Правительство Российской Федерации
Федеральное государственное бюджетное образовательное учреждение
высшего профессионального образования
«Санкт-Петербургский государственный университет»

Межкафедральная лаборатория биомедицинской химии

Ал Мулла Хадеер Хассан Ахмед Мостафа

Химическая модификация поверхности клеток человека для получения биогибридов

Магистерская диссертация (Дипломная работа)

Допущена к защите.

зав. лаб.:

д.х.н., профессор Тенникова Т.Б.

Научный руководитель:

д.б.н., в.н.с Шаройко В.В.

Рецензент:

к.х.н. Руденко А.О.

Санкт-Петербург

2020

SAINT-PETERSBURG STATE UNIVERSITY

Interdepartmental Laboratory of Biomedicinal Chemistry

Hadeer Hassan Ahmed Mostafa Al Mulla

Chemical modification of human cell surface for biohybrids production

Master's Thesis (Graduation Thesis)

Admitted for defence.

Head of the lab:

DSc, professor Tennikova T.B.

Scientific supervisor:

DSc, leading scientist Sharoyko V.V.

Reviewer:

PhD Rudenko A.O.

Saint-Petersburg
2020

To my Parents

To my brother,

Mohammed

To my sisters,

Haidy

Hala

Sara

CONTENTS

Abbreviations

CuAAC	Cu-catalyzed azide-alkyne cycloaddition
SPAAC	Strain-promoted [3 + 2] azide-alkyne cycloaddition
IEDDA	Inverse-electron-demand Diels–Alder
Tz	Tetrazines
TCO	trans-cyclooctene
DIFO	difluorinated cyclooctyne
GalNaAz	N-azidoacetylglucosamine
6AzFuc	6-azidofucose
SiaNAz	N-azidosialic acid
Ac_4ManNAz	N-Azidoacetylmannosamine-tetraacylated
BCN-CNPs	Bicyclo[6.1.0]nonyne modified imageable glycol chitosan nanoparticle
Ac3ManNAz	1,3,4-tri-O-acetyl-N-azidoacetylmannosamine
DBCO-650	Dibenzyl cyclooctyne-SETA 650
DBCO-lipo	Dibenzyl cyclooctyne conjugated PEGylated liposome
EPR	Enhanced permeability and retention
DBCO-VC-Dox	Dibenzyl cyclooctyne-valine-cysteine-doxorubicin conjugate
DCL-AAM	Histone deacetylase/cathepsin L-responsive acetylated azidomannose
DOX	Doxorubicin
DBCO-NPs	Dibenzyl cyclooctyne-modified poly (lactide-co-glycolide) nanoparticles
MSCs	Mesenchymal stem cells
PLGA	Poly (lactide-co-glycolide)
VEGF	Vascular endothelial growth factor
VPF	vascular permeability factor
PlGF	placental growth factor
PDGF	platelet-derived growth factor
VEGFRs	Vascular endothelial growth factor receptors
NRP	Neuropilin
HBDs	Heparin-binding domains
HS	heparan sulfate
HSPGs	Heparan sulfate proteoglycans
ECM	Extracellular matrix
MMPs	matrix metalloproteinases
HIF	hypoxia-inducible factor
HRE	hypoxic response elements
CBP	cAMP-regulated-enhancer (CRE)-binding protein (CREB)-binding protein
VHL	von-Hippel Lindau
IL	interleukin
TNF	tumor necrosis factor
TGF	transforming growth factor

EGF	epidermal growth factor
TKRs	tyrosine kinase receptors
Ig	immunoglobulin
Flt	fms-like tyrosine kinase
KDR	Kinase insert domain receptor
Flk1	Fetal Liver Kinase 1
MAPK	mitogen-activated protein kinase
Raf	rapidly accelerated fibrosarcoma
MEK	mitogen-activated protein kinase
ERK	extracellular signal-regulated kinase
FAK	focal adhesion kinase
PI3K	phosphotidylinositol-3 kinase
PKB	Protein kinase B
PKC	protein kinase C
PLCγ	phospholipase C gamma
AMD	age-related macular degeneration
DR	diabetic retinopathy
BBB	blood brain barrier
FDA	Food and Drug Administration
CRC	colorectal cancer
MBC	metastatic breast cancer
NSCLC	non-small cell lung cancer
RCC	renal cell carcinoma
RVO	Retinal Vein Occlusion
DME	Diabetic Macular Edema
TKIs	tyrosine Kinase Inhibitors
RTKI	Receptor tyrosine Kinase Inhibitors
GIST	imatinib-resistant gastrointestinal stromal tumors
FGFR	fibroblast growth factor receptor
PDGFR	platelet derived growth factor receptor
EGFR	epidermal growth factor receptor
PABA	p-aminobenzoic acid
MTHFR	Methylene tetrahydrofolate reductase
5,10-methylene THF	5,10-methylenetetrahydrofolate
SAM	s-adenosylmethionine
dUMP	deoxyuridine monophosphate
dTMP	deoxythymidine monophosphate
FR	folate receptor
RFC	reduced folate carrier
PCFT	proton-coupled folate transporter
OP	organic phosphate
CML	chronic myeloid leukemia

AML	acute myeloid leukemia
IHC	immunohistochemistry
^{99m}Tc	^{99m}technetium
SPECT	single photon emission computed tomography
CT	computed tomography
DAVLBH	desacetylvinblastine hydrazide
ADCC	antibody-dependent cellular cytotoxicity
CDC	complement-dependent cytotoxicity
DMEM-F12	Dulbecco's modified Eagl's medium
DMSO	dimethyl sulfoxide
HBSS	Hank’s balanced salt solution
DBCO	Dibenzocycolctyne
DCC	N,N'-Dicyclohexylcarbodiimide
NHS	N-Hydroxysuccinimide
TFA	Trifluoroacetic acid
DMF	Dimethylformamide
MTT	3-(4,5-dimethylthiazol-2-yl)-2,5-diphenyltetrazolium bromide
FBS	fetal bovine serum
TEA	Triethylamine
DIPEA	N,N-Diisopropylethylamine

Chapter 1

Introduction

Research at the interface of chemistry and biology has resulted in major advances in bio-sensing, diagnostics, drug delivery and theranostics. Biohybrid materials are based on the combination of rationally designed synthetic compounds and unique properties of living systems. These approaches allow construction of biomaterials and bio-hybrid material for biomedical applications, such as the delivery of therapeutics (drugs, cells, and genetic material), tissue engineering, diagnostics, and imaging, theranostics [1].

Modified cells have been used as transporters of pharmaceuticals. Some types of cells have natural homing mechanisms that can be exploited in drug delivery and further optimized chemically or genetically. Drug-loaded cells (pharmacytes) can be based on T lymphocytes, macrophages, erythrocytes, lymphocytes, bacteria, and stem cells. Biohybrids utilize the properties of living cells such as the ability to home to diseased tissues, abundant surface ligands, long half-life, and flexible morphology. Even though substantial efforts have been made to understand the key features of cell-mediated drug carriers, these approaches have only rarely been used for ocular treatments [1].

Aim of this thesis is the development of the chemical and biological technologies for the construction of biomaterials and biohybrids platforms based on the strain-promoted azide-alkyne cycloaddition (SPAAC) reaction.

Research objectives

Innovative chemical technologies for the preparation of the biohybrid structures will be developed on the base of mammalian cells. To this aim the living cells will be hybridized with biologically active molecules. In this study the following tasks will be solved:

1. Development of optimal conditions for creation of biohybrids in SPAAC reaction between N-azidoacetylmannosamine, incorporated in surface peptidoglycan of cells, and dibenzocyclooctyne conjugate of fluorescent dye Cy5.

2. Synthesis of an anti-VEGF peptide and dibenzocyclooctyn conjugate for subsequent creation of biohybrids capable of selectively binding a VEGF protein.

3. Synthesis of folic acid and dibenzocyclooctyne conjugate for subsequent creation of biohybrids capable of selectively recognizing tumor cells overexpressing folate receptor.

1.1 The Reactions of Bioconjugation

Bioconjugation is an important issue that can connect chemistry, biology, and material science. Although great efforts have been made to promote bioconjugation chemistry forward, some key limitations of current available strategies have greatly restricted some applications in biology and biomedicine [2].

Bioconjugation is a chemical technique used to form covalent bond between a biological molecule with another moiety (Figure 1.1). These moieties may include other biomolecules (e.g., nucleic acid, or protein), synthetic polymers (e.g., polyethylene glycol), and small molecules such as ligands (e.g., biotin), drugs, or fluorescent dyes [3]. This technique uses a variety of reagents for the crosslinking, immobilization, modification, and labeling of peptides and proteins. Bioconjugation reactions play a critical role in the modification of biomolecules. Because of recent advances in the study of biomolecules, Synthetically modified biomolecules can have a variety of functions, including cellular tracking, imaging specific biomarkers, and target drug delivery [4].

Figure 1.1 Forming a basic conjugate often involves the reaction of two molecules and a crosslinking agent that covalently links the components together. In some conjugation schemes an activation agent is used that results in the linking of two molecules without an intervening cross-bridge between them [5].

1.1.1 Chemoselective Ligation: Bioorthogonal Reagents

Many of reactions that are available for bioconjugation purposes generally are designed to work with biological molecules and their functions. The main goal of most bioconjugate techniques is to use the functional groups on biomolecules to label with another biomolecule or join to synthetic probes. However, it is often desirable to link one molecule to another without the potential for cross-

reactivity with biomolecules. Chemoselective ligation describes the coupling of one reactive chemical group specifically with another reactive group without side reactions in aqueous solution or in the presence of biological material [6].

Unfortunately, the diversity of biomolecules in organisms and cells presents problems for the goal of total bioorthogonality and chemoselectivity, as the number and variety of reactive sites on the biomolecules is extraordinary. Even the crosslinkers or labeling reagents designed to be site-specific in their reactions often display cross-reactivity with functional groups on biomolecules other than the ones intended for coupling [6].

Bioorthogonal reagents should contain a reactive group that only will react with another specific reactive group without any potential for cross-reactivity with biomolecule functionalities. The bioorthogonal reactive group could be added to a complex mixture of biomolecules in aqueous solution without reacting with any of them. Furthermore, the ideal bioorthogonal system should be immune to instability in aqueous solutions, such as the tendency to oxidize or hydrolyze. True bioorthogonal reagents of this type will join to each other only in the presence of intracellular environments or in defined biomolecule solutions [6].

The chemoselective ligation reactions can be considered to have a degree of bioorthogonal characteristics. In each system, the chemoselective pair of reactants can be separately linked to the labeling reagents and used to modify biological molecules, surfaces, or organic compounds. Subsequently, these labeled components can be brought together to facilitate conjugation between the two bioorthogonal reacting species [6].

In addition, for several reactant strategies in chemoselective ligation, one of the reagent pairs can be designed into a biological monomer which can be used by cellular processes to become incorporated into biopolymers. This advantage provides a unique in vivo labeling capability through the feeding of monomer analogs to cells or organisms, such as modified amino acids or sugar derivatives, which then get selectively added into proteins, peptides, carbohydrates, or lipids. Thus, the application of bioorthogonal chemoselective ligation is to label specifically the molecules of life directly within living systems and without cross-reactions with other biological functional groups [5,6].

1.1.2 Bioorthogonal chemistry

Bioorthogonal chemistry is chemical reaction which can be performed in living systems without interaction with the inside biomolecules or interference with biological processes. Since its first introduction by Carolyn R. Bertozzi in 2003 [7].

The use of bioorthogonal reaction to probe biomolecules in living systems typically involves a two-step strategy, that has become known as the bioorthogonal chemical reporter strategy. First, a metabolic substrate, enzyme inhibitor, or small molecule ligand is linked to a bioorthogonal functional group (chemical reporter) and introduced to the biological system. The structural perturbation imposed by the functional group (chemical reporter), must be minimal so as not to affect the molecule's natural bioactivity. Once the labeled molecule has been delivered to its target (e.g., a metabolically labeled glycan, protein, or lipid, or an inhibitor-bound receptor or enzyme), the second step involves a bioorthogonal conjugation reaction to label the biomolecule with fluorophores or affinity tags (Figure 1.2) [8,9].

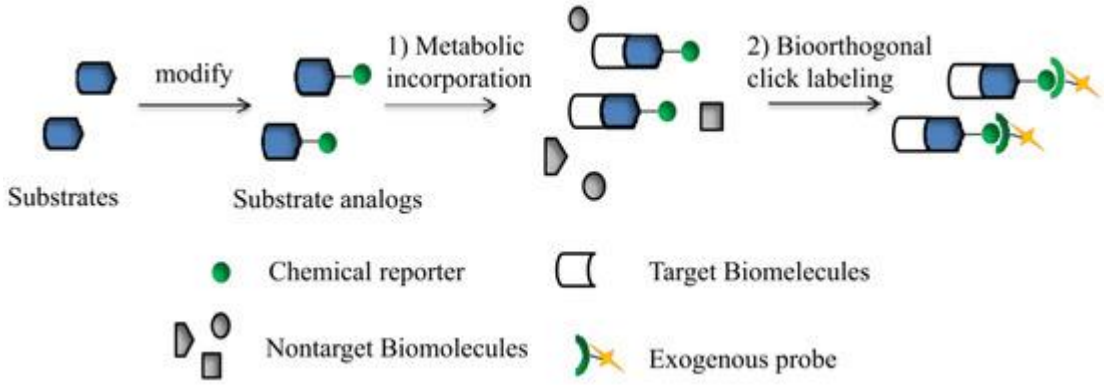

Figure 1.2 Two-step bioorthogonal chemistry strategy. (1) A bioorthogonal functional moiety (chemical reporter) was installed into substrates (blue shapes) to generate substrate analogs which can selectively incorporated into the target biomolecules (white shapes) through metabolism; (2) Chemical reporters selectively covalent with exogenous probes by click reaction for further detection and isolation [10].

The development of bioorthogonal reaction has unusually restrictive boundary requirements for the covalent reaction between the two components. The reaction must form a stable covalent linkage between two functional groups that are bio-inert and ideally nontoxic. The reaction must be rapid in kinetics so that product is formed at a reasonable rate even when reactant concentrations are very low, as is required in many biological labeling experiments. Also, such fast kinetics must be

achieved in a physiological environment (37 °C, pH 6–8). For optimal use as chemical reporters, at least one of the bioorthogonal reactive partners should be small and highly stable [8,9]. In addition, the chemical reporter and its complementary probe must have adequate metabolic stability and bioavailability for use in cells or organisms [11].

Bioorthogonal chemistry has widely employed applications in the field of chemical biology. In the past decade, a limited number of reactions including Staudinger ligation and click reaction have been well developed, which have also been widely used for labeling biomolecules in the context of living cells and whole organisms (Figure 1.3). In general, most of the bioorthogonal click reactions rely on azide as a functional bio-orthogonal handle. The kinetically stable azide neither exists among the functional groups in living systems nor cross-reacts with them, making it truly bio-orthogonal. Additionally, due to its small size, the introduction of the abiotic and bioinert azide into a molecular target constitutes an insignificant structural perturbation. These unique attributes of azide have been exploited in the development of various bio-orthogonal click reactions, which have since been widely used in many biological applications, particularly for selective in vivo biomolecule labeling, targeted imaging, and drug delivery [12,13].

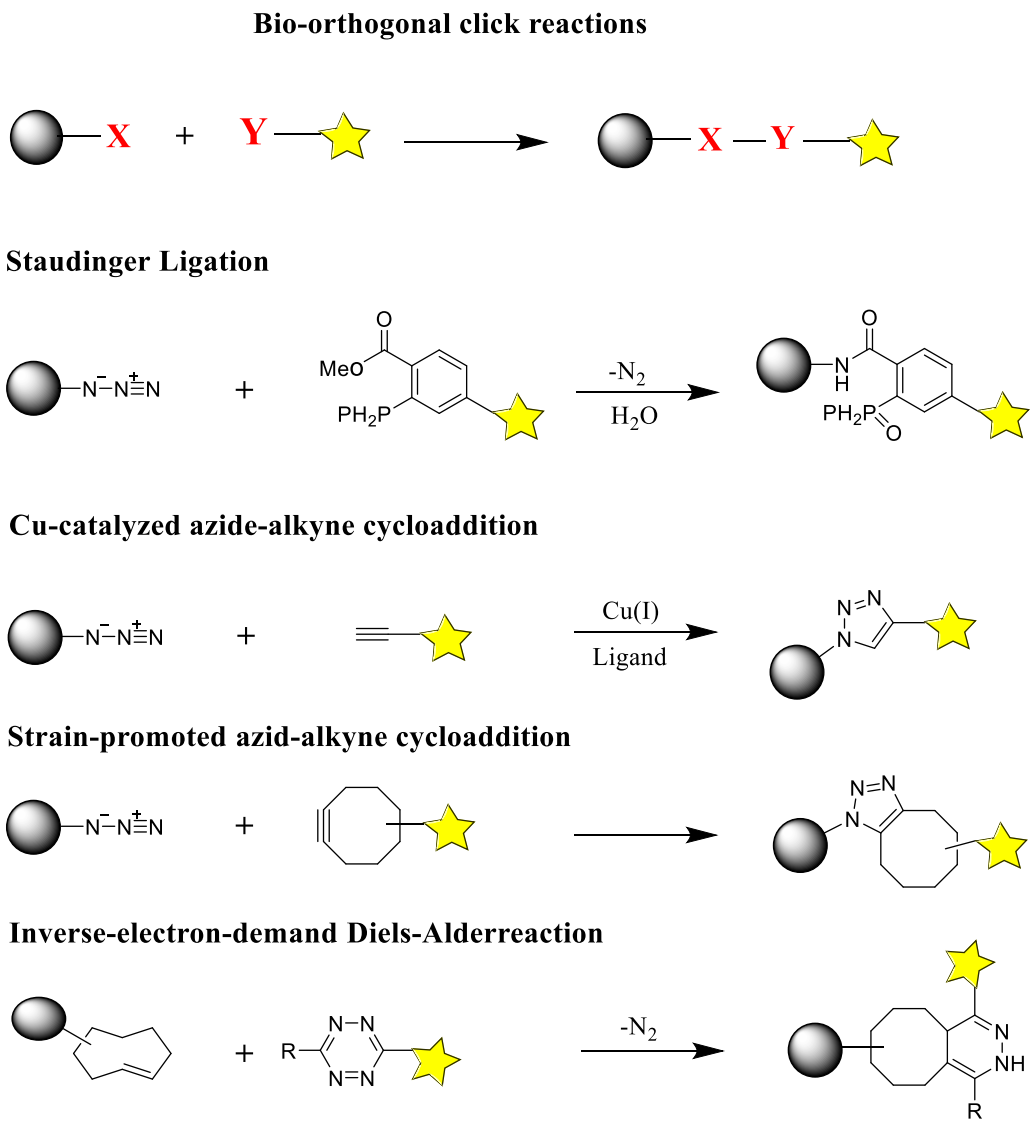

Figure 1.3 Bio-orthogonal Click Reactions Commonly Used for In Vivo Biological Labeling and Imaging Applications. The commonly employed bio-orthogonal click reactions for in vivo biological labeling and imaging include: Staudinger ligation; Cu-catalyzed azide-alkyne cycloaddition (CuAAC); strain-promoted (Cu-free) azide-alkyne cycloaddition (SPAAC); and the inverse-electron-demand Diels–Alder (IEDDA) reaction [12].

1.1.2.1 The Staudinger Ligation

The Staudinger ligation was the first developed of bioorthogonal ligation reaction. In 1919 Hermann Staudinger reported that the reduction of azides with triphenylphosphines (soft nucleophiles) in water under mild conditions to produce aza-ylide intermediates (Scheme 1.1). Advantageous features of this reaction were the small size of the azide, its absence from biological

systems, and its kinetic stability. Also, the azide can act as a "soft electrophile" that prefers "soft nucleophiles" (such as phosphines) situates this functional group in a reaction space that is distinct from most of biology, wherein nucleophiles are typically "hard". That organic azides would be well tolerated by cells and organisms was hinted at by the established use of aryl azides as photocrosslinkers. Additionally, phosphines, the other reactive group, are naturally absent from living systems. Mechanistically, the classic Staudinger reduction proceeds through azides are reducing by phosphines under mild conditions, followed by loss of nitrogen to produce an aza-ylide intermediates. In aqueous environments, the aza-ylide intermediates are rapidly hydrolyzed to to provide a pair of products: a phosphine oxide and an amine (Scheme 1.1). The Staudinger reduction appeared as a prototype for bioorthogonal reaction development because the two participants were abiotic, mutually and selectively reactive, essentially unreactive with biological functionalities, and tolerant of water. The bioorthogonal nature of this transformation suggested potential applications of the azide as a chemical reporter, provided an initial covalent linkage formed (intermediate) could be forged between the two reactants, was later lost to hydrolysis [8,9,14]. Thus, Bertozzi and co-workers modified the classic Staudinger reaction to redirect the aza-ylide intermediate to a stably ligated product. Now known as the Staudinger ligation, was achieved by introducing an intramolecular trap (ester group ortho) to the phosphorous atom on one of the aryl rings. the aza-ylide intermediate then reacts with the electrophilic ester carbonyl group and generates upon hydrolysis in water, yielded a stable amide-linked product is freed from the phosphine oxide moiety (Scheme 1.1) [7,15].

Staudinger ligation has been the choice for a wide range of bioconjugation applications and useful for in vivo labeling, it suffers from several shortcomings, which have undermined its widespread adoption for in vivo labeling and imaging. These include the nonspecific oxidation of phosphine reagents in the biological systems, which limits their shelf life, and slow reaction kinetics of the Staudinger ligation. The slow kinetics of Staudinger ligation have hampered its utilization for in vivo bioconjugation. To overcome this, high concentrations of phosphine reagent are required, which will lead to a high backgrounds signal for fluorescence imaging applications due to the difficulty in removing excess probe reagent. Therefore, other bioorthogonal reactions with more rapid reaction kinetics alternative to Staudinger ligation have been actively exploited [12,16].

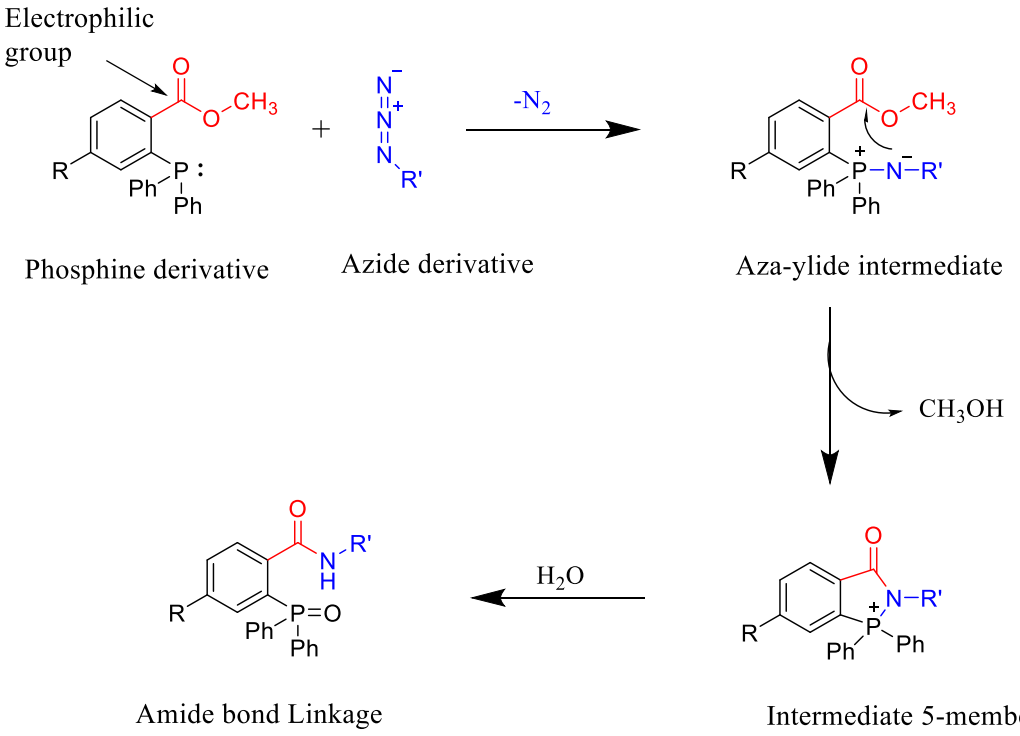

Scheme 1.1 The Staudinger ligation reaction. A triarylphosphine and an azide first react to form an aza-ylide intermediate. The nucleophilic nitrogen atom is trapped in an intramolecular fashion, and the cyclized intermediate hydrolyzes in water to form a stable amide-linked product [5].

1.1.3 Click chemistry Reactions

Click chemistry is a new concept of chemical synthesis, which opens up new ways for chemists to develop chemical synthesis pathways. Click chemistry was defined by Sharpless and co-workers in 2001, describe a set of powerful and practical method for synthesizing a large number of new compounds at low cost by linking carbon and heteroatoms (C-X-C) via rapid, highly reliable and selective chemical reactions using readily available raw materials [17,18].

Click chemistry can also be called as Linkage Chemistry, Dynamic, Combinatorial Chemistry or Quick Linking Combinatorial Chemistry. Click chemistry, also known as tagging, describes the reaction that joins molecular fragments as simple, efficient and versatile. The two units with specific click structures can be joined by click reaction. It emphasizes the development of new combinatorial chemistries on the basis of the synthesis of efficient and highly selective carbon-heteroatom bond (C-X-C) and effectively prepares molecules with high diversity through these simple reactions. Click

chemistry has become one of the most useful and attractive synthetic strategy in many fields, such as drug development and the synthesis and preparations of biomedical materials and polymers [17]. Among the click chemistry reactions, the copper (I)-catalyzed azide-alkyne 1,3-dipolar cycloaddition (CuAAC) reaction has been used as a bioorthogonal reaction in the life science research fields (Scheme 1.2.A), the strain-promoted [3 + 2] azide-alkyne cycloaddition (SPAAC) reaction, which is a new type copper-free click chemistry developed by Bertozzi et al. in 2004, has brought about the successful application of click reactions to living cells without copper-induced cytotoxicity (Scheme 1.2.B). Moreover, inverse electron demand Diels-Alder (IEDDA) reaction between the cycloaddition of s-tetrazine and trans-cyclooctene (TCO) derivatives, successfully developed by Blackman et al. And resulted in a faster copper-free click chemistry than SPAAC reactions (Scheme 1.2.C) [19–21].

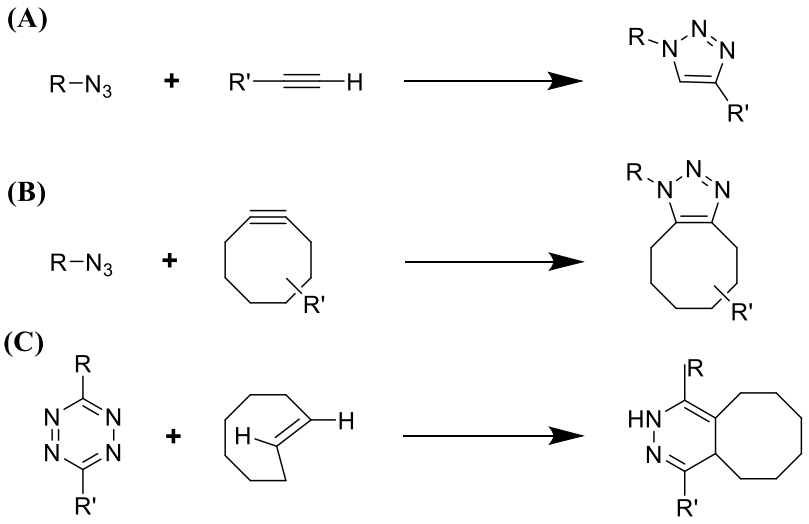

Scheme 1.2 Click chemistry reactions. (A) CuAAC reaction with azide and linear alkyne; (B) SPAAC reaction with azide and cyclooctyne; (C) IEDDA reaction with tetrazines (Tz) and trans-cyclooctene (TCO) [19].

The characteristics of click chemistry reactions

1. Click chemistry reactions are fast, modular, wide in scope, and simple to perform under mild conditions and are rarely affected by water and oxygen. The presence of water can even accelerate the reaction.

2. Click chemistry reactions are highly stereoselective, give high yield product and generate by-products that are non-toxic.

3. Click chemistry reactions are usually exothermic, which is achieved by high-energy reactants and stable products.

4. Click chemistry reactions produce the products that can be purified simply by nonchromatographic methods, such as crystallization or distillation without complex chromatographic separation needed, and the product must be stable under physiological conditions [17,18,22].

Azide-Alkyne Cycloaddition

A number of cycloaddition reactions are useful for bioconjugation. These reactions are highly specific reactant pairs that have a chemoselective nature, which means they mainly react with each other and not other functional groups, such as those found on biomolecules [5].

1.1.3.1 Cu-Catalyzed Azide-Alkyne Cycloaddition (CuAAC)

In the Staudinger ligation, the azide serves as an electrophile subject to reaction with soft nucleophiles. An alternate mode of reactivity for the azide is its participation as a 1,3-dipole in a [3+2] cycloaddition that can undergo reactions with dipolarophiles such as activated alkynes [11]. The prototype reaction was reported by Michael in 1890s [7]. Later, in 1950s Rolf Huisgen introduced the concept of 1,3-dipolar cycloadditions, the reactivity of azide as a 1,3-dipole is used to facilitate a [3+2] cycloaddition between azides and terminal alkynes to provide stable triazole linkage (Scheme 1.3). Like Staudinger ligation, the classical [3+2] cycloaddition of azides and unactivated alkynes to form triazoles reaction is far away from being developed into bioorthogonal reaction due to its slow reaction kinetics and harsh reaction conditions. To overcome this, the reaction requires elevated temperatures or pressures that are not compatible with living systems [12,23].

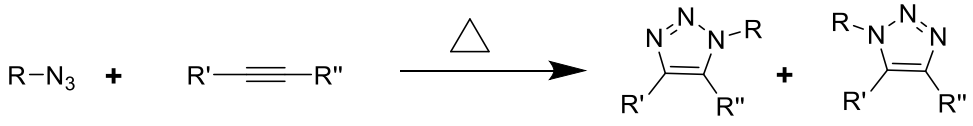

Scheme 1.3 The 1,3-dipolar cycloaddition of azides and alkynes to yield regioisomeric triazole products [8].

In early 2000s, Sharpless and Meldal discovered that a regiospecific reaction can proceed rapidly to form 1,4-disubstituted 1,2,3-triazoles could be effectively catalyzed by Cu(I) (Figure 1.4).

This is the well-known “click” chemistry, termed the copper-catalyzed azide-alkyne 1,3-dipolar cycloaddition (CuAAC), takes advantage of Cu-acetylide formation to activate terminal alkynes toward reaction with azides. The result of Cu(I) catalysis is a reaction that proceeds roughly seven orders of magnitude higher than the uncatalyzed cycloaddition, and the reaction can be further accelerated in the presence of specific ligands for Cu(I). CuAAC has all the properties of a “click” reaction (including efficiency, selectivity, and simplicity). CuAAC has gained widespread use in organic synthesis, chemical biology, combinatorial chemistry, polymer chemistry, and materials chemistry. The formal cycloaddition between azides and terminal alkynes can also be catalyzed by Ru(II)to obtain 1,5-disubstituted 1,2,3-triazole products, but this reaction is used far less frequently than CuAAC [7,8].

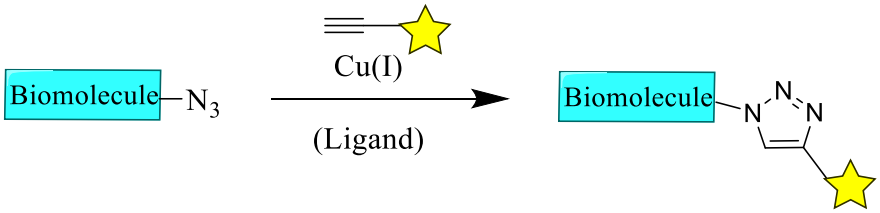

Figure 1.4 Cu(I) catalyzed formal cycloaddition between an azide and terminal alkyne to yield a 1,4-triazole product [8].

CuAAC has been widely used as a bioconjugation strategy in the field of chemical biology [7]. Therefore, click chemistry has been used in detection of very small quantities of azide-labeled biomolecules. The reagents required for click chemistry are simple and small. In addition, CuAAC gives one flexibility regarding the choice of chemical reporter group because both azides and terminal alkynes are stable, compact, and readily metabolically incorporated. CuAAC also benefits from fast reaction kinetics without compromising selectivity. These advantages have resulted in many fields of chemistry exploiting CuAAC [8]. Unfortunately, CuAAC not biocompatible enough and has a limited scope in the chemical biology applications due to the toxicity of Cu(I). The disadvantage of the copper-catalyzed cycloaddition is the cellular toxicity of the metal catalyst. Although more biofriendly metal-ligand combinations could potentially be discovered, the reaction is not ideal for labeling biomolecules in living cells [11,24,25].

1.1.3.2 Strain-Promoted Azide-Alkyne Cycloaddition (SPAAC)

To overcome the cytotoxicity of the CuAAC reaction, Bertozzi used strained cyclooctynes instead of linear alkynes. the Cu-free modification is achieved by incorporating the alkyne within a strained cyclooctyne system. The alkyne in strained form makes it highly reactive and can undergo cycloaddition with azide quickly under physiological environment. As a result, cyclooctynes react with azides at room temperature, without the need for a catalyst. This reaction is named as the Cu-free click reactions is strain-promoted [3+2] azide-alkyne cycloaddition (SPAAC) to form triazole products and has been widely used for bioconjugation in not only living cells but also living animals without observable toxic effects (Figure 1.5). While, poor water solubility of cyclooctynes limits their uses in biological environment. Chemical modification on the cyclooctynes has been demonstrated as a way to improve their solubility [7,26]. In addition, the strain-promoted cycloaddition has improved biocompatibility, its reaction rate is similar to that of Staudinger ligation and significantly slower than that of CuAAC. To improve the reaction kinetics, cyclooctyne derivatives such as difluorinated cyclooctyne (DIFO), in which the electron-withdrawing fluorine atoms can be incorporated into cyclooctyne reagents with improved reactivity beneficial for in vivo bio-orthogonal imaging of azidelabeled sugars. Since then, cyclooctyne analogs with improved water solubility and kinetics have been increasingly developed to further enhance the efficacy of the azide-alkyne cycloaddition reaction in living systems [12,25].

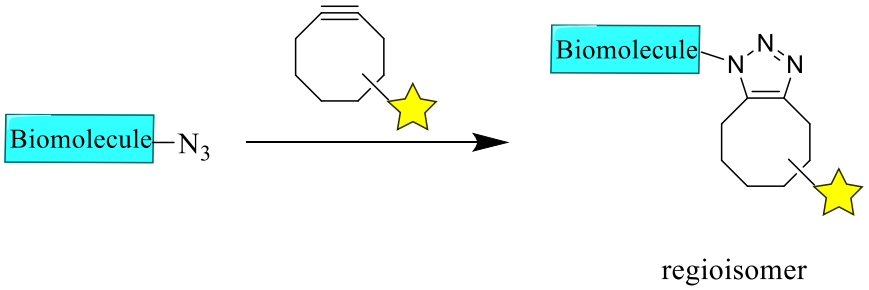

Figure 1.5 The strain-promoted cycloaddition between an azide and cyclooctyne to yield a triazole product [8].

1.1.4 Application of Bioorthogonal Chemistry for Glycan Bioconjugations

The biological activities of biomolecules on the cell surface may reveal crucial information about cellular states. Glycans have been increasingly recognized as a dynamic indicator of cellular states. Glycan is an attractive target for bio-imaging as it plays key roles in number of biological

processes. Therefore, the ability to monitor the kinetics of glycosylation in living systems will deepen our understanding of the mechanisms of glycosylation-related diseases and improving disease diagnosis and therapeutics. Classic methods for monitoring glycans rely on molecular recognition with probe bearing lectins or antibodies that are limited due to the poor tissue permeability and toxicity [7,12].

To overcome the limitations of conventional molecular labeling techniques, bio-orthogonal click reactions have been actively coupled with metabolic engineering to construct highly specific and sensitive molecular labeling strategies. This technique has enabled the chemical labeling of glycans in live cells and in vivo with bioorthogonal groups in various applications, such as molecular imaging and proteomic analysis of glycoproteins. Generally, a metabolic labeling and imaging strategy based on bio-orthogonal click chemistry proceeds in two stages [12].

Metabolic engineering is a click chemistry tool that allows for the modification of living cells with chemical tags. Metabolic glycoengineering offers means for modify glycans on the surface of cells in a defined way. As biocomponents such as sugars, amino acids, or lipids are metabolized in the living cells, using biomolecules with chemical tags can incorporate chemical tags into proteins, glycans, and lipids in living cells [19,27]. The unnatural monosaccharides (e.g., azidosugars) residues with chemical tags can be incorporated into glycans in cells through a biosynthesis pathway to present chemical tags, including azide, alkene, and alkyne, on the cells surface. There are mainly fours subtypes of azido sugars have been synthesized and developed for metabolic glycan labelling, such as N-azidoacetylmannosamine (ManNAz), N-azidoacetylgalactosamine (GalNaAz), N-azidoacetylglucosamine (GlcNAz), and 6-azidofucose (6AzFuc) (Figure 1.6) [10,28,29].

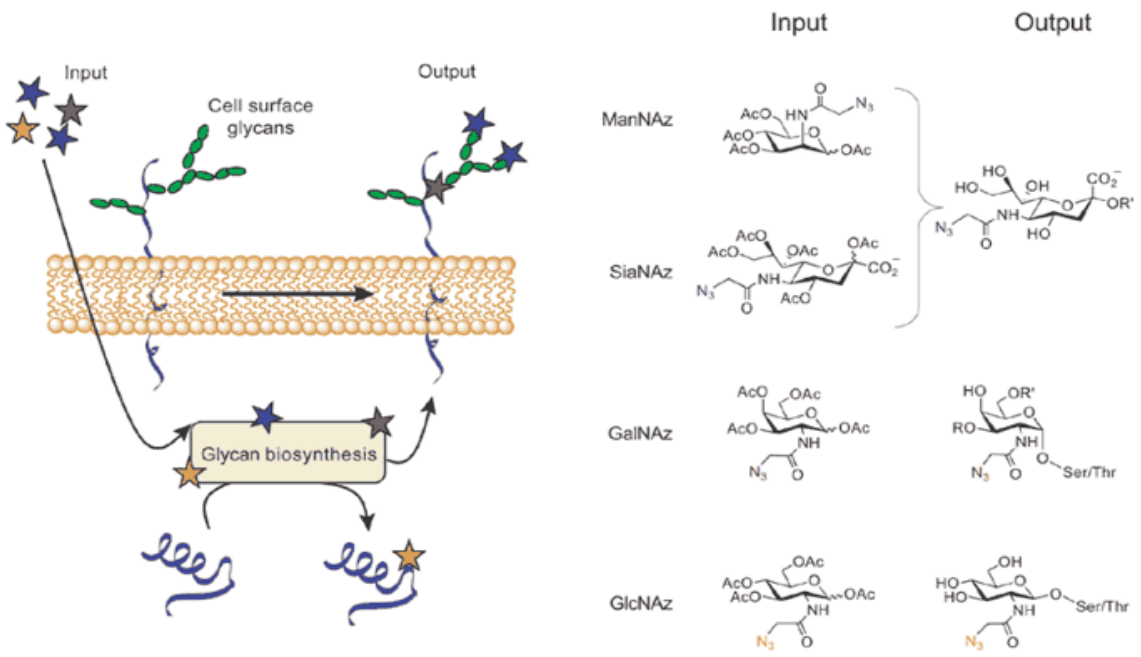

Figure 1.6 Azides can be incorporated into glycoconjugates using glycan biosynthetic pathways. Azido analogs of ManNAc (ManNAz) and sialic acid (SiaNAz) are metabolized by cells and converted to cell surface azido sialosides. Similarly, an azido analog of GalNAc (GalNAz) can be metabolically introduced at the core position of mucin-type O-linked glycoproteins. An azido analog of GlcNAc (GlcNAz) can be incorporated into cytosolic and nuclear glycoproteins [11].

In general, monosaccharides building blocks functionalized with bioorthogonal chemical tags can be incorporated into target glycans on cells surface through a biosynthesis pathway to present chemical tags, including azide, alkene, and alkyne, on the surface of cells (Figure 1.7) [7,30]. In metabolic glycoconjugation, N-azidoacetylmannosamine (Ac_4ManNAz) is widely used for engineering of the cell surface. Ac_4ManNAz is metabolized into N-azidoacetyl neuraminic acid and is incorporated into glycans, such that azide groups are expressed in the glycans on the cells surface. Furthermore, Ac_4ManNAz is not affected by the characteristics of culture cells (attachment, differentiation, and migration) with a lower toxicity in animal tissues. Table 1.1 and Table 1.2 summarize the non-toxic dose ranges of the reagents reported in vitro and in vivo studies using click chemistry and metabolic glycoengineering. Azide groups on cell surfaces after metabolic glycoengineering gradually disappear due to the hydrolysis of glycans by neuraminidase in cells after internalization. However, it has been reported that azide groups were detected on the cell surface for at least 14 days, suggesting that metabolic glycoengineering is a suitable tool for cell labeling or functionalization through click chemistry [19]. After metabolic incorporate the bioorthogonal group

into glycans on cell surface, a complementary imaging probe is then conjugated to the glycans via bioorthogonal reaction, enabling the visualization of the tagged glycoconjugates [7].

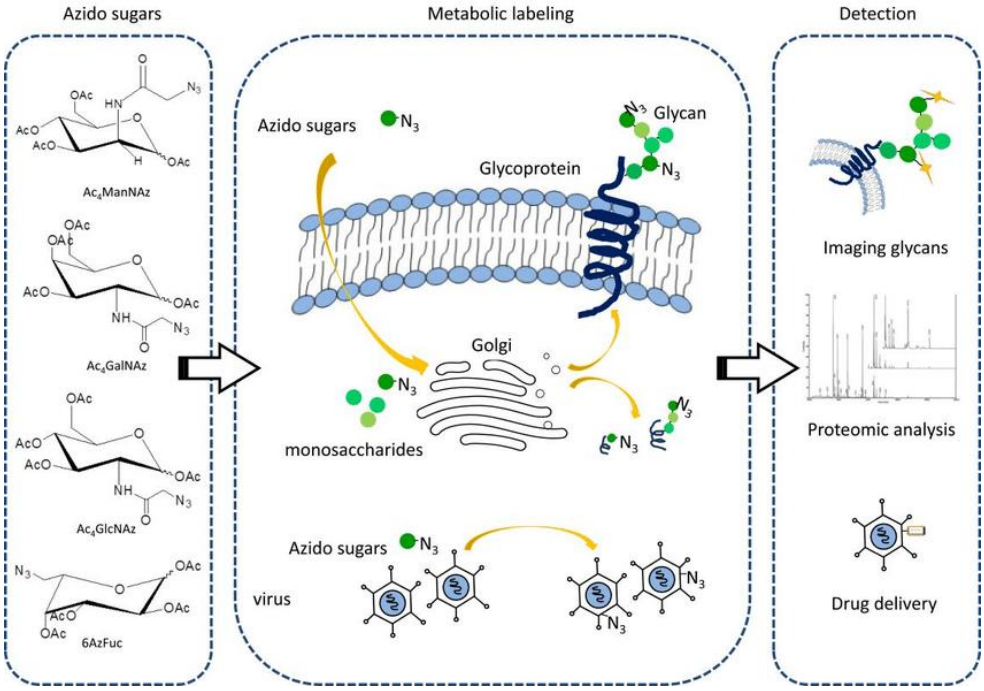

Figure 1.7 Metabolic engineering strategy. Different types of unnatural monosaccharides residues (azido sugars): N-azidoacetylmannosamine (ManNAz), azidoacetylgalactosamine (GalNAz), N-azidoacetylglucosamine (GlcNAz), and 6-azidofucose (6AzFuc) can be incorporated into glycoconjugates using glycan biosynthetic pathways. After displayed on cell surfaces or virus capsid, it can be applied to image glycans in vivo, identify targets by mass spectrometry and deliver cancer specific drugs [10].

Table 1.1 Non-toxic concentration range of the reagents used in click chemistry and glycoengineering in vitro [19].

Compound	Non-Toxic Concentration	Incubation Time	Cell Type
$Ac_4ManNAz$	5 µM	3 days	B16
	10 µM	3 days	A549
	20 µM	3 days	MSC (human)
	50 µM	3 days	NIH3T3
	50 µM	1 day	ASC (human)
		3 days	Jurkat T lymphocyte
		3 days	Chondrocyte (rabbit)
		7 days	MSC (human)
$Ac_3ManNAz$	<5 µM	2 days	Primary hippocampal neurons (rat)
	100 µM	2 days	U87
BCN-CNP-Cy5	500 µg/mL	1 day	ASC (human)
DBCO-650	50 µM	1 h	Chondrocyte (rabbit)
DBCO-Cy5	20 µM	1 h	ASC (human)
	100 µM	48 h	A549
TCO-DBCO	100 µM	30 min	NIH3T3
			A549
			Jurkat T lymphocyte
Tz-DBCO	100 µM	30 min	NIH3T3
			A549
			Jurkat T lymphocyte

B16, murine melanoma cell line; A549, human lung adenocarcinoma cell line; NIH3T3, murine embryo fibroblast cell line; ASCs, adipose-derived mesenchymal stem cells; BCN-CNP-Cy5, Cy5-labeled bicyclo[6.1.0]nonyne modified imageable glycol chitosan nanoparticle; $Ac_3ManNAz$, 1,3,4-tri-O-acetyl-N-azidoacetylmannosamine; DBCO-650, dibenzylcyclooctyne-SETA 650; Tz, tetrazines; TCO, trans-cyclooctene.

Table 1.2 Non-toxic dose range of the reagents used in click chemistry and glycoengineering in vivo [19].

Compound	Non-Toxic Dose	Administration Route	Animal Type
	300 mg/kg/day daily for 7 days	ip	Mouse
Ac_4ManNAz	10 mg/kg/day daily for 3 days	it	Mouse
	40 mg/kg/day daily for 3 days	iv	Mouse
	10 nmol	Oral	Mouse
Ac_4ManNAz-LP	40 mg/kg/day of Ac4ManNAz daily for 4 days	iv	Mouse
BCN-Lipo	10 mg/kg	iv	Mouse
DBCO-Cy5	5 nmol	iv	Mouse
DBCO-Cy5.5	5 μg (4.25 nmol)	iv	Mouse
DBCO-lipo	10 mg/kg	iv	Mouse
DBCO modified polymeric nanoparticles	100 μg/body	iv	Mouse
DBCO-ZnPc-LP	2.5 mg/kg	iv	Mouse
3,6-dimethyl-1,2,4,5-Tz	6 mg/kg	iv	Mouse
Tz-Cy5.5	8 nmol	iv	Mouse
GEBP11-TCO	4 nmol	iv	Mouse

Ac_4ManNAz-Lp, Ac_4ManNAz-loaded liposome; BCN-Lipo, bicyclo[6.1.0]nonyne-modified liposome; DBCO-lipo, dibenzyl cyclooctyne conjugated PEGylated liposome; DBCO-ZnPc-LP, dibenzyl- cyclooctyne-modified zinc (II)-phthalocyanine-loaded liposome; GEBP11-TCO, a vascular-homing peptide (GEBP11)-trans-cyclooctene.

1.1.5 Applications of Click Chemistry for Drug Delivery in the Diagnosis and Treatment of Diseases.

Copper-free click chemistry recently has been used as an effective tissue-targeting method for drug delivery in the diagnosis and treatment of diseases due to its high stability, specificity, and quick reaction rate. Some researchers have demonstrated that the labeling method using metabolic glycoengineering and copper-free click chemistry is useful for the visualization of glycans in vivo. The studies demonstrated that copper-free click chemistry could be a useful application tool for in vivo tissue engineering molecule imaging, and cell tracking. In addition, copper-free click chemistry has been used for tissue-targeted delivery of imaging agents and anti-cancer agents. Tissue or cancer cell-specific drug delivery is highly desirable in cancer therapy, in order to improve therapeutic efficacy, avoid adverse effects, and for detecting cancer cells in order to determine tumor size and metastasis [19].

Tumor-Specific Labeling with Azide Groups

The combination of metabolic glycoengineering and click chemistry is a powerful tool for the labeling and targeting of cancer cells. Ac_4ManNAz is widely used to introduce azide groups on the cancer cells surface because it can easily introduce azide groups both in vitro and in vivo without significant toxic effects. Ac_4ManNAz and its analogs are distributed not only to targeted tumor tissues but also into normal tissues after systemic injection. For successful cancer-specific drug delivery to achieve tumor-specific labeling with azide groups by using metabolic glycoengineering and click chemistry (Figure 1.8) [19,31].

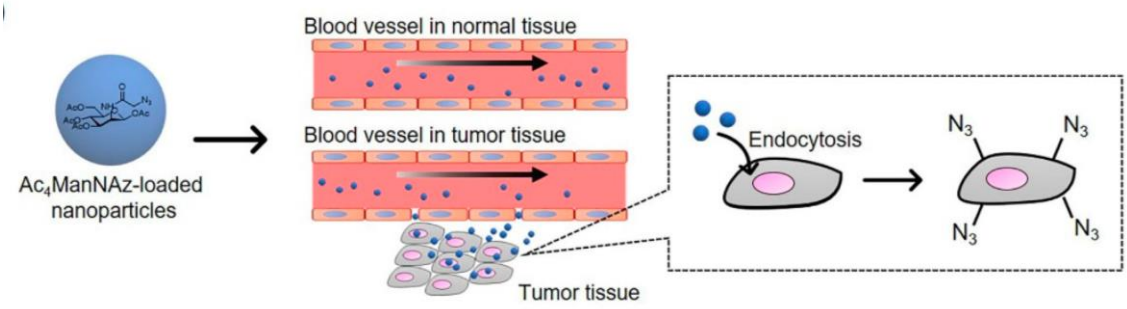

Figure 1.8 Ac_4ManNAz-loaded nanoparticles specifically accumulate in tumor tissue through the EPR effect and are taken up by tumor cells. Azide group presents on the surface of tumor cells [19].

Lee et al. synthesized Ac_4ManNAz-loaded CNPs to improve Ac_4ManNAz accumulation in tumor tissues. The azide groups were directly introduced into tumor tissues by intravenous injecting Ac_4ManNAz-loaded NPs into tumor-bearing mice. Most of nanoparticles, including Ac_4ManNAz-loaded CNPs, are easily accumulate in tumor tissues due to the EPR effect. This study showed that the intravenous injection of Ac_4ManNAz-CNPs effectively and specifically generated azide groups on the surface of tumor tissues [19,32].

Xie et al. also demonstrated that azide sugar-loaded folate-modified liposomes loaded with azide sugar were useful for labeling cell-surface glycans of folate receptor-overexpressing cancer cells with azide groups. Overexpression of folate receptors in various cancer cells are widely used in cancer therapy as target molecules for drug delivery. In this study, the folate modified-liposomes loaded with azide sugar were effectively taken up by folate receptor-overexpressing HeLa cells via endocytosis,

and could deliver sufficient amounts of azide sugars into the cytosol to introduce azide groups onto the surface of HeLa cells [19,33].

Tumor-Targeting Delivery by Click Chemistry for Cancer Therapy

To carry out cancer-targeting therapy safely and efficiently, cancer-targeting strategies using click chemistry chemical-drug conjugates and bioorthogonal chemical receptors to carry out cancer-targeting therapy safely and efficiently. Wang et al. has developed a tumor-targeting strategy for improving drugs accumulation in tumors by using metabolic glycoengineering and DBCO-drug conjugate (Figure 1.9). First, they synthesized the DBCO-valine-cysteine-doxorubicin conjugate (DBCO-VC-Dox), which was degraded by a cancer-overexpressing cathepsin B protease followed by the release of Dox. DCL-AAMwas intravenously injected into tumor-bearing mice for the generation of azide groups on the surface of tumor tissue. Then, DBCO-VC-Dox was intravenously injected into DCL-AAMor PBS-treated mice. The amount of DBCO-VC-Dox in the DCL-AAM-treated group was increased compared to the PBS group in the tumor tissue, while there was a negligible difference in terms of DBCO-VC-Dox accumulation were observed in the normal tissue. Moreover, the combination of DCL-AAM and DBCO-VC-Dox significantly suppressed tumor growth in mice. This study showed that specific-tumor labeling with azide groups enhanced drug accumulation in targeted tumors and the therapeutic effect of anti-cancer agents via the SPAAC reaction [19,34].

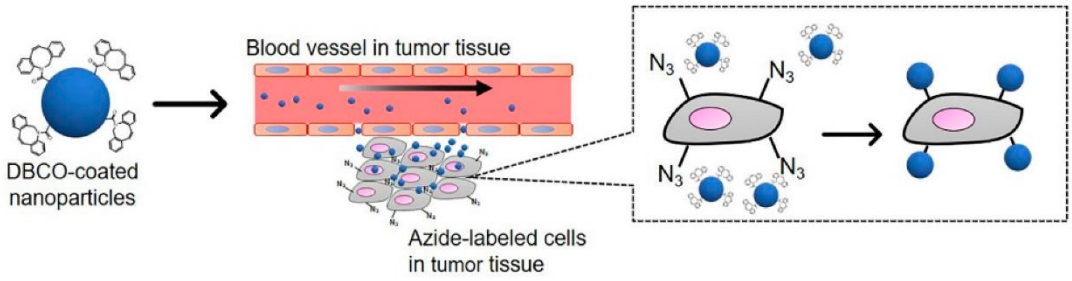

Figure 1.9 DBCO-coated nanoparticles accumulate in tumor tissue and is conjugated with azide group in tumor cells via SPAAC reaction [19].

Layek et al. demonstrated that the MSCs-based targeting strategy improved the tumor targeting efficacy of drug-loaded nanoparticles. Mesenchymal stem cells (MSCs) treated with Ac_4ManNAz to label azide groups without affecting the migration or viability of MSCs. Then, the glycoengineered MSCs were intraperitoneally injected into metastatic ovarian tumor-bearing mice, followed by the

intraperitoneal injection of paclitaxel-loaded DBCO-modified poly (lactide-co-glycolide) (PLGA) nanoparticles (DBCO-NPs). The administration of azide-labeled MSCs along with DBCO-NPs showed significant inhibition of tumor growth and improved the overall survival of mice. These studies have provided that a two-step drug delivery strategy based on generating bioorthogonal chemical receptors and the SPAAC reaction could be useful as a cancer-targeting therapy [19,35].

1.2 Vascular Endothelial Growth Factor

The vascular endothelial growth factor (VEGF) also known as vascular permeability factor (VPF), is a specific type of protein and their receptors (VEGFRs) play important roles in both vasculogenesis, the development of the embryonic vasculature from early differentiating endothelial cells, while angiogenesis, the process of forming new blood vessels from pre-existing vasculature, and lymphangiogenesis, the process of forming new lymph vessels [36]. The platelet derived growth factor (PDGF) proteins and their receptors (PDGFRs) are involved in regulation of cell proliferation, survival and migration of several cell types. Dysfunction of the endothelial cell regulatory system is a key feature of cancer and various diseases associated with abnormal vasculogenesis, angiogenesis and lymphangiogenesis [37].

Angiogenesis is essential for embryonic development, normal tissue growth, repair, and regeneration, the female reproductive cycle, the establishment and maintenance of pregnancy, and the repair of wounds and fractures. In addition to angiogenesis which takes place in the healthy individual, angiogenic are involved in a number of pathological processes, such as tumor growth and metastasis, and other conditions in which blood vessel proliferation, especially of the microvascular system, is increased, such as age-related macular degeneration, rheumatoid arthritis, diabetic retinopathy. Inhibition of angiogenesis is useful in preventing or slowing progression of these pathological processes [37].

Although therapies directed to blockade of VEGF/PDGF signaling through their receptors have shown promise for inhibition of angiogenesis and tumor growth, there remains a need for development of new VEGF inhibitors or improved compounds and therapies for the treatment of cancers and ophthalmic diseases [36].

1.2.1 VEGFA and VEGF receptors

Vascular endothelial growth factor/vascular permeability factor (VEGF/VPF) is a major regulator of tumor-associated angiogenesis and promotes tumor growth, invasion and metastasis [38].

The VEGF gene family plays an integral role in angiogenesis, vasculogenesis, and lymphangiogenesis. VEGF, also known as VEGF-A, is the prototype member of a family of proteins that consists of six different glycoproteins: VEGF-B, VEGF-C, VEGF-D, VEGFE (a virally encoded protein), placental growth factor (PlGF), and the snake venom VEGF-F [39]. These proteins, which are structurally related to the platelet-derived growth factor (PDGF) family of proteins, have a range of tissue distributions and functions. They are secreted to form homodimers, which interact with a family of three receptor tyrosine kinases: VEGFR1, VEGFR2, and VEGFR3 and two non-enzymatic receptors (neuropilin-1 and -2) [40,41].

1.2.2 VEGF Isoforms

VEGF (vascular endothelial growth factor)-A is the most prominent member of the PDGF (platelet-derived growth factor)/VEGF family of secreted dimeric growth factors, controlling blood vessel growth in both physiological and pathological angiogenesis [42,43]. VEGF-A was first identified as a vascular permeability–inducing factor secreted by tumor cells, and thus referred to as vascular permeability factor (VPF) [42,44]. VEGF-A, exists as a homodimeric glycoprotein consisted of two identical 23 kDa subunits [45]. The human VEGF-A gene is organized in eight exons, separated by seven introns and is localized in chromosome 6p21.3 [44]. Alternative exon splicing of the human *VEGF-A* gene results in the generation of four different isoforms, having 121, 165, 189, and 206 amino acids, respectively, after signal sequence cleavage (VEGF121, VEGF165, VEGF189, VEGF206) (Figure 1.10) [46–48].

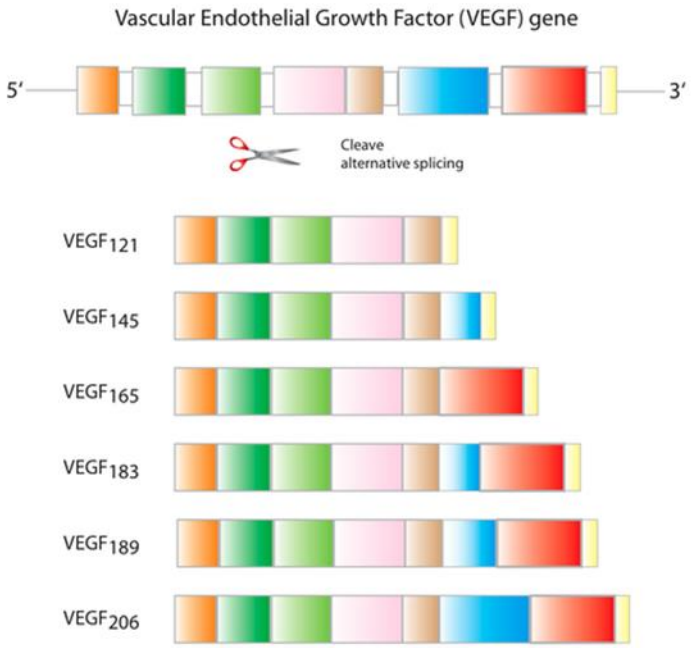

Figure 1.10 Alternative splicing of the mRNA for VEGF-A.

All VEGF isoforms share the same N-terminal amino acid sequence, which contains the binding sites for VEGFR-1 and VEGFR-2, but they may or may not contain sequences encoded by exons 6 and 7 in the C-terminus. This C-terminal region encodes two heparin-binding domains (HBDs), each of which confers the ability to bind heparan sulfate (HS) and Heparan sulfate proteoglycans (HSPGs) on cell surfaces and basement membranes, thus determining the localization of the VEGF-A isoforms in the extracellular space. The heparin-binding domains help VEGF-A to anchor to the extracellular matrix (ECM) and are involved in binding to heparin sulfate and presentation to VEGF receptors (VEGFR). VEGF isoforms with higher heparin affinity are rapidly sequestrated by the heparan sulfate proteoglycans located at the endothelial cell surface and in the ECM. In addition, these proteoglycans are an extracellular storage of VEGF isoforms and enhance the interactions with their own receptors [38,43,49].

The longer splice form VEGF189 and VEGF206 bind avidly to heparin and heparin-like moieties encoded by exon 6 and exon 7 in the extracellular matrix and on the cell surface, while VEGF121, the shortest isoform, lacks basic residues corresponding to exon 6 and 7, leading to loss of extracellular matrix sequestration. The predominant isoform VEGF165, lacking exon 6, exists as both cell-bound factor and freely diffusible protein with the bound fraction undergoing proteolysis by

plasmin and matrix metalloproteinases (MMPs). Beside differences in bioavailability and bioactivity, these isoforms also have different receptor specificities. VEGF165, through exon 7-encoded domains, binds to the tyrosine kinase receptors VEGFR1 and VEGFR2, as well as neuropilin (NRP)-1 and NRP-2, while $VEGF_{145}$ binds to NRP-2 [41,45,50]. VEGFA165 is the most common expressed isoform in normal tissues and in tumors, although less common isoforms, such as VEGFA145 and VEGFA183, have also been identified. VEGFA165 has an intermediary behavior between the highly diffusible VEGFA121 and the extracellular matrix (ECM) bound VEGFA189, and is considered to be the most physiologically relevant VEGFA isoform [51].

Other members of the VEGF gene family also undergo alternative splicing with the exception of VEGF-C. Likewise, VEGF-B, whose biological functions are not entirely clear, and VEGF-D, which is involved in lymphangiogenesis, both have multiple alternatively spliced isoforms [45].

1.2.3 Regulation of VEGFA gene expression

The expression and activity of VEGFA are modulated by several mechanisms including hypoxia, oncogene and tumor suppressor dysregulation, inflammatory mediators, transcription factors, and mechanical forces of shear stress and cell stretch [45].

The VEGF-A gene is one of numerous genes regulated by hypoxia-inducible factor (HIF)-1α. The VEGF-A is primarily stimulated under hypoxic conditions, such as within large solid tumors, mediated by the hypoxia-inducible factor (HIF), which also triggers the expression of other hypoxia-regulated genes. HIF-1α dimerizes with the constitutively expressed HIF-1β to form a transcription factor that binds to hypoxic response elements (HRE) in the promoter region of the VEGF gene. Further interaction with transcriptional co-activators such as p300 and CBP induces the transcription of HIF target genes including VEGF, VEGFR1, and many other genes regulating angiogenesis, cell survival cell proliferation, apoptosis, and motility [45,52]. In contrast, under normoxic conditions, HIF is hydroxylated by a class of oxygen- and iron-dependent enzymes known as HIF prolyl hydroxylases, leading to HIF-1α interaction with the von-Hippel Lindau (VHL) tumor suppressor protein. As a result, HIF becomes a target for proteosomal degradation and polyubiquitylation. Inactivating mutations in VHL, such as those occurring in the VHL hereditary cancer syndrome or in

renal cell carcinomas, result in inefficient degradation of HIF-1α and in VEGF-A upregulation in normoxic conditions [51,53].

VEGFA expression is also regulated by other factors, such as Inflammatory cytokines, including interleukin IL-1α, IL-1β, IL-6, tumor necrosis factor (TNFα), and growth factors such as transforming growth factor (TGF)α, TGFβ, epidermal growth factor (EGF), platelet-derived growth factor (PDGF), hypoxia, nitric oxide and by oncogenic mutations. The latter include VHL mutations, as well as mutations affecting the RAS pathway and the WNT–KRAS signaling pathway [51,54,55].

1.2.4 VEGF Signaling Pathway

VEGF ligands mediate their angiogenic effects via several different receptors [48]. There are three receptor protein-tyrosine kinases for the VEGF family of ligands (VEGFR1, VEGFR2, and VEGFR3) and two non-enzymatic receptors (Neuropilin (NRP)-1 and NRP-2) [37]. Moreover, Binding sites for VEGFA on endothelial cells, several of the VEGF family ligands bind to heparan sulfate proteoglycans that are found on the plasma membrane and in the extracellular matrix [39,56].

VEGFRs are typical tyrosine kinase receptors (TKRs) carrying an extracellular component containing seven immunoglobulin (Ig)–like domains, a single transmembrane segment, a juxtamembrane segment, an intracellular protein-tyrosine kinase domain that contains a kinase insert of 70–100 amino acid residues, and a carboxyterminal tail in the cytoplasmic domain [39,57].

Two VEGF receptors belonging to the tyrosine-kinase receptor family: the VEGFR-1 (also known as fms-like tyrosine kinase 1 [Flt-1]) is expressed in trophoblast cells, monocytes, and renal mesangial cells, and the VEGFR-2 (also known as KDR and FLK1) is also expressed in hematopoietic stem cells, megakaryocytes, and retinal progenitor cells. while A highly homologous RTK, VEGFR-3 (also known as FLT4), which is expressed on the surface of lymphatic endothelial cells and binds VEGF-C and VEGF-D (which promote both angiogenesis and the development of lymphatic vessels) [40,58].

A nonkinase receptors, (neuropilin-1 and -2), initially shown to mediate guidance of neurite growth, acts as a high-affinity co-receptor and enhances the binding affinity of VEGF-A to VEGFR-2 and is expressed on the surface of endothelial and tumor cells [38].

All members of the VEGF family stimulate cellular responses by binding to tyrosine kinase receptors (VEGFRs) on the cell surface .Of the two Receptor tyrosine kinases (RTKs), VEGFR2 is the main mediator of the roles of VEGF-A in cell proliferation, angiogenesis and vessel permeabilization. Upon VEGF-A binding to VEGFR2 on endothelial cells leads to dimerization of receptor and tyrosine kinase autophosphorylation [59,60]. On ligand binding, VEGFRs transduce intracellular signals through a range of mediators. Proliferation of cell and replication of the DNA are mediated by both the MAPK and Ras-Raf-MEK-ERK pathways; the migration of cell, either via FAK and Paxillin, PI3Kinase/Akt, or MAPK activation; and cell survival, via PI3-Kinase and Akt/PKB activation. In the case of VEGFR2, which is the most characterized, these include phosphotidylinositol-3 kinase (PI3K)/Akt, mitogen-activated kinases, the nonreceptor tyrosine kinase Src, as well as PLCγ (phospholipase C gamma)/PKC (protein kinase C), which promote lymphangiogenesis, angiogenesis, vascular permeability, and vascular homeostasis (Figure 1.10) [40].

The various members of the VEGF family have differing binding specificities for VEGFRs, which have helped in elucidating their function (Figure 1.11) [48]. All the VEGF isoforms share common tyrosine kinase receptors (VEGFR-1 or Flt-1, VEGFR-2 or KDR/Flk-1, VEGFR-3 or Flt-4), which are primarily expressed by endothelial cells. Placenta growth factor (PlGF) and VEGFB bind selectively to VEGF receptor 1 (VEGFR1), whereas All of the VEGF-A isoforms bind to both VEGFR1 and VEGFR2 with high affinity and plays an essential role in vasculogenesis and angiogenesis, although VEGFR2 is the major signalling receptor for VEGF-A. It has also been shown to induce lymphangiogenesis through VEGFR2. VEGF-E specifically interacts with VEGFR2, whereas VEGF-C and VEGF-D bind to VEGFR3, a key regulator of lymphangiogenesis; however, following proteolytic processing they can also bind to and activate VEGFR2. Heparin-binding VEGF-A isoforms and PlGF also bind the co-receptor neuropilin (NRP)-1. This interaction between VEGF-A and NRP1 increases the binding affinity of VEGF-A for VEGFR2. VEGF-A or PlGF may directly act on NRP1, independently of VEGF receptor activation. NRP2 regulates lymphangiogenesis, primarily through its interaction with VEGFR3 [42,61,62].

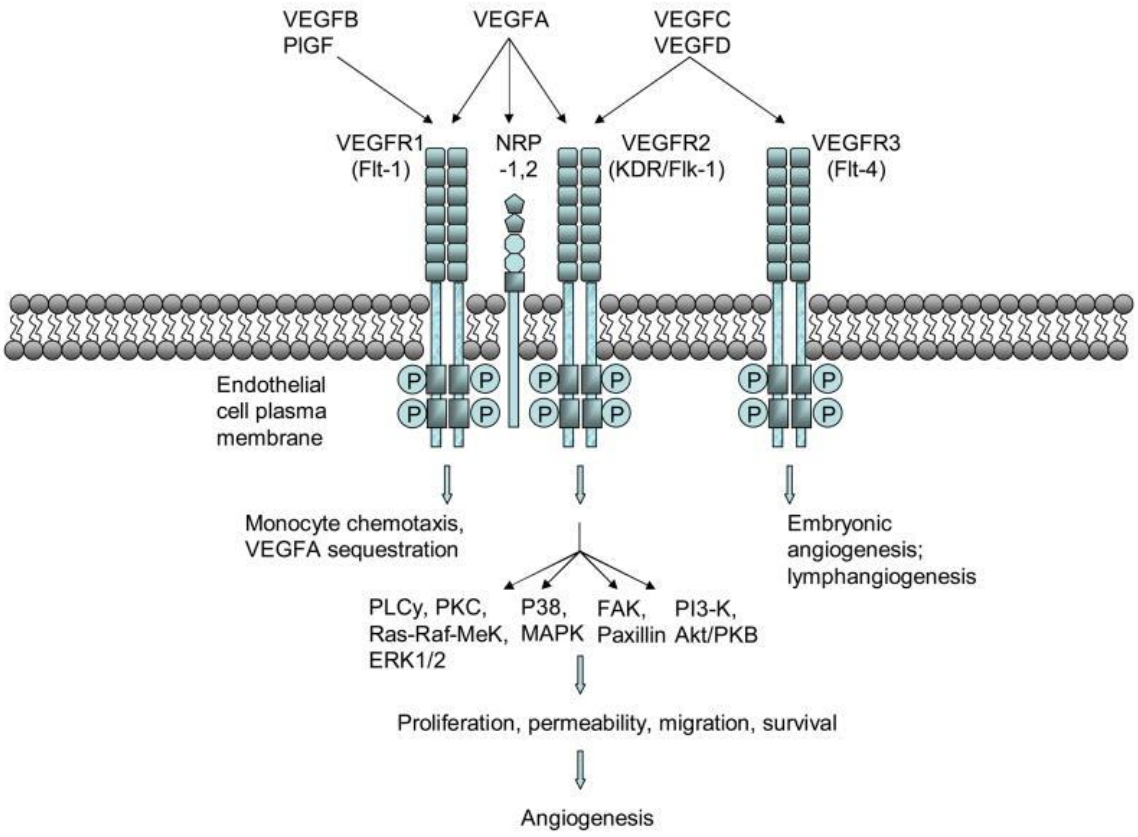

Figure 1.11 VEGF Signalling Pathway [45].

VEGFR1 may function as a decoy receptor, sequestering VEGF-A and preventing it from binding to VEGFR2. It can, however, regulate the expression of a variety of genes in the endothelium, including matrix metalloproteinase 9 (MMP9) and certain growth factors such as hepatocyte growth factor and connective tissue growth factor, which play an important part in tissue homeostasis and regeneration. VEGFR1 is also expressed by monocytes and macrophages and, in some cases, also by tumor cells, in which it can mediate tumor cell proliferation in response to VEGF-A or PlGF. VEGFR2 mediates endothelial cell mitogenesis and vascular permeability (Figure 1.12) [51,63].

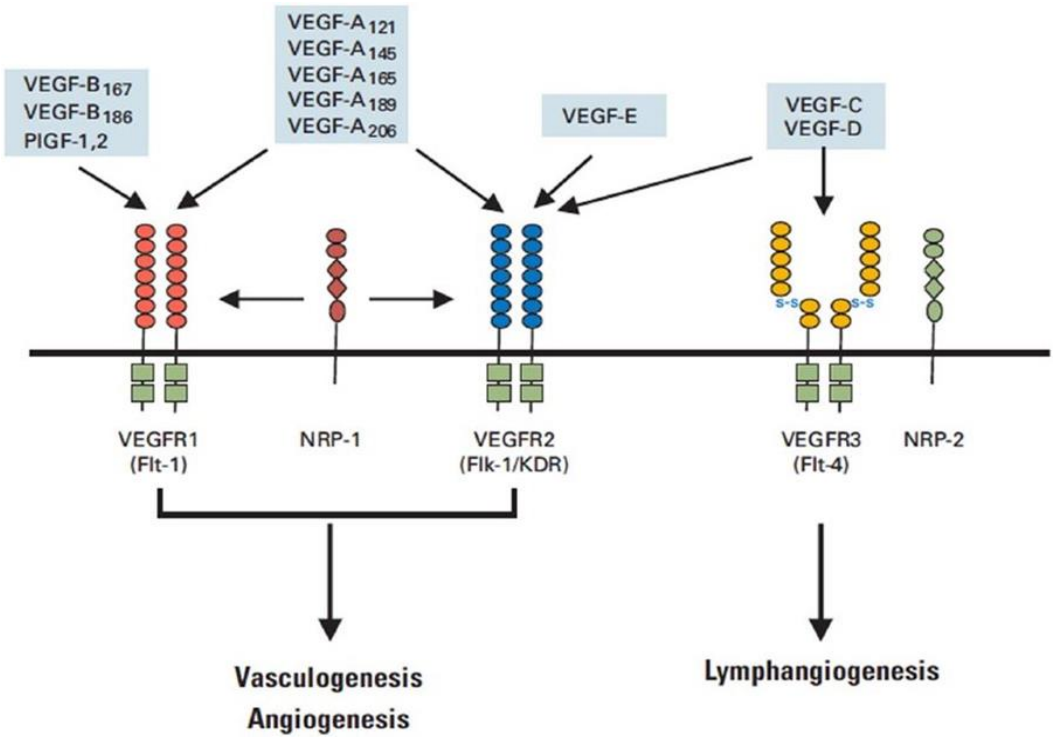

Figure 1.12 Binding specificity of various vascular endothelial growth factor (VEGF) family members and their receptors [48].

1.2.5 Inhibition of VEGF family signaling

Angiogenesis has a key role in maintaining the continued growth of tumors. VEGFA secreted by tumor cells and surrounding stroma stimulates the endothelial cells proliferation and survival, leading to the formation of new blood vessels, which may be structurally abnormal and leaky. VEGFA mRNA is overexpressed in most human tumors, where its expression correlates with invasiveness, metastasis, increased vascular density, tumor recurrence and poor prognosis. Accordingly, several strategies to inhibit the VEGFA–VEGFR signaling pathway for the treatment of cancer have been explored [51,64].

Preventing angiogenesis is hypothesized to arrest tumor growth through several mechanisms. The initial hypothesis was that antiangiogenic agents prevent the formation of new blood vessel and prune the existing tumor vessels, leading to tumor deprivation of oxygen and nutrients. The second potential mechanism is Vascular normalization by which antiangiogenic agents may achieve an antitumor effect when combined with cytotoxic therapies [65].

Diseases that are candidates for therapeutic inhibition of VEGF signaling include neovascular age-related macular degeneration (AMD) of the eye, diabetic retinopathy (DR), endometriosis, psoriasis, rheumatoid arthritis (RA), and tumor growth and spread. Various strategies for restraining tumor growth and progression include inhibiting VEGF signaling pathway by blocking the activity of VEGF by using antibodies directed against VEGF or VEGFR2 or by using small molecule inhibitors directed against VEGF receptor kinases (Table 1.3) [39]. Many drugs that block the VEGF pathway are in clinical development. They differ primarily in their route of administration, specificity and potency of VEGF blockade, and additional targets blocked [65].

1.2.5.1 Antibodies to VEGF

The advantage of antibodies is highly specific for VEGF, with limited cross-reactivity and fewer side effects. The half-life of the antibodies is generally long, which allows less frequent dosing. Conversely, antibodies are costly to produce and must be administered by intravenous infusion. They are high molecular weight protein molecules with limited penetration of the normal blood brain barrier (BBB). However, this may be less of an impediment when targeting endothelial cells that line tumor blood vessels or in the setting of a disrupted BBB [65].

Bevacizumab

Bevacizumab (Avastin) is a humanized anti-VEGFA monoclonal antibody that was the first antiangiogenic drug approved by the U.S. Food and Drug Administration in 2004. Bevacizumab specifically binds to the VEGFA protein, thereby inhibiting the process of angiogenesis. Maintaining the VEGF ligand inhibition may prevent tumor growth and may result in tumor shrinkage with time (Figure 1.13) [66,67].

Currently, bevacizumab is approved for first and second-line treatment of metastatic colorectal cancer (mCRC) in conjunction with 5-fluorouracil-irinotecan or 5-fluorouracil-oxaliplatin-based chemotherapy [68]. It is also approved to use in combination with chemotherapy for the treatment of advanced colorectal cancer (CRC), metastatic breast cancer (MBC), advanced non-small cell lung cancer (NSCLC), and advanced renal cell cancer. More recently, it has been approved by FDA as a single agent for second-line treatment in adult patients with recurrent glioblastoma multiforme who had tumor progression after initial treatment, and in conjunction with interferon α to treat metastatic renal cell carcinoma (RCC) [69–71].

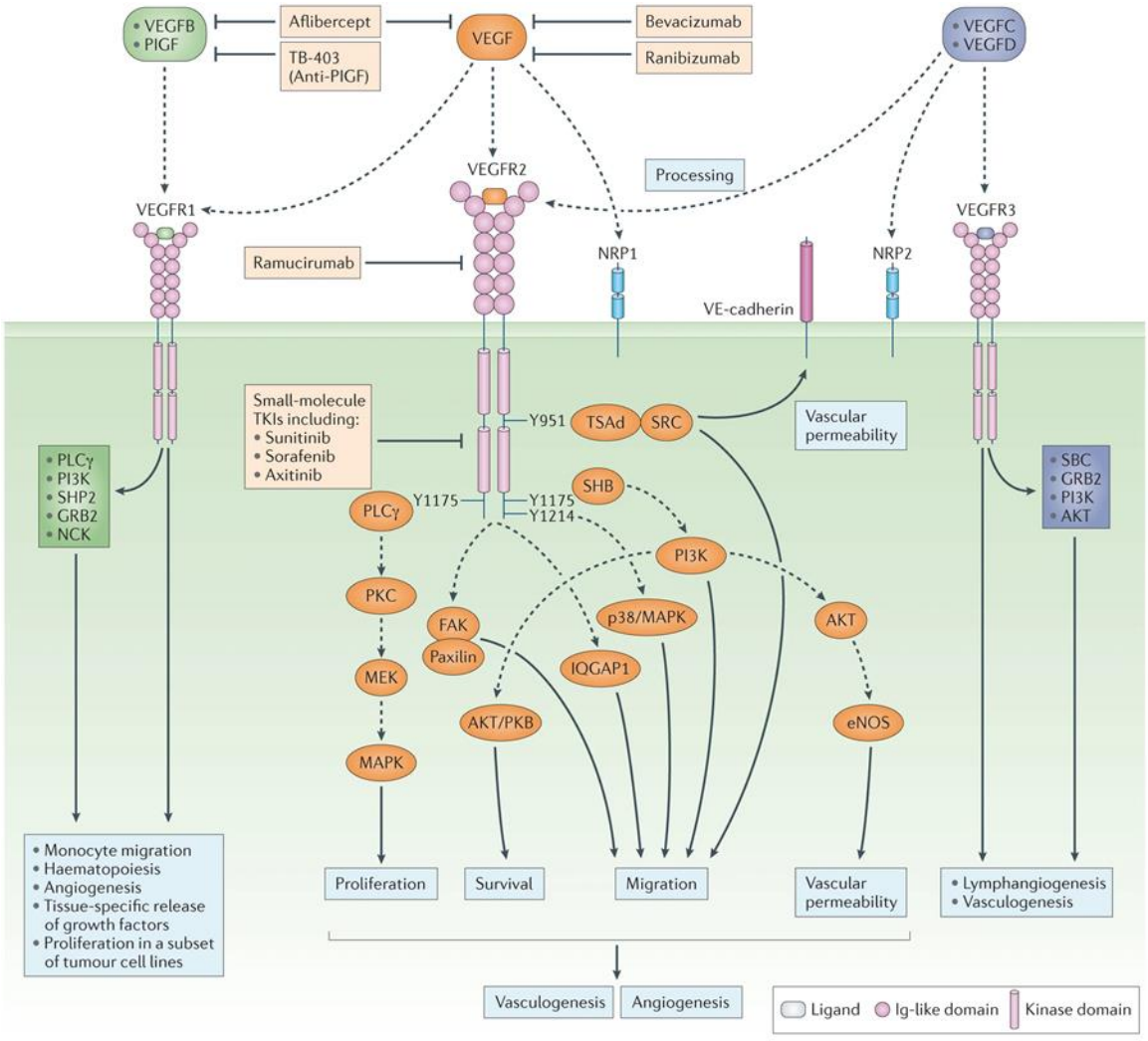

Figure 1.13 VEGF signalling pathways and inhibitors.

Aflibercept and Ramucirumab

Aflibercept (Eylea), a recombinant VEGFR chimeric fusion protein that consists of VEGF-binding portions from the extracellular domains of human VEGFR 1 and 2 fused to the Fc portion of human immunoglobulin G1. It functions as a decoy receptor for proangiogenic members of the VEGF family: VEGFA, VEGFB and PIGF. Aflibercept is approved for use in metastatic colorectal cancer as well as Neovascular (Wet) Age-Related Macular Degeneration (AMD), Macular Edema Following Retinal Vein Occlusion (RVO), Diabetic Retinopathy (DR), and Diabetic Macular Edema (DME), while ramucirumab (Cyramza), an anti-VEGFR2 monoclonal antibody, is approved for use in various solid tumors (Figure 1.13) [72–74].

Ranibizumab and Pegaptanib

Ranibizumab (Lucenis), a recombinant humanized anti-VEGF Fab fragment, and pegaptanib (Macugen), a pegylated oligonucleotide aptamer selectively targeting VEGF165, have both received FDA approval for treatment of neovascular age-related macular degeneration (AMD) in 2004 and 2006, respectively [75,76]. Notably, ranibizumab both retarded vision loss and improved vision in a signification fraction of patients and was superior to photodynamic therapy. Ranibizumab has been also approved for the treatment of macular edema following central retinal vein occlusion (CRVO) [45].

1.2.5.2 Tyrosine Kinase Inhibitors

Small molecule tyrosine Kinase Inhibitors **(**TKIs) interfere with tyrosine or serine/threonine kinase growth factor receptor signaling by attaching to the intracellular adenosine triphosphate–binding pocket of the receptor. The advantage of these agents is orally active. Most of the agents in this class lack specificity for one tyrosine kinase receptor, thus allowing broad inhibition of a variety of growth factor pathways, albeit at the risk of increasing potential side effects. Many of TKIs are in the clinical development. The primary factors that distinguish these drugs are their potency and selectivity at different receptors [65].

Sunitinib and Sorafenib

Sunitinib, a broad-spectrum multi-targeted oral RTKI, received initial FDA approval in January 2006 for imatinib-resistant gastrointestinal stromal tumors (GIST) and in February 2007 for the treatment of advanced renal cell carcinoma (RCC) [77]. Similarly, Sorafenib is orally bioavailable and exhibit broad-spectrum activity against numerous kinases including VEGF receptors, It was approved for first-line treatment of metastatic RCC in 2005 and for the treatment of unresectable hepatocellular carcinoma in 2007 (Figure 1.13) [78].

Table 1.3 Angiogenesis inhibitors approved by FDA [71].

Drug/ Company	Type of inhibitor	Targets	Indication
Bevacizumab (Avastin; Genentech/Roche)	Humanized Monoclonal antibody	Human VEGF-A	Metastatic colorectal cancer, NSCLC, Recurrent glioblastoma, and Metastatic renal cell carcinoma
Aflibercept (Eylea; Regeneron Pharmaceuticals)	Chimeric soluble receptor	VEGF-A, VEGF-B, and PIGF	Wet macular degeneration and metastatic colorectal cancer
Ranibizumab (Lucentis; Genentech/Novartis)	Fab fragment of antibody	VEGF-A	Neovascular age-related macular degeneration (AMD), Macular Edema Following (RVO), and Diabetic Macular Edema (DME)
Pegaptanib (Macugen; Pfizer/Valeant)	Pegylated polynucleotide aptamer	VEGF-A165	Wet age-related macular degeneration
Sorafenib (Nexavar; Bayer and Onyx Pharmaceuticals)	Tyrosine Kinase Inhibitors	VEGFR, PDGFRs, KIT, Raf kinase	Metastatic renal cell carcinoma, hepatocellular carcinoma, and thyroid cancer
Sunitinib (Sutent; Pfizer)	Tyrosine Kinase Inhibitors	VEGFRs, PDGFRs, KIT, FLT-3	Metastatic renal cell carcinoma, gastrointestinal stromal tumor, unresectable pancreatic, and neuroendocrine tumors
Axitinib (Inlyta; Pfizer)	Tyrosine Kinase Inhibitors	VEGFRs, PDGFRs, KIT	Metastatic renal cell carcinoma
Pazopanib (Votrient; GlaxoSmithKline)	Tyrosine Kinase Inhibitors	VEGFRs, PDGFRs, KIT	Metastatic renal cell carcinoma, and soft tissue sarcoma
Vandetanib (Caprelsa; AstraZeneca)	Tyrosine Kinase Inhibitors	VEGFRs, EGFR, RET	Metastatic medullary thyroid cancer
Cabozantinib (Cabometyx; Exelixis)	Tyrosine Kinase Inhibitors	VEGFR2, MET, RET	Metastatic renal cell carcinoma (RCC), and metastatic medullary thyroid cancer
Regorafenib (Stivarga; Bayer and Onyx Pharmaceuticals	Tyrosine Kinase Inhibitors	VEGFRs, TIE2, PDGFRs, KIT, FGFRS	Metastatic colorectal cancer (CRC), and metastatic gastrointestinal stromal tumors (GIST)

VEGF-A, vascular endothelial growth factor A; VEGF-B, vascular endothelial growth factor B; PlGF, placental growth factor; VEGFR, vascular endothelial growth factor receptor; PDGFR, platelet derived growth factor receptor; FGFR, fibroblast growth factor receptor; KIT, v-kit feline sarcoma viral oncogene homolog; RAF, v-raf-1 murine leukemia viral oncogene homolog 1; FLT-3, fms-related tyrosine kinase 3; EGFR, epidermal growth factor receptor; RET, ret proto-oncogene; MET, met proto-oncogene; TIE, TEK tyrosine kinase endothelial.

1.3 Folic Acid

Folic acid is water soluble vitamin B9, composed of a pterin ring connected to p-aminobenzoic acid (PABA) and conjugated with one or more glutamate residues (Figure 1.14). Humans do not generate folate endogenously because they cannot synthesize PABA, nor can they conjugate the first glutamate. It is present in most vegetables and animal products [79].

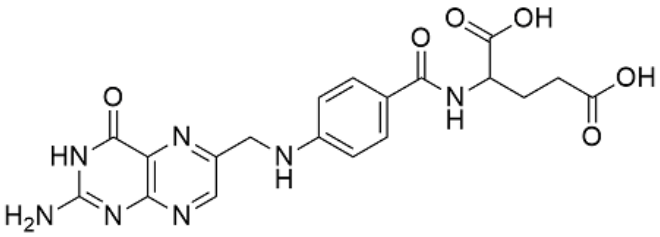

Figure 1.14 The Chemical Structure of Folic Acid.

Folate is essential for normal functioning of cells, as it is involved in mediating the transfer of one-carbon donors for the biosynthesis of purines and pyrimidines that are important in RNA and DNA synthesis and replication, cell division, and growth and survival, particularly for rapidly dividing cells [80,81]. Furthermore, folate provides methyl groups for de novo deoxynucleotide synthesis and for intracellular methylation reactions. Methylene tetrahydrofolate reductase (MTHFR) plays a central role in folate metabolism by catalyzing the conversion of 5,10-methylenetetrahydrofolate (5,10-methylene THF) to 5-methyltetrahydrofolate (5-methyl THF), which is the main circulating form of folate in the blood and a cosubstrate for the conversion of homocysteine to methionine (Figure 1.15), which is important for the biosynthesis of S-adenosyl methionine, an essential supplier of methyl groups for the methylation of many compounds including DNA, RNA, proteins, and phospholipids. Low levels of 5,10-methylene THF can cause an increased dUMP/dTMP ratio, which could result in the incorporation of uracil into DNA in place of thymine, leading to an increased risk for DNA mutations, DNA strand breakage and abnormal methylation reactions. In addition, low levels of 5-methyl THF can lead to decreased s-adenosylmethionine (SAM) levels, which could result in DNA hypomethylation leading to activation of cellular oncogenes, genomic instability, and DNA damage. Folate deficiency is associated with many diseases, including fetal neural tube defects, cardiovascular disease and cancers [82,83].

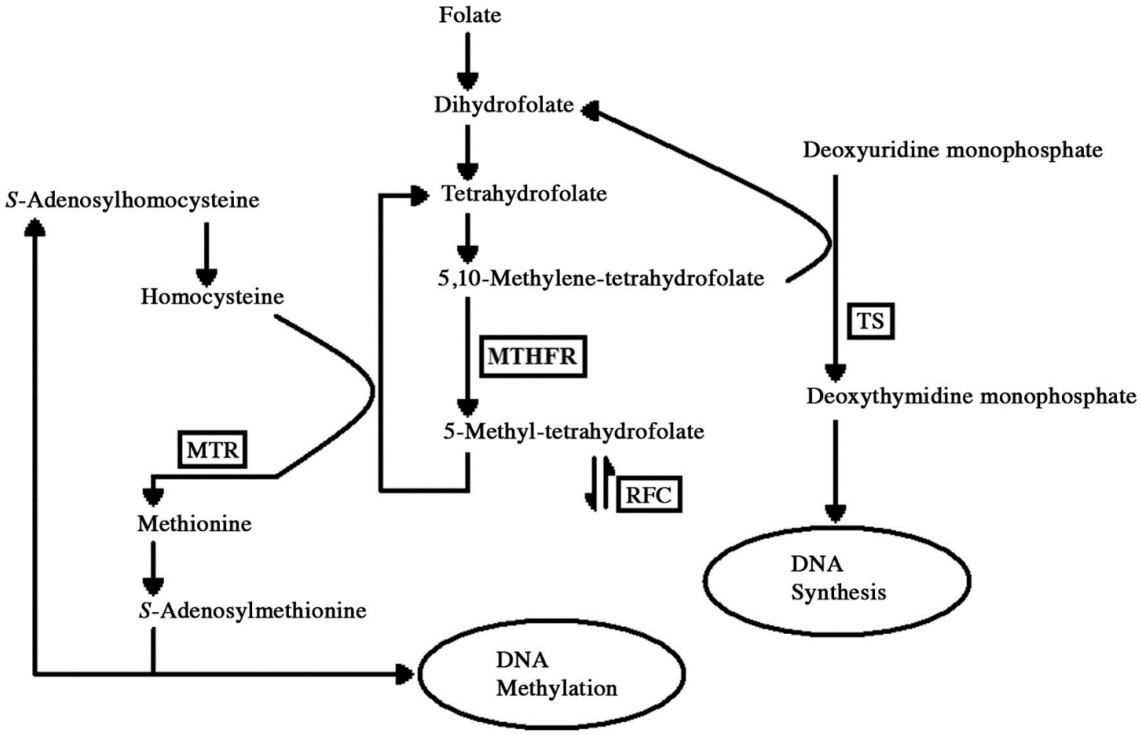

Figure 1.15 Folate metabolic pathway [84].

Because folate is lipophilic, it needs to be actively transported into the cell via the low-affinity, high-capacity, ubiquitously expressed reduced folate carrier (RFC; bidirectional anion-exchange mechanism). The 12-transmembrane-domains RFC protein is expressed in normal cell and is the predominant folate transporter. It preferentially binds to reduced forms of folate and subsequently carries them into the cytoplasm via a bidirectional anion-exchange mechanism. Folates are also transported by high-affinity folate receptor (FRs) (Figure 1.16) [80,85]. In humans, there are multiple isoforms of the FR (FRα, FRβ, FRγ, and FRδ), which are cysteine-rich glycoproteins that mediate folate uptake through endocytosis. FRα, FRβ, and FRδ are attached to the cell surface by a glycosylphosphatidylinositol anchor, while FRγ is a soluble protein secreted by lymphoid cells. When folic acid or reduced folate binds to the FR, the cell-surface receptor–ligand complex is transported into the cell via receptor-mediated endocytosis for ligand release. Table 1.4 shows the distribution of FR isoforms in normal and tumor tissue [85,86]. All of these FR isoforms have their own tissue-specific distribution and folate binding potential. FRα, the most widely studied FR isoform, has restricted expression in normal cells but high expression levels in the majority of tumors of epithelial origin. The FRβ has been shown to be expressed mainly by the placenta and hematopoietic cells, such

as activated macrophages. The FRδ is expressed on regulatory T cells, and dietary folic acid has been shown to promote survival of these cells. FRγ is a secreted protein expressed in hematopoietic cells [80].

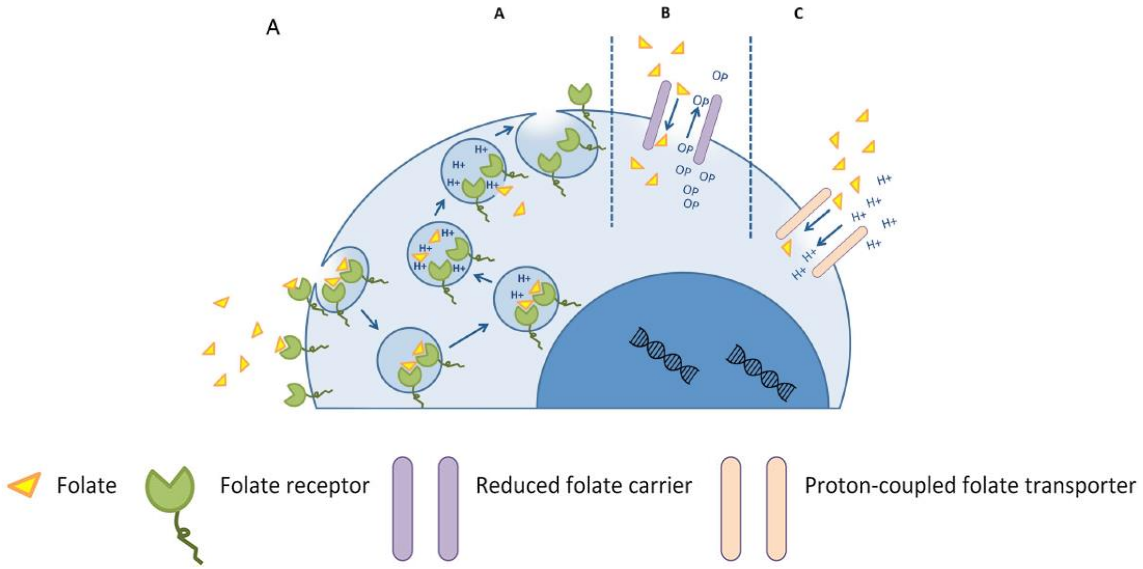

Figure 1.16 a Folate can be transported into the cell by three different proteins: the folate receptor (FR) (panel A), the reduced folate carrier (RFC) (panel B), and the proton-coupled folate transporter (PCFT) (panel C). After folate binds the FR, the cell membrane invaginates and forms a vesicle. Subsequently, the vesicle acidifies, leading to the dissociation of folate fromthe FR. Folate is then released from the intact vesicle by an unknown process that is optimal at low pH. Folate can also be transported by the organic anion antiporter RFC, which functions optimally at pH=7.4. The high transmembrane organic phosphate (OP) gradient mediates the uphill folate transport. Finally, the proton symporter PCFT uses the transmembrane proton (H+) gradient to mediate uphill folate transport. The PCFT functions optimally in low-pH conditions [80].

Because FRα is expressed on the cell surface in a tumor-specific manner, it provides the potential to allow not only tumor localization, but also selected delivery of therapeutic agents to the malignant tissue and minimizing collateral toxic side-effects. There are a number of unique advantages to utilizing FR as a diagnostic and therapeutic target. First, FRα is expressed on the luminal surface of epithelial cells in most proliferating normal tissues and is inaccessible to circulation. In contrast, FRα is expressed all over the cell in malignant tissue and is accessible via circulation. Second, FR has the ability to bind to the small molecule of folic acid, that can rapidly penetrate solid tumors and is amenable to chemical conjugation with other molecules. Once a folate conjugate is bound to FR, it is internalized into the cell and the FRα is rapidly recycled via the FR-mediated

endocytic pathway to the cell surface, as shown in Figure 1.17 These factors all emphasize the potential role of FRα in the diagnosis and treatment of specific tumor types [85,87].

Table 1.4 Tissue distribution of FR family members [85].

Protein name (gene name)	Normal tissue distribution (cellular expression)	Tumor tissue overexpression
FRα (FOLR1)	Some polarized epithelia: • Fallopian tube (fimbriated end) • Proximal kidney tubules (apical brush border) • Type I and II pneumocytes in the lungs (apical) • Choroids plexus (apical versus the cerebrospinal fluid) • Submandibular salivary glands (luminal) • Bronchial glands (luminal) • Retinal pigment epithelial cells (basolateral) • Trophoblasts in placenta	Epithelial tumors of: • Ovary, fallopian tube, and primary peritoneum • Kidney • Lung • Ependymal brain • Uterus, breast, colon • Malignant pleural mesothelioma
FRβ (FOLR2)	Hematopoietic tissues [spleen, thymus, peripheral blood (monocytes = low levels; activated macrophages = high levels)] Placenta	Hematologic malignancies (AML, CML)
FRγ (FOLR3)	Hematopoietic tissues: spleen, bone marrow, thymus	Hematologic malignancies Epithelial tumors of ovary, endometrium, cervix
FRδ (FOLR4)	Oocytes Regulatory T cells	Unknown

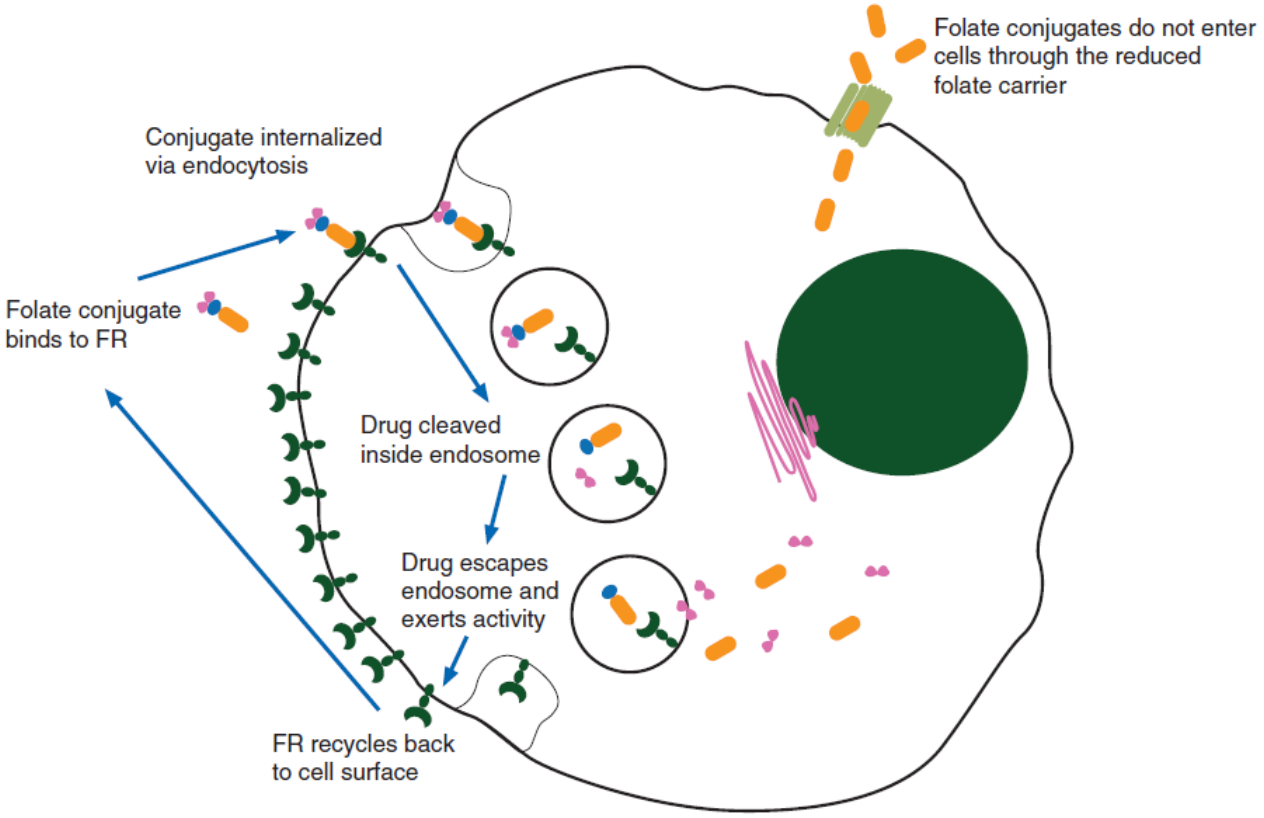

Figure 1.17 Schematic presentation of tumor-cellular uptake of folate and folate conjugate. FR, folate receptor [85].

1.3.1 Role of FR expression in personalized cancer therapy

Assessing tumor FR expression can be both a prognostic and a diagnostic tool. Various semiquantitative and quantitative methods have been used to assess FRα levels in tumor biopsy specimens or in the circulation; however, there are inherent challenges with many of these techniques, particularly in a clinical setting (Table 1.5) [85,88].

Table 1.5 Overview of the in vitro techniques for FR detection and measurement [85].

Methodology	Major characteristics	Sensitivity
Radioligand binding assay	Quantitative assay Applicable to body fluids Need for a long-half-life isotope (^{3}H) Detection of functional FR Does not discriminate between FRα and FRβ	Low (medium after microfiltration)
Sandwich assay	Quantitative assay Applicable to body fluids Need for highly selected pairs of antibodies Detection of FR-specific isoforms Does not discriminate between active and inactive molecules	Medium
IHC	Amenable to automation but quantification procedures still in progress Detection of cellular and subcellular location Applicable to archival tissues Low cost	Medium
Reverse-transcription quantitative PCR	Semiquantitative assay, amenable to automation High dynamic range but amplification needed Does not provide information about the protein expression Still not standardized for FR RNA from archival tissues	High

FR, folate receptor; IHC, immunohistochemistry; PCR, polymerase chain reaction.

An attractive option is the in vivo use of a companion imaging agent that allows the whole-body, noninvasive, real-time assessment of FRα expression, facilitating the monitoring of FR status without invasive tissue biopsies during the course of treatment. The interaction between folic acid and FRα has been identified as a useful vehicle for allowing imaging probes to be localized on FR-expressing cells. The probe is conjugated to the folic acid molecule, binds with high affinity to the FR and emits an imaging signal. Current methods for detecting probe/folic acid conjugates include fluorescence imaging, magnetic resonance imaging, ultrasound imaging, single photon emission computed tomography (SPECT), computed tomography, and positron emission tomography. A number of folate conjugates have been evaluated in the context of tumor imaging. One of particular interest is etarfolatide (EC20), an imaging agent composed of ^{99m}technetium (Tc) complexed to a short folate linked peptide (Figure 1.18) [85,89].

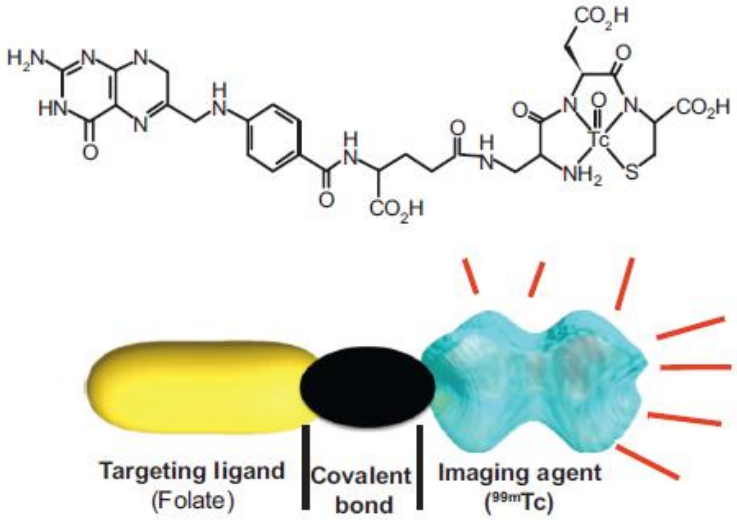

Figure 1.18 Structure of diagnostic imaging agent: ^{99m}Tc-etarfolatide. ^{99m}TcEC20 consists of two parts: an FR binding moiety (folic acid) and a chelating moiety that forms a pocket to chelate ^{99m}Tc. EC20, etarfolatide [90].

^{99m}Tc is a commonly used radiographic tracer that mainly decays by gamma emission and has a short half-life. When complexed to folic acid and injected into the circulation, it localizes to FR-expressing tissues and binds to FR with high affinity. Uptake of ^{99m}Tc-etarfolatide is high in FRα-positive tumors, with rapid accumulation in the target tissue. SPECT can then visualize Expression of FR (Figure 1.19). Importantly, excess probe conjugates are rapidly cleared via the kidneys from the blood reducing non-specific background and allowing images to be obtained quickly [85,91,92].

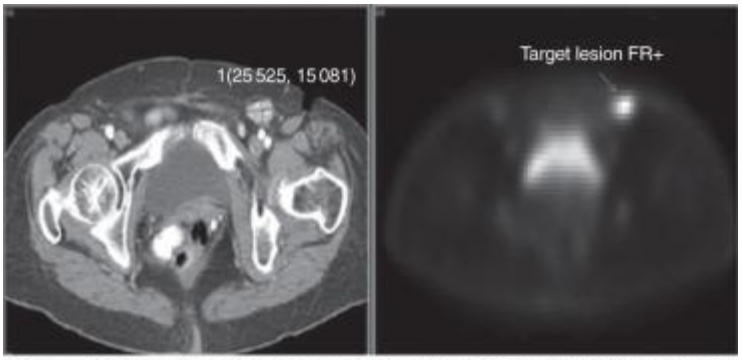

CT image (left) of pelvic ovarian mass. Corresponding EC20 SPECT images (right) showing ^{99m}TC-EC20 uptake in target lesion

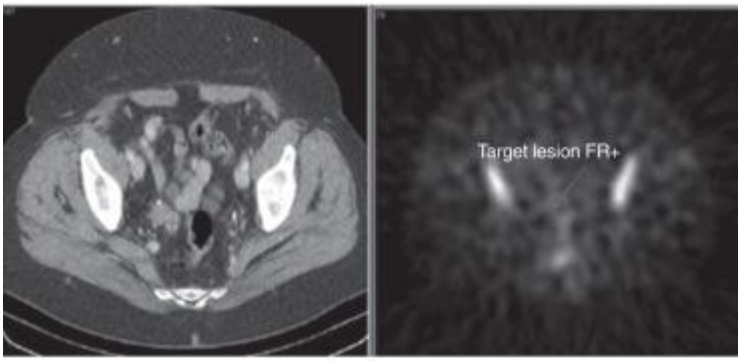

CT image (left) of pelvic ovarian mass. Corresponding EC20 SPECT images (right) showing no ^{99m}TC-EC20 uptake in target lesion

Figure 1.19 SPECT imaging of FR-expressing tumors: ^{99m}Tc-EC20 accumulates in FR-positive tumors but not FR-negative tissues. CT, computed tomography; EC20, etarfolatide; FR, folate receptor; SPECT, single-photon emission CT [85].

^{99m}Tc-etarfolatide, which is noninvasive, folate-targeted, single-photon emission computed tomography based companion imaging agent, provides the potential to rationally identify patients for treatment with vintafolide without the need for biopsy. The use of imaging with etarfolatide allows identification of patients whose disease expresses functionally active FR and, therefore, has the potential to respond to FR-targeted treatment [85,93].

1.3.2 FR-targeted therapeutics in personalized cancer therapy

The selective expression of the FR on cancerous tissues makes it attractive for targeted therapy. At present, two main strategies of FR-targeted therapy are in clinical development: folate conjugates and mAbs (Table 1.6). The development of antifolates is an alternative or even combinatorial strategy of FR-targeted therapy that selectively target the FR. One example is the novel FRα-targeted thymidylate synthase inhibitor, BGC 945 (ONX-0801), which is selectively transported into FRα-

overexpressing tumors, potentially resulting in minimal toxicity to healthy tissues. An ongoing phase I clinical trial is being conducted to assess the safety and pharmacokinetics of BGC 945 in patients with solid tumors [85].

Table 1.6 Comparison of FR-targeting therapeutic approaches in cancer [85].

	Vintafolide	Farletuzumab
Structure	Folate conjugate	Humanized monoclonal antibody
Target	FRα and FRβ	FRα
Affinity to FR (KD)	Nanomolar range 10^{-10}–10^{-11}	Micromolar range 10^{-9} –10^{-10}
Competition with endogenous folates	Yes	No
Molecular weight	1917	~150 000
Mechanism of action	Tumor cytotoxicity by: Preventing cell division through mitotic spindle inhibition (experimentally documented) Causing apoptosis of mitotically active cells (experimentally documented)	Tumor cytotoxicity by: Antibody-dependent cellular cytotoxicity (experimentally documented) Complement-mediated cytotoxicity (experimentally documented) Induction of cell death associated with autophagy (experimentally documented) Inhibition of association of FRα and lyn kinase (hypothesized)
Administration route	i.v.	i.v.
Pharmacokinetics (half-life)	26 min	121–260 h following multiple weekly infusions

FR, folate receptor; i.v., intravenous; KD, equilibrium dissociation constant.

1.3.2.1 FR-targeted mAbs

Farletuzumab (MORAB-003) is a fully humanized FRα-binding mAb that does not prevent folate from binding to the FR nor does it block FR-mediated transport of folate into the cell. Upon binding to FRα expressed on tumor cells, farletuzumab exerts its antitumor activity by different modes of action: (i) promotion of tumor cell lysis via antibody-dependent cellular cytotoxicity (ADCC) and complement-dependent cytotoxicity (CDC); (ii) induction of sustained autophagy, resulting in a decrease in the proliferation of tumor cell; (iii) inhibition of the interaction between FRα and lyn kinase, thus reducing intracellular growth signaling [85,94,95].

1.3.2.2 Folate cytotoxic drug conjugates

Covalent linkage of folate to a variety of molecules, including imaging agents or chemotherapy, allows targeted delivery to FR expressing cells. For drug delivery, the folate-drug conjugate binds with high affinity and specificity to the FR and enters cells via endocytosis, these conjugates do not appear to be substrates for the ubiquitously expressed RFC and may therefore selectively target tumor tissue. Moreover, they do not interfere with the folate cycle or inhibit cellular uptake of antifolates such as pemetrexed or methotrexate [85].

Vintafolide is a water-soluble FR-targeting drug conjugate consisting of a folate moiety covalently linked via a peptide spacer and reducible disulfide linker to desacetylvinblastine monohydrazide (DAVLBH) (Figure 1.20). DAVLBH is a vinca alkaloid that can prevent cell division through the inhibition of mitotic spindle, causing apoptosis of mitotically active cells. Once vintafolide is endocytosed by the FR expressing cell, the disulfide bond linking folate with DAVLBH is cleaved through a reductive process, and the drug is released. Because vintafolide directly targets FR expressing cells, non-FR-expressing cells have limited exposure to DAVLBH (Figure 1.17) [85,93,96].

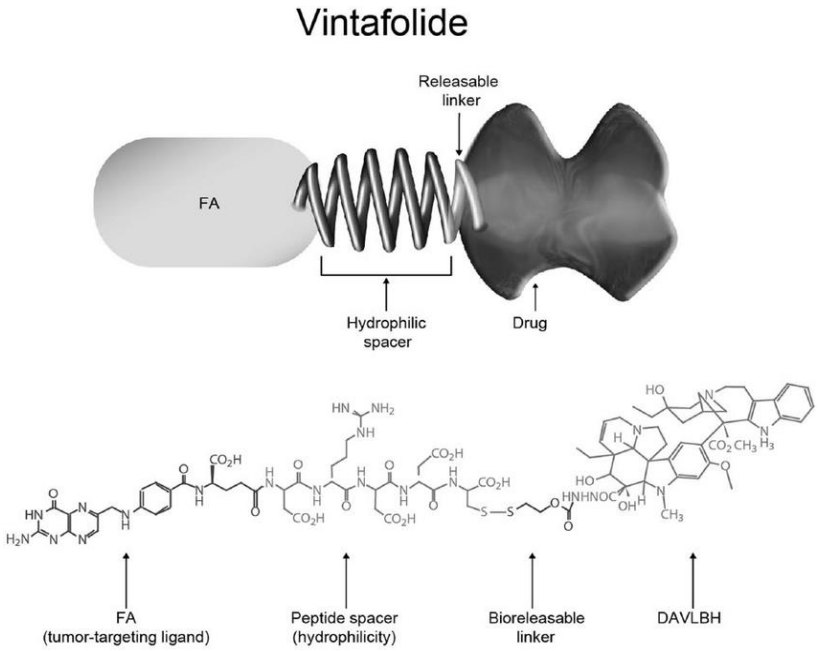

Figure 1.20 Molecular design and structure of vintafolide. Each molecule of vintafolide contains one FA moiety, which serves as a stable high-affinity binding ligand for the FR, and one vinca alkaloid unit (DAVLBH). DAVLBH, desacetylvinblastine monohydrazide [93].

Chapter 2

Materials and Methods

2.1 Materials

Anti-VEGF peptide VEPNc[CDIHVnLWEWEC]FERL was synthetized by Dr. Ivan Gurianov (Department of Chemical Sciences, University of Padova, Padova, Italy).

T-lymphocytes human cell line Jurkat (Institute of Cytology, RAS, Russia), human retinal pigmented epithelial cells ARPE-19 (ATCC® CRL-2302™ collection, USA), human retinoblastoma WERI-Rb-1 (ATCC® HTB-169™ collection, USA), human prostate cancer cells PC-3 (ATCC ® CRL-1435™ collection, USA).

Culture media DMEM-F12, RPMI-1640, dimethyl sulfoxide (DMSO), Trypsin-EDTA (0.25%), Hank's balanced salt solution (HBSS), penicillin/streptomycin, 100X, tissue culture grade, 3-(4,5-dimethylthiazol-2-yl) -2,5-diphenyltetrazolium bromide (MTT), (Paneko, Russia).

Tetraacylated N-azidoacetylmannosamine (Ac_4ManNAz; Sigma, Germany), DBCO NHS esters, Cy5-DBCO and Sulfo-Cy5-DBCO (Lumiprobe, Russia), folic acid (anhydrous; Vekton, Russia), N-hydroxysuccinimide (Vekton, Russia), N,N'-Dicyclohexylcarbodiimide (DCC; Vekton, Russia), triethylamine (Vekton, Russia), acetone (Vekton, Russia), diethylether (Vekton, Russia), trifluoroacetic acid (Vekton, Russia), dichloromethane (Vekton, Russia), DMF (Vekton, Russia), diisopropylethyl amine (Vekton, Russia).

Instruments

Basic Equipment

- Cell culture hood (CYTOS - Biosafety Cabinet)
- NuAire Laboratory CO_2 Incubator
- Digital Water Bath
- Refrigerator and freezer (+4/–20°C)
- Cell counter (LUNA-II™ Automated Cell Counter)

- Reverse microscope Motic, AE21
- Fluorescent Microscope (Cytell Cell Imaging System)
- Biosan FTA-1, Aspirator with trap flask
- Autoclave Tuttnauer EA 2340 D-Line (20L)
- Varioskan LUX Multimode Microplate Reader
- IKA RV 8 Rotary Evaporator
- Heating mantle ES-4110
- Heidolph MR Hei-Standard magnetic stirrer.
- Eppendorf Concentrator plus.
- Shimadzu ATX224 UniBloc Analytical Balance.
- Pipettes and pipettors

Disposable materials

- Cell culture vessels (e.g., Cell Culture flasks, Petri dishes, Falcon tubes, Sterile 96-well filter bottom plates)
- Waste containers
- Eppendorf tubes, Falcon tubes, Round-bottomed flask, volumetric pipette (5, 10ml).

2.2 Methods

2.2.1 Metabolic labeling and chemoselective ligation of living cells

Jurkat cells were cultured in complete growth media RPMI-1640. After 24 hours, the medium was aspirated and fresh medium containing 50 μM tetraacylated N-azidoacetylmannosamine ($Ac_4ManNAz$) was added. Cells were incubated at 37 ° C in an atmosphere of 5% CO_2 for 72 hours. Then, the culture medium was removed, and the cells were washed twice with Hank's balanced saline (HBSS). For fluorescence imaging of the modified cell surface, 1 ml of HBSS containing 2.5, 5 or 10 μM sulfo-Cy5-DBCO was added, and the plates were incubated at room temperature for 15 minutes. Then, HBSS was aspirated and the cells were washed 3 times with HBSS. The analysis of the T-lymphocyte Jurkat cell biohybrids was carried out using the CytellTM Imaging System (GE, USA).

ARPE-19 cells were cultured in complete growth media DMEM-F12 containing 50 µM tetraacylated N-azidoacetylmannosamine (Ac_4ManNAz) for 72 h and maintained in a humidified 5% CO_2 atmosphere at 37 °C. Then, the culture medium was removed, and the cells were washed twice HBSS. For fluorescence imaging of the modified cell surface, 1 ml of HBSS containing 2.5, 5 or 10 µM sulfo-Cy5-DBCO (dibenzocyclooctyne) was added, and the plates were incubated at room temperature for 15 minutes. Then, HBSS was aspirated and the cells were washed 3 times with HBSS.

Sulfo-Cy5-DBCO is an azide- reactive fluorescent dye that is well suited for detection and labeling of chemically, enzymatically, or metabolically azide-modified biopolymers or peptides. The DBCO group reacts with an azide to produce a stable triazole (Figure 2.1), which is also referred to as the Cu(I)-free or strain-promoted click reactions.

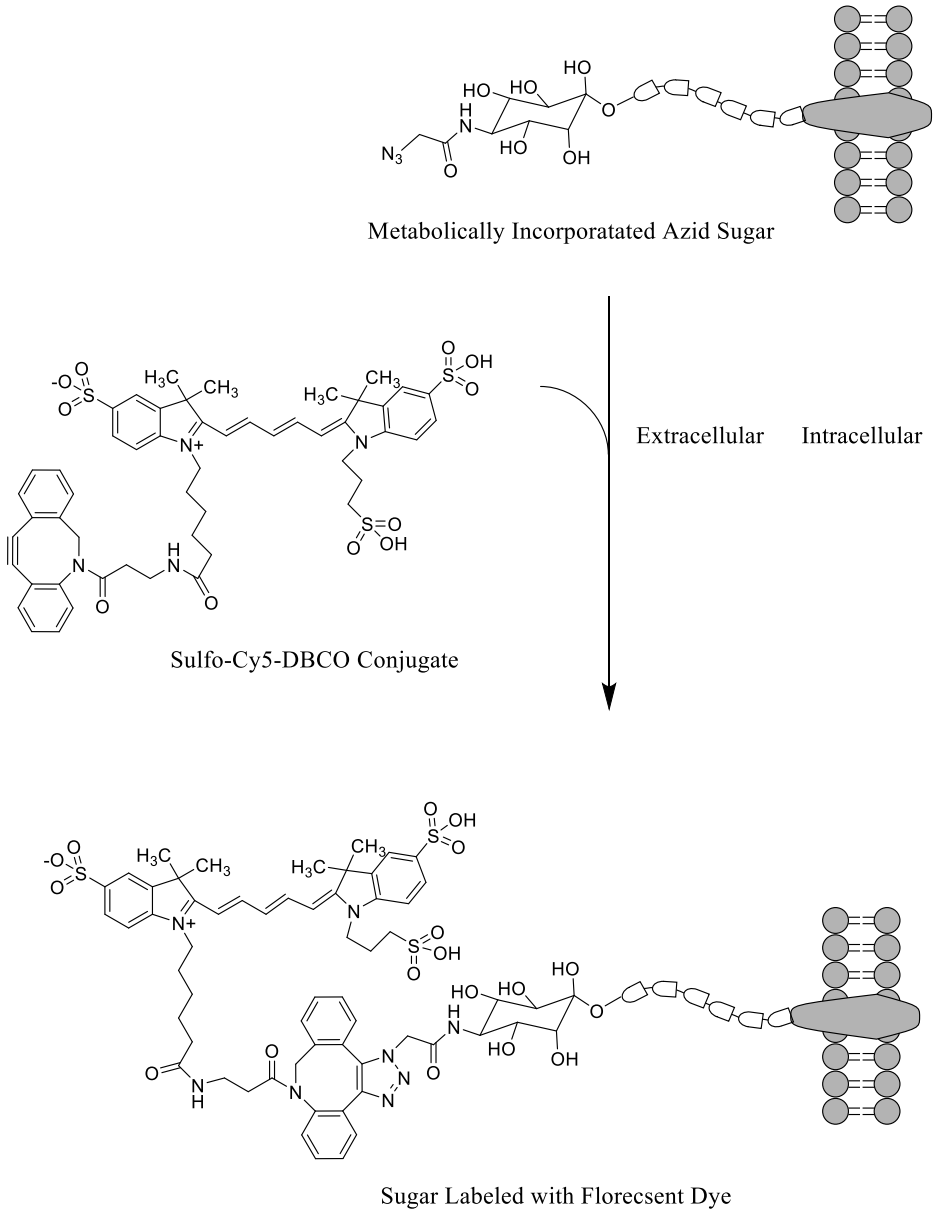

Figure 2.1 Reaction scheme of Sulfo-Cy5-DBCO fluorescent dye (DBCO-dibenzocyclooctyne) and azide

2.2.2 MTT-cell Viability Assay

MTT (3-(4,5-dimethylthiazol-2-yl)-2–5-diphenyltetrazolium bromide) assay is one of the most used colorimetric assay is used to measure cellular metabolic activity as an indicator of cell proliferation, viability and cytotoxicity. The MTT assay was the first homogeneous cell viability assay developed for a 96-well format that was suitable for high throughput screening (HTS) [97,98]. This colorimetric assay is based on the reduction of a yellow tetrazolium salt (MTT) to purple formazan crystals by metabolically active cells (Figure 2.2). Viable cells contain NAD(P)H-dependent

oxidoreductase enzymes that reduce the MTT reagent to an insoluble purple formazan by cleavage of the tetrazolium ring by dehydrogenase enzymes [97,99].

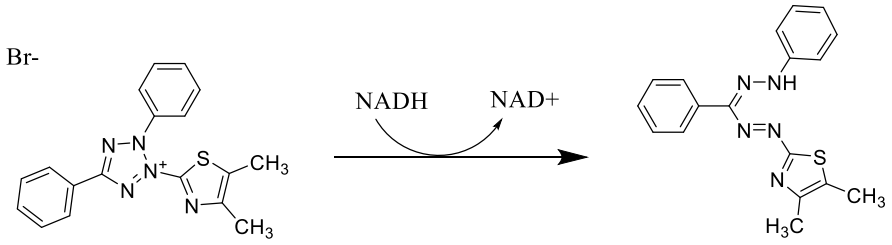

3-(4,5-dimethylthiazol-2-yl)-2,5-diphenyltetrazolium bromide **(MTT)**

(E,Z)-5-(4,5-dimethylthiazol-2-yl)-1,3-diphenylformazan **(Formazan)**

Figure 2.3 Structures of MTT and colored formazan product [97].

The water insoluble formazan can be solubilized by using isopropanol, DMSO or other solvents and The absorbance of this colored solution can be quantified by measuring at 570 nm using a plate reading spectrophotometer. The darker the purple color solution (The Greater the formazan concentration), the greater the number of viable, metabolically active cells [97].

The cytotoxicity of $Ac_4ManNAz$ in a concentration range of 1-100 μM was studied on the ARPE-19 cell line. Cells were cultured in a CO_2 incubator at 37 °C in a humidified atmosphere containing air and 5% CO_2 in a DMEM-F12 nutrient medium (Dulbecco's modified Eagl's medium) containing 10% (v / v) thermally inactivated fetal bovine serum, 1% L-glutamine, 50 U / ml penicillin and 50 μg / ml streptomycin. The analysis of cytotoxicity is carried out spectrophotometrically using a tetrazolium dye 3-(4,5-dimethylthiazol-2-yl) -2,5-diphenyltetrazolium bromide (MTT), which is restored under the action of NAD(P)H-dependent cell oxidoreductases with the formation of stained formazan product with a maximum absorption at a wavelength of 540 nm, the content of which is proportional to the number of viable cells.

For the experiment, 5.0×10^3 cells / 100 μl / well were seeded in 96-well plates and cultured for 16-24 ho for attachment. Then 100 μl of DMEM-F12 medium containing $Ac_4ManNAz$ in various concentrations is added and the cells are incubated for an additional 72 hours. At the end of the incubation period, DMEM-F12 medium is removed and 100 μl / well of a new portion of DMEM-F12 medium and 30 μl / well of MTT reagent solution (5 mg / ml) are added. Cells in the plates are incubated with a CO_2 incubator for 1 h at 37 ° C. After removal of the supernatant, the formazan

crystals formed by the metabolically viable cells were dissolved in DMSO (100 µl/well) and the absorbance of each well was measured at 540 nm and 690 nm on a Varioskan LUX multimodal plate reader (Thermo Scientific). To correct the background, the optical density at 690 nm was subtracted from the values of optical density at 540 nm for the corresponding wells. Data were normalized as a percentage with respect to control cells, i.e. cells incubated without test substances.

2.2.3 Synthesis of anti-VEGF and Dibenzocyclooctyne conjugate

Anti-VEGF peptide with the following amino acid sequence VEPNc[CDIHVnLWEWEC]FERL was conjugated with DBCO NHS ester according a protocol published at the web resource https://www.lumiprobe.com/protocols/nhs-ester-labeling. The obtained conjugate was purified by dialysis (MW cut off 1000) against distilled water for 3 days at a temperature of +4 ºC.

2.2.4 Synthesis of Ethylenediamine Folic Acid and Dibenzocyclooctyne conjugate

Functionalization of the terminal γ-carboxyl group of folic acid is one of the most important strategies for targeted delivery of chemotherapeutic agents and dyes to cancer cells which overexpress folate receptors. However, folic acid conjugation is limited by its unique solubility and by selectivity issues requiring an expensive preparative reverse-phase chromatographic purification in order to isolate γ-folate conjugates [100].

The use of strain-promoted azide–alkyne cycloadditions reaction (SPAAC) with a γ-folate–cyclooctyne conjugate is consider a novel synthetic tool for the synthesis of new folic acid conjugates with excellent γ-purity. In order to demonstrate the potential of this process several new folate conjugates were synthesized with high γ-purity and without using any type of chromatographic purification by reacting conjugate with several fluorescent probes, and polymers bearing azide. In addition, the cycloaddition reaction between conjugate and an azido-derived fluorescent dye was successfully performed in cellular media leading to an increase of fluorescence in the cells that overexpress folate receptors. strain-promoted azide-alkyne cycloaddition reaction allows chemically modifying the surface of living cells with various tissue-specific ligands to impart targeted properties to these cells [100].

In particular, folic acid, which ensures targeted delivery of chemotherapeutic and diagnostic tools for tumor cells exhibiting increased expression of receptors for this acid (FOLR1). This small water soluble vitamin B9 is essential for the normal cell functioning and its receptors were found to be overexpressed in a considerable percentage of cancer cell lines. Until now, a number of small folic acid conjugates with fluorescent probes or drugs have been described and are being evaluated in clinical trials. Apart from these developments, the synthetic tools available for conjugation of folic acid are relatively underdeveloped and remain highly challenging. This vitamin is structurally consisted of pteroic acid covalently bound to a glutamic acid residue. However, only the γ-conjugates have the medicinal relevance, as they have higher affinity toward the receptors compared with α-conjugates. Recently, folate receptor-α (FRα) protein was isolated and crystallized providing important insights into the interaction between the receptor and folate. The pterin head of Folic acid bind to the receptors, being stabilized by numerous of hydrogen bridges and hydrophobic interactions. Even the glutamate residue is stabilized by six hydrogen bonds, four of them with the α-carboxylic acid. These observations indicate that only γ-folate conjugates have highly affinity toward the receptors [100].

Hence, herein is described a new folic acid conjugation route based on strain-promoted alkyne–azide cycloadditions (SPAAC) for folate-based cancer cell targeting. the development of a small folate conjugate that incorporates a non-metal based “clickable” functional group allowing fast, selective and quantitative conjugation to folic acid. This conjugate should also have an ethylenediamine spacer in order to ensure high affinity to folate receptors.

The cyclooctyne DBCO-NHS ester was selected as the most appropriate clickable probe as Dibenzocyclooctyne (ADIBO, DBCO) is one of the most reactive cycloalkynes for strain promoted alkyne azide cycloaddition (SPAAC) – a copper free Click chemistry reaction. This is an amine-reactive NHS ester that provides easy attachment of the reactive moiety to almost any primary or secondary amine group, such as that of protein, peptide, or small molecule amine (Figure 2.4).

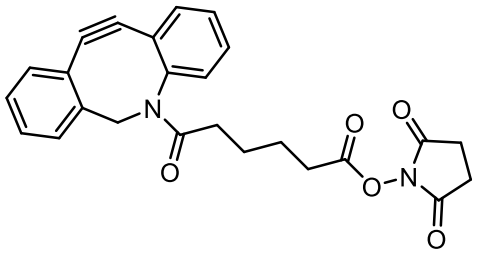

Figure 2.5 Dibenzocyclooctyne (DBCO) NHS ester.

The γ-conjugate folate-diethylenediamine-DBCO was synthesized in high purity employing a direct amide coupling strategy (Scheme 2.1), without using chromatographic purification. The procedure was demonstrated for the synthesis, identification of a dibenzocyclooctyne (DBCO) derivative of folic acid, study of its reactivity in the SPAAC reaction with cell line T-lymphocyte Jurkat cells labeled with N-azidoacetylmannosamine tetraacetate ($Ac_4ManNAz$) and study of the specificity of the obtained primary biohybrid model for human retinoblastoma cells Weri-Rb1. The developed chemical and biological approaches for constructing biohybrid platforms containing the targeted ligand - folic acid can form the basis new approaches to personalized cell therapy or therapeutics of cancer.

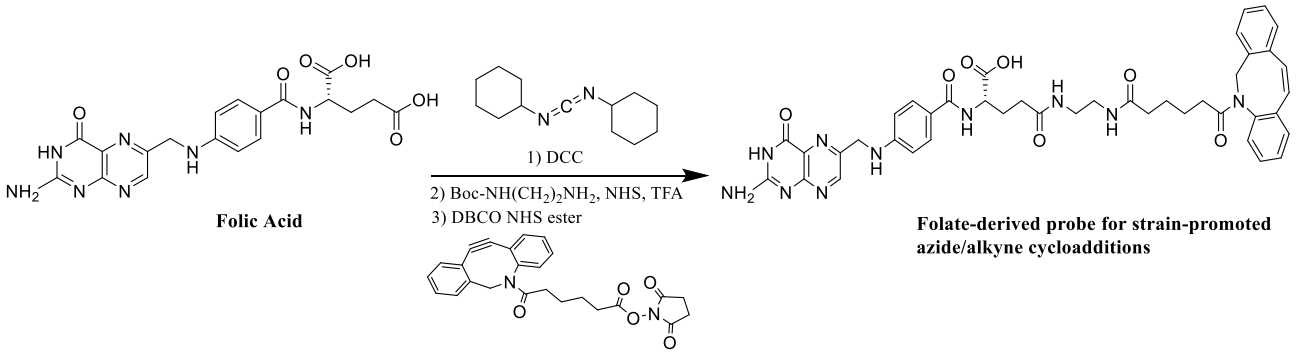

Scheme 2.1 Synthesis of folic acid conjugate.

Synthesis

Folic Acid

In the synthesis dried folic acid was used. In a bottom flask put calcium chloride and a Petri dish contain 4.2426 g of folic acid and dried under low pressure vacuum device for 1 min then leave covered for 36 h in dark. Anhydrous folic acid structure was confirmed by 1H NMR and IR techniques. As shown in Figure 2.6, a characteristic wide band of stretching vibrations of NH and OH

is observed, which overlap the bands of stretching vibrations of CH (3000-2567 cm^{-1}) and overtones of the aromatic ring, and a doublet (3415, 3323 cm^{-1}) confirms the presence of a primary amino group (NH_2). The intense band C = O (1695 cm^{-1}) refers to the carboxyl groups of folic acid; C – C vibrations (1600–1570 cm^{-1}) of aromatic rings. Further, the C – N, C – O stretching vibrations which can overlap with CH deformation vibrations. In the area of fingerprints, bands of bending vibrations of NH, OH are observed.

Acetone and Hexane

Acetone and hexane 50 ml were distilled once without drying agents by using IKA RV 8 Rotary Evaporator at 35-40 ºC.

Drying Dichloromethane

Dichloromethane was freshly distilled over calcium hydride prior to use, in a round bottom flask 100 ml of dichloromethane distilled over calcium hydride by using (Heating mantle ES-4110) at 30 ºC.

THF, DMSO and DMF were used without any purification.

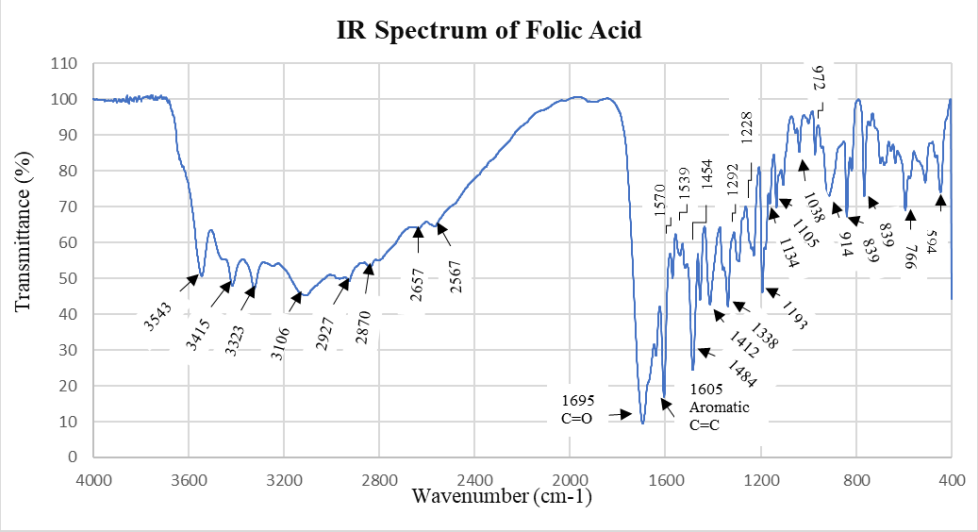

Figure 2.6 IR Spectrum of Folic Acid

FT-IR (KBr, cm^{-1}): 3543-2000(νOH, νNH); 2927-2872 (νCH3); 1695 (νC=O); 1605 (νC–C); 1570-1454 (νC–N, δNH), 1412 (δC–O–H); 1292-1228 (ν_{as}C–O); 1193-1134 (ν C–N); 1105-1038 (ν_{s}C–O); 839-766 (δNH, δOH).

The 1H NMR spectra of folic acid is consistent with the one available in the literature (Figure 2.7).

2.2.4.1 N-BOC ethylenediamine

In a round-bottomed flask was dissolved 4 ml (60 mmol, 10 eq.) of ethylene diamine in 100 ml of dry dichloromethane and stirred (Speed 1400 rpm) at 0 ºC. Then, it was added drop-by-drop a solution of BOC anhydride (1.31g, 6 mmol, 1eq.) in 20 ml of dry dichloromethane. After the addition was finished the reaction mixture was stirred for 24 hours at room temperature, the solvent was removed under low pressure by using IKA RV 8 Rotary Evaporator (Speed 120 rpm, pressure 800 at 40 °C) to yield a viscous oil (27.0914 g). It was redissolved in a solution of 2M Na_2CO_3 (60 ml) and extracted twice with 60 ml of dichloromethane. The organic phase was dried with Na_2SO_4, evaporated to dryness. N-Boc ethylenediamine (1,1 g, 92 % yield) was isolated as an uncolored oil with enough purity to be used in subsequent reactions.

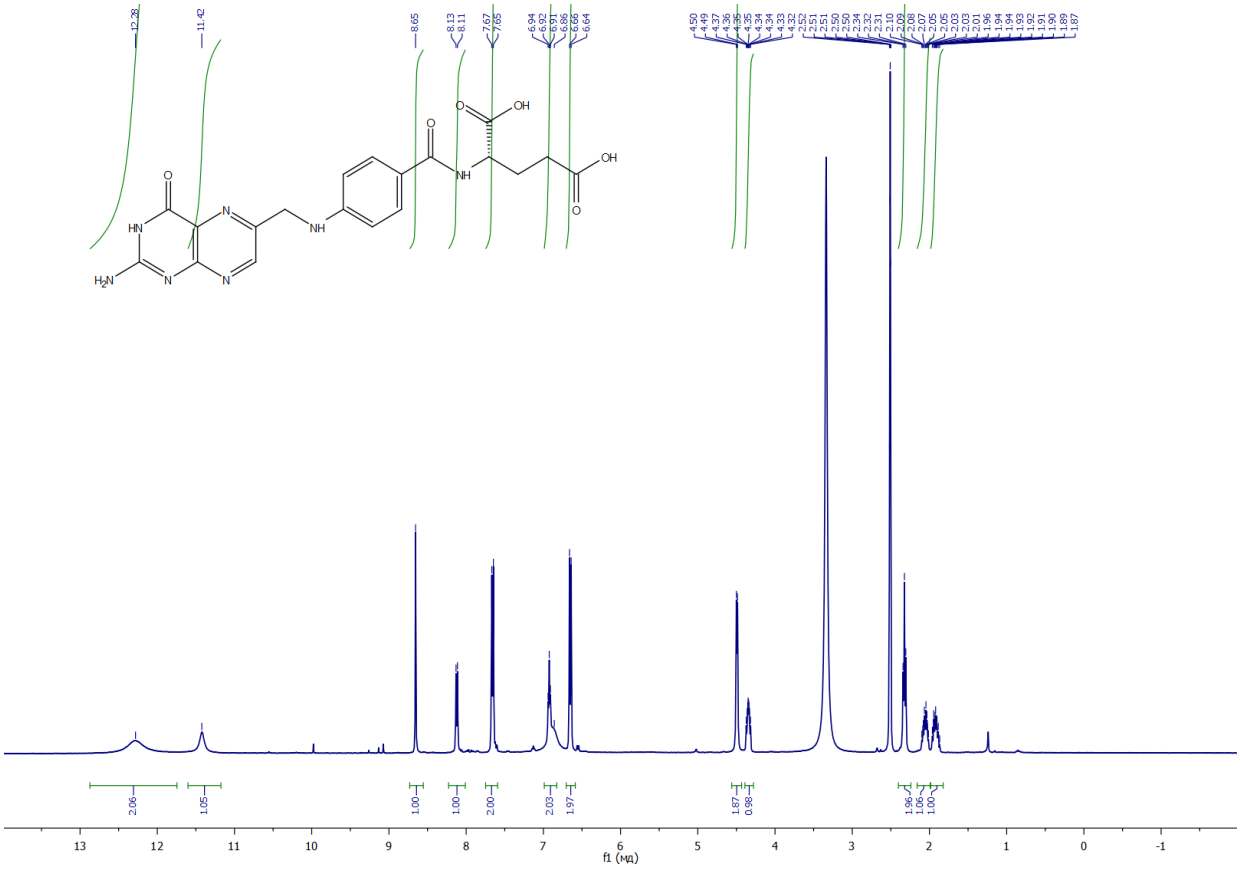

Figure 2.7 NMR Spectrum of Folic Acid

^{1}H NMR (400 MHz, DMSO-d_6) δ 12.28 (s, 2H), 11.42 (s, 1H), 8.65 (s, 1H), 8.12 (d, J = 7.7 Hz, 1H), 7.66 (d, J = 8.5 Hz, 2H), 7.03 – 6.74 (m, 2H), 6.65 (d, J = 8.5 Hz, 2H), 4.49 (d, J = 5.9 Hz, 2H), 4.42 – 4.15 (m, 1H), 2.32 (t, J = 7.4 Hz, 2H), 2.16 – 2.00 (m, 1H), 1.92 (m, 1H) ppm.

Figure 2.8 illustrate HPLC chromatogram of the folic acid. The retention time for folic acid was 9.6 min. The chromatographic purity of folic acid was ≥95 %.

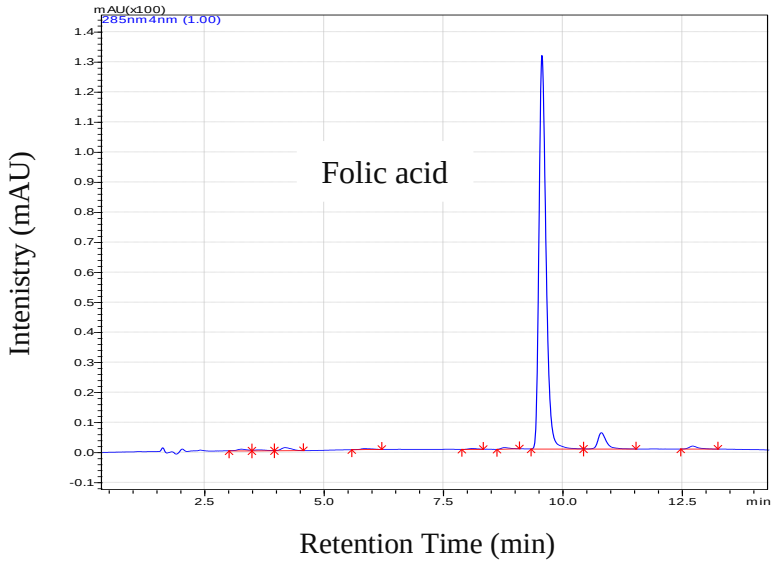

Figure 2.8 Reverse phase HPLC analysis of Folic acid.

UV detection: 285 nm, column: Luna C18 (150 * 2.1 mm, 5 µm), M.P. 0.1% H_3PO_4 / CH_3CN, flow rate: 0.3 ml/min, sample volume: 20 µl.

2.2.4.2 N-BOC ethylenediamine-folate

In a round-bottomed flask was dissolved 640 mg of Folic acid (1.45 mmol, 1 eq. anhydrous powder) in 25 ml Dimethyl sulfoxide (DMSO) using water ultrasonic bath. After the dissolution was complete (about 30 min with mild heating 50-60 °C) 333.74 mg (2 eq.) of N-hydroxysuccinimide and 598.32 mg (2 eq.) of N,N'-Dicyclohexylcarbodiimide (DCC) were added successively. The reaction mixture was stirred for 16 h at room temperature, after which the urea precipitate was removed by centrifugation (20 min, speed 10000 rpm, 20 °C). Then, it was added 404 µl (2 eq.) of triethylamine followed by 465 mg (2 eq.) of N-BOC-ethylene diamine dissolved in 5 ml of DMSO. The mixture was again stirred overnight (speed 750 rpm at 25°C), before was added to a mixture of 20% acetone (25 ml) in 80% diethyl ether (100 ml). The thin yellow precipitated was carefully centrifuged (20 min, speed 10000 rpm, 18 °C) and washed four times with (25 ml) acetone and two times with (25 ml) diethyl ether (607 mg, 69.61 % yield). The folic acid was conjugated with N-BOC ethylene diamine almost exclusively in the terminal carboxylic acid as confirmed by ^{1}H NMR (1500 µl of DMSO, 0.020 mg of N-BOC ethylenediamine-folate).

2.2.4.3 Ethylenediamine-folate

The ethylenediamine-folate conjugate was prepared according with a literature protocol. N-BOC-ethylenediamine folate (150 mg) was dissolved in 1 ml of trifluoroacetic acid and stirred for two hours (speed 852 rpm, 25 °C). The solvent was removed under pressure by using IKA RV 8 Rotary Evaporator (Speed 120 rpm, pressure 742 units, 50 °C) with aid of dichloromethane (1 ml) and the red-dark residue was dissolved in the minimal amount of dry DMF (1 ml). The addition of triethylamine (720 µl) resulted in the precipitation of a yellow powder, which was centrifuged (10 min, 6000 rpm, 18 °C) and washed four times with acetone (20 ml) and two times with diethyl ether (20ml) and dried under vacuum by using Concentrator Device (3 h, 60 °C, mode U-AQ)}(88.8 mg, 72% yield).

2.2.4.4 DBCO-Ethylenediamine-folate

In a round-bottomed flask was dissolved (52 mg, 0.104 mmol) of ethylenediamine-folate in 4 ml of Dimethyl sulfoxide (DMSO) and added diisopropylethyl amine (68 µl, 0.5 mmol, 4 eq) and DBCO NHS ester (48 mg, 0.111 mmol, 0.9 eq) and stirred until a clear solution is obtained (about 30 minutes). The reaction mixture was poured into a mixture of 20% acetone (4 ml) in 80% diethyl ether (16 ml). The thin yellow precipitated was carefully centrifuged (10min, speed 6000rpm, 18 ° C) and washed two times with (10 ml) acetone and two times with (10 ml) diethyl ether and dried under vacuum by using Concentrator Device (3h, 60 °C, mode U-AQ)} (56mg, 65% yield).

Chapter 3

Results and discussion

3.1 Development of optimal conditions for creation of biohybrids in SPAAC reaction.

Our technology for producing biohybrids consists in metabolic (biological) labeling of immune cells with N-azidoacetylmannosamine tetraacetate (Ac_4ManNAz) during their *in vitro* culture. In order to develop and optimize a novel method for cell labeling and tracking, firstly, human cells (suspension T-lymphocyte Jurkat cell line and adherent prostate carcinoma PC3 cell line) were treated with N-azidoacetylmannosamine-tetraacetate (Ac_4ManNAz) during their *in vitro* culture, so that Ac_4ManNAz is integrated into glycoconjugates on the surface of cells during metabolic reactions of glycan biosynthesis. Secondly, the unnatural azide groups on the surface of immune cells were specifically conjugated with Cy5-DBCO or Sulfo-Cy5-DBCO fluorescent dye (DBCO-dibenzocyclooctyne) through bioorthogonal copper-free click chemistry.

Fluorescent dyes Cy5-DBCO and sulfo-Cy5-DBCO were used to develop and optimize the technology for producing biohybrids. Primary experiments showed that a fluorescent dye Cy5-DBCO freely penetrates the cell membrane in a concentration range of 1 nM-10 μM and accumulates in the cytoplasm of Jurkat cells and ARPE-19 cells. Therefore, for further experiments, a more hydrophilic fluorescent dye sulfo-Cy5-DBCO was used.

As shown in Figure 3.1, the Ac_4ManNAz-treated Jurkat cells were successfully labeled through the SPAAC between the unnatural azide groups on the cell surface and the cyclic alkyne groups of Sulfo-Cy5-DBCO fluorescent dye. Based on the azide groups introduced into the cellular glycoproteins, Sulfo-Cy5-DBCO fluorescent dye specifically bound to the surface of the Ac_4ManNAz-treated cells in suspension to show strong signals at the cell surface, but no signals were detected from the control cells without the Ac_4ManNAz treatment (Figure 3.1). The results indicate that the azide groups were artificially introduced onto Jurkat cell surface via metabolic labeling.

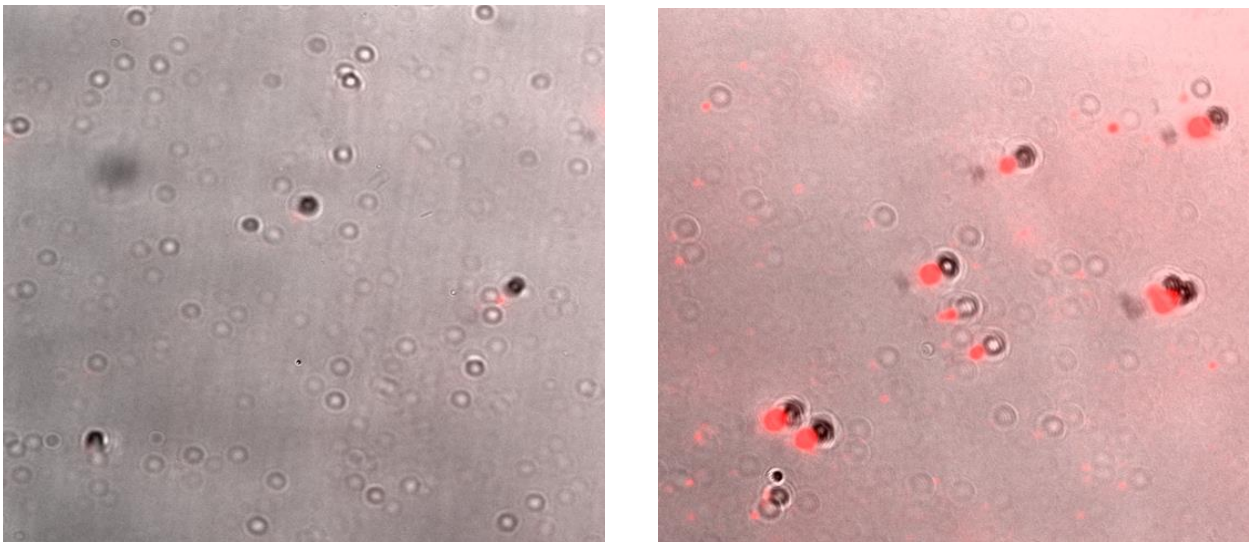

Control (without $Ac_4ManNAz$) **Cultured with $Ac_4ManNAz$**

Figure 3.1 Chemoselective ligation of T-lymphocyte Jurkat cell line with 2.5 μM sulfo-Cy5-DBCO (incubation time 15 min, at room temperature in darkness). Fluorescence signal acquired by Cytell Imaging System (GE, USA), E_{ex}=644 nm, E_{em}=665 nm (red). Scale bar: 10 μm.

At a minimum concentration (2.5 μM), the sulfo-Cy5-DBCO fluorescence signal was detected only on the surface of PC3 cells incubated with azido sugar and was almost not observed in the cytosol of cells, which indicates the occurrence of the azide-alkyne cycloaddition click reaction on the cell surface (Figure 3.2).

The presence of a negatively charged sulfo groups of sulfo-Cy5-DBCO prevents passive diffusion of the dye into the cytosol of living PC3 cells. Nevertheless, with an increase in the concentration of sulfo-Cy5-DBCO in the incubation medium, its nonspecific diffusion into the cell increased (c = 5 and 10 μM, Figure 3.2 B-C). Thus, 2.5 μM is the minimum concentration of sulfo-Cy5-DBCO, which allows the detection of fluorescence without causing nonspecific penetration of the dye into the PC3 cell. We also studied the effect of bovine fetal serum (a component of the incubation medium) on the effectiveness of the reaction of chemoselective ligation. The Figure 3.2.D shows that presence of bovine fetal serum in incubation medium does not affect the effectiveness of the reaction of chemoselective ligation.

When analyzing 3D sections of PC3 cells, it is evident that the fluorescence signal is predominantly accumulated on the periphery of PC3 cells, which indicates the occurrence of the azide-alkyne cycloaddition reaction on the cell surface (Figure 3.3).

A.

PC3 cells

C = 2.5 μM

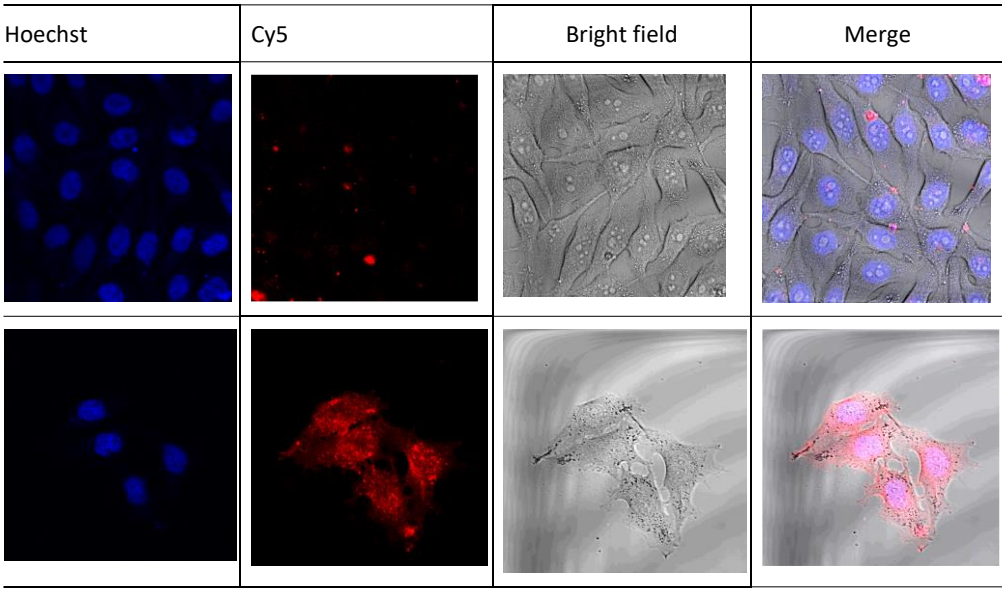

C = 5 μM

B.

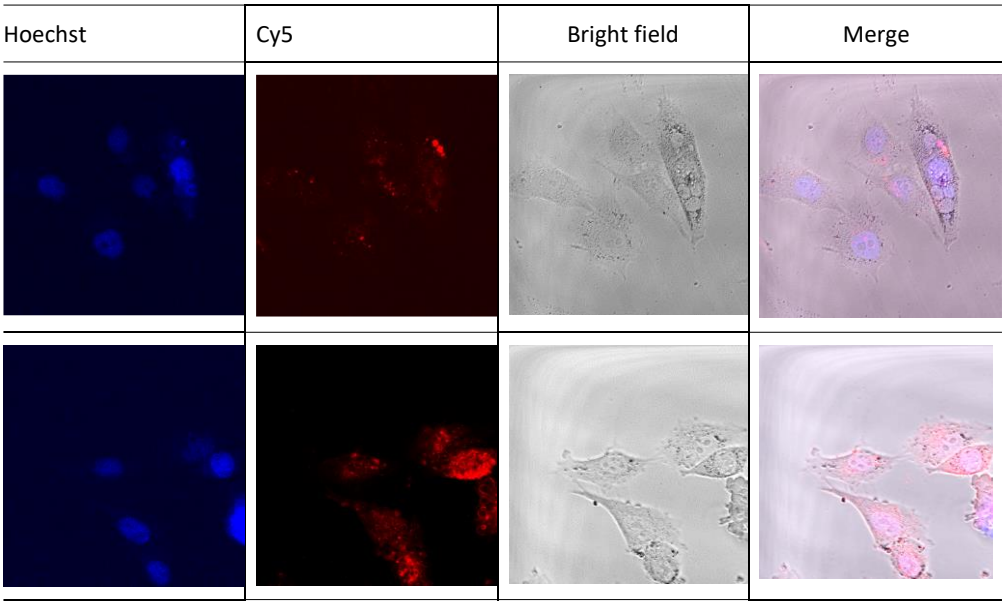

C.

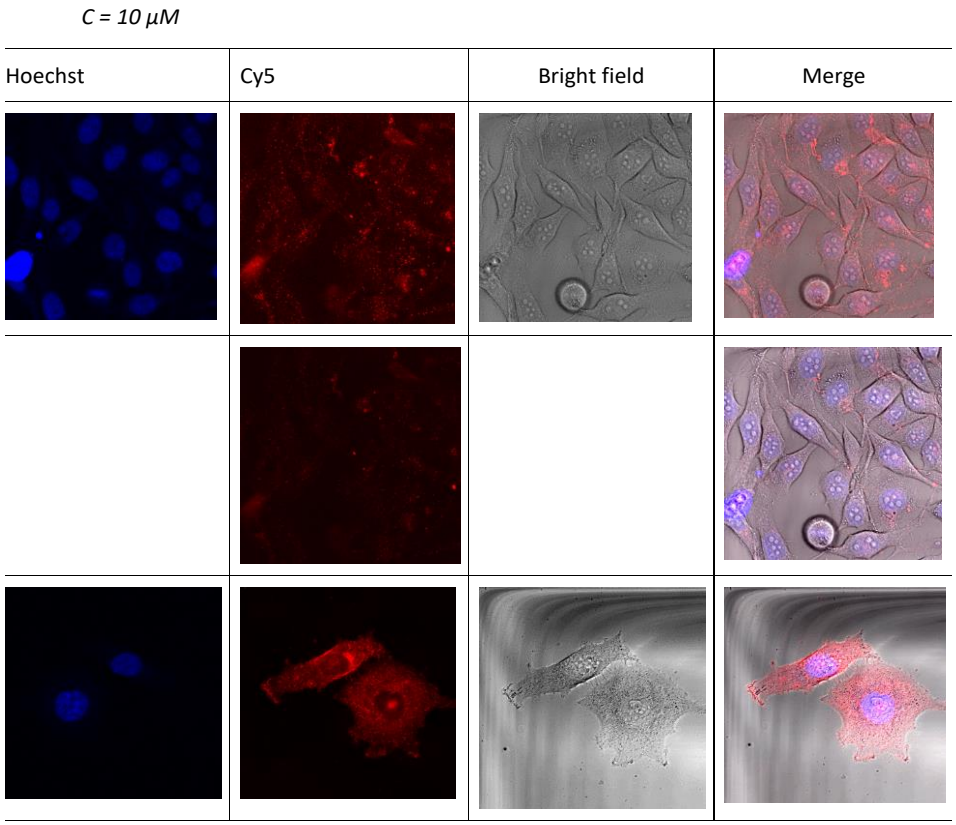

D.

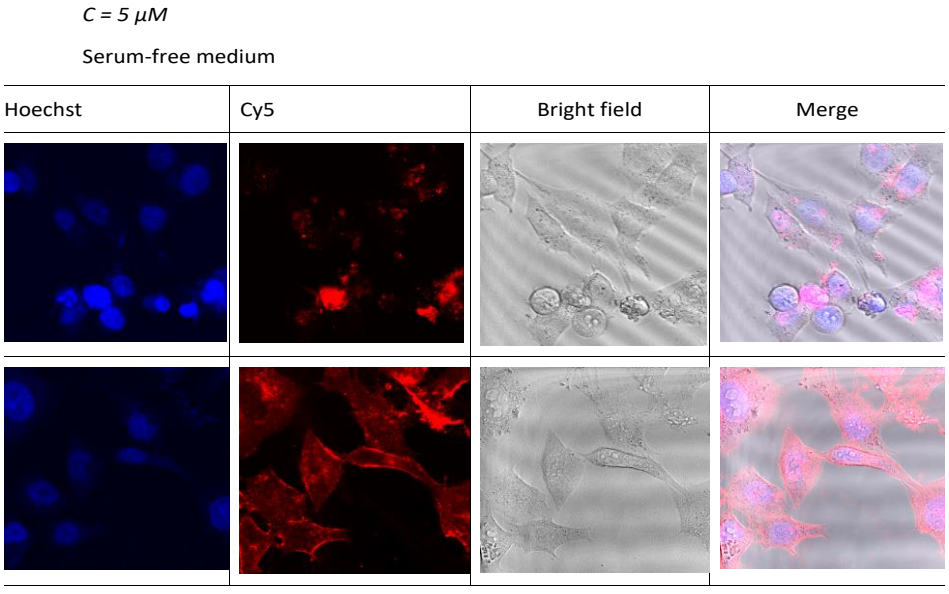

Figure 3.2 Chemoselective ligation of PC3 cells line at various concentrations of sulfo-Cy5-DBCO (2.5 - 10 μM) (A-C) and in serum free medium (D). Nuclear staining with Hoechst 33258 (blue), sulfo-Cy5-DBCO (red).

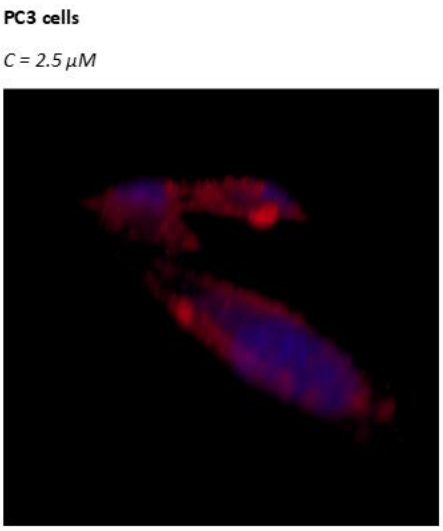

Figure 3.3 Chemoselective ligation of PC3 cells line at 2.5 μM of sulfo-Cy5-DBCO. From 3D stack image. Nuclear staining with Hoechst 33258 (blue), sulfo-Cy5-DBCO (red).

To determine the cytotoxicity of Ac_4ManNAz treatment for introduction of azide groups, cell viability was measured after the treatments of varying dose of Ac_4ManNAz (0 - 100 μM). MTT data obtained on ARPE-19 cells cultured with Ac_4ManNAz for 72 h. As can be seen from Figure 3.4, in the studied concentration range from 1 to 100 μM Ac_4ManNAz does not have any cytotoxic effect. Thus, it was shown that the presence of a functional azide group in mannose sugar does not affect cell viability and does not cause a cytotoxic effect.

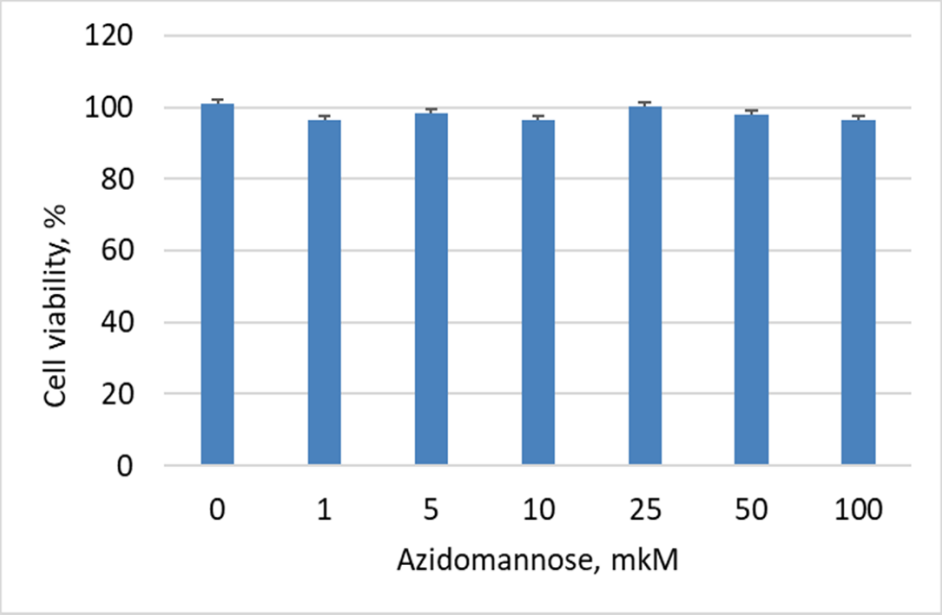

Figure 3.4 Effect of Ac_4ManNAz on ARPE-19 cell viability (72 h culture).

Thus, we obtained results on chemoselective ligation of the surface of living human cells using a fluorescent dye sulfo-Cy5-DBCO. Our data showed that the use of a sulfo-Cy5-DBCO is preferable compared to Cy5-DBCO, since the presence of charged sulfo groups in molecular structure of Cy5 impedes the passive diffusion of the dye through the cell membrane. Importantly, Sulfo-Cy5-DBCO-labeled Jurkat and PC3 cells presented strong emission in the red region of the spectrum with negligible cytotoxicity and the amounts of azide groups and Sulfo-Cy5-DBCO could be easily controlled

The resulting technology will be used to obtain biohybrids containing anti-VEGF peptides necessary for binding of VEGF protein and biohybrids containing folic acid conjugate for recognition of cancer cells overexpressing the folate receptor. The developed chemical and biological technologies for the construction of biohybrid platforms will be able to form the basis of new approaches to personalized therapy of a wide range of diseases.

3.2 Creation of biohybrids capable of selectively binding a VEGF protein

Perturbation of the regulation of VEGF signaling pathways and its synthesis is the main cause of number of diseases. VEGF is a known growth factor involved in cancer cell growth and metastasis; in addition, overexpression of VEGF can cause vascular disease in the retina of the eye. Therefore, creation of biohybrids based on anti-VEGF peptides which can block VEGF signaling pathways is a current task.

Small peptide inhibitors can be highly effective for blocking VEGF signaling pathways. An anti-VEGF peptide VEPNc[CDIHVnLWEWEC]FERL is capable of selectively binding endothelial growth factor VEGF was synthesized. This peptide contains 19 proteinogenic L-amino acids residues, except nL – Norleucine. In addition, the peptide contains two L-cysteine residues that form an intramolecular disulfide bond.

Firstly, to obtain a biohybrid containing anti-VEGF peptide on the cell surface, anti-VEGF peptide was conjugated with DBCO NHS ester (Scheme 3.1).

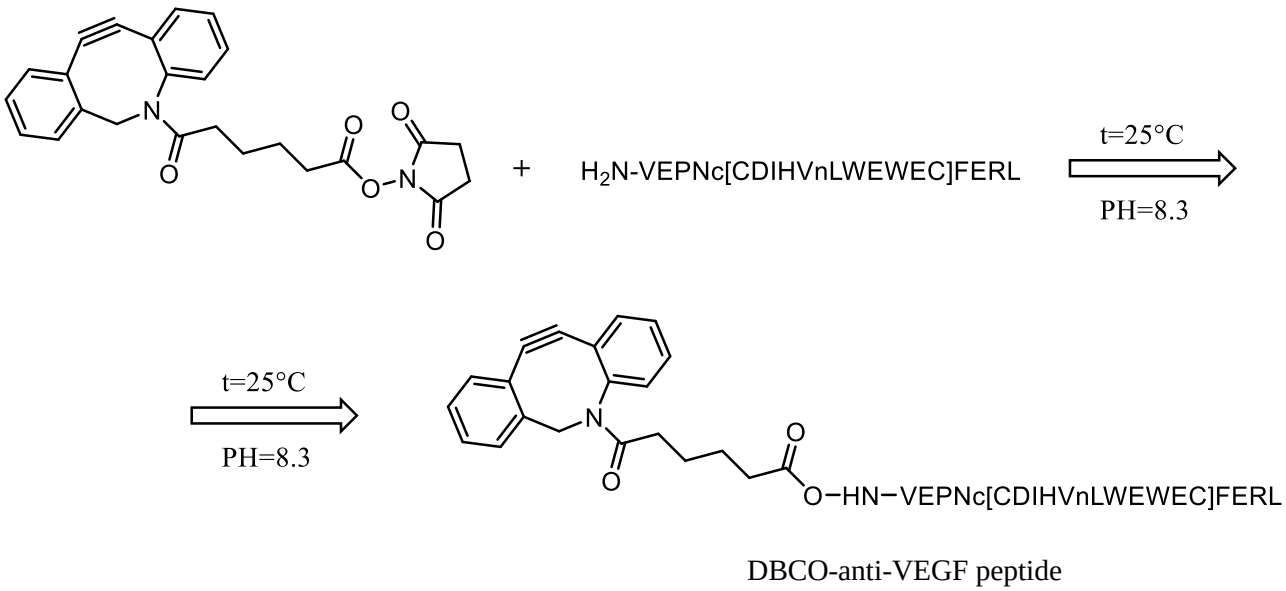

DBCO-anti-VEGF peptide

Scheme 3.1 Synthesis of DBCO-anti-VEGF peptide conjugate.

Secondly, the obtained DBCO-anti-VEGF peptide conjugate after purification was employed to create biohybrid (Jurkat-anti-VEGF) in the SPAAC reaction (Scheme 3.2).

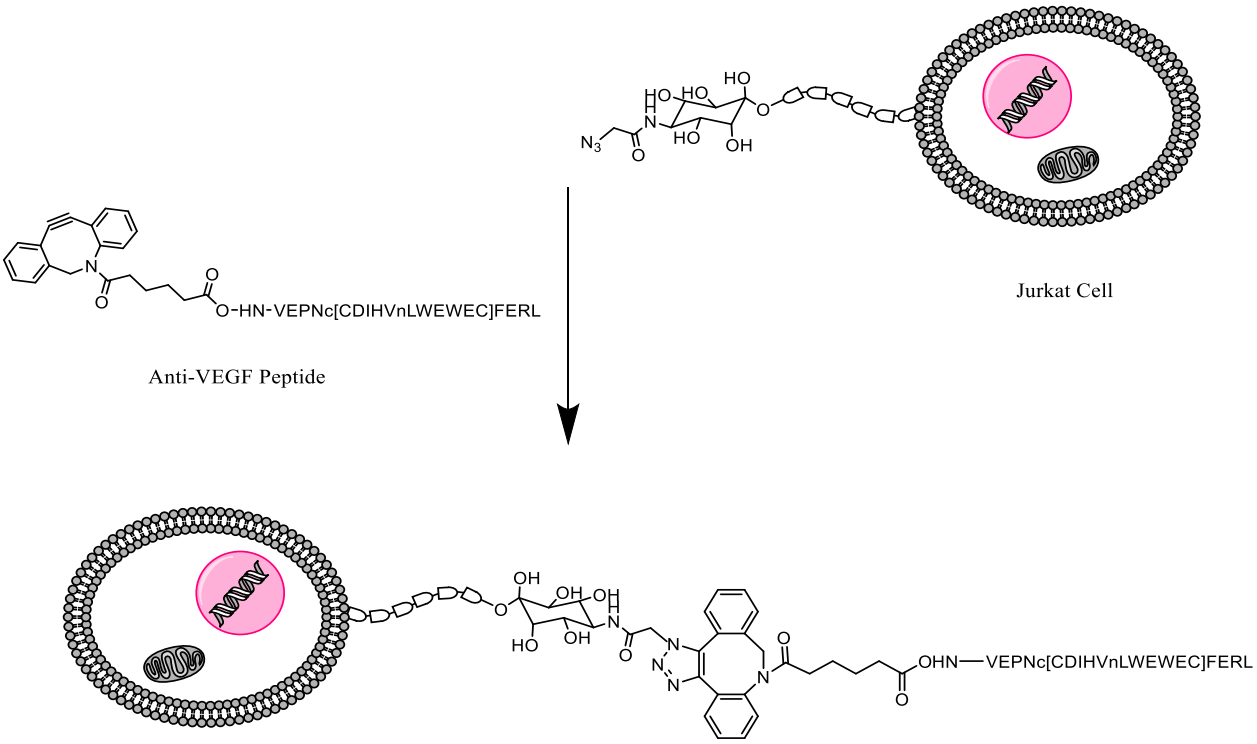

Scheme 3.2 Strategy of creation of biohybrid of T-lymphocyte Jurkat cells with anti-VEGF peptide (Jurkat-anti-VEGF peptide).

Figure 3.5 shows the results of measuring the fluorescence of metabolically labeled T-lymphocytes Jurkat cells with Ac_4ManNAz with following reaction of chemoselective ligation with DBCO-anti-VEGF peptide.

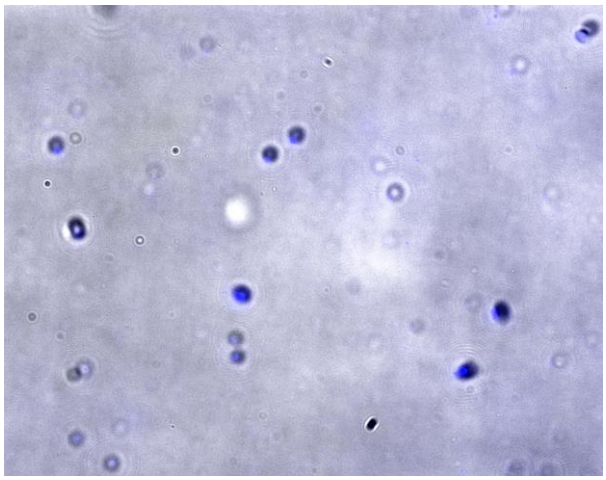

T-lymphocytes Jurkat cells with anti-VEGF peptide (Jurkat-anti-VEGF peptide)

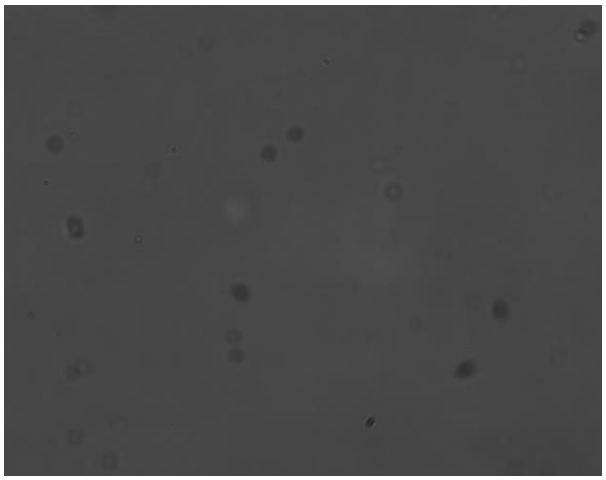

Bright field

Figure 3.5 Chemoselective ligation of T-lymphocyte Jurkat cell line with DBCO-anti-VEGF peptide (incubation time 15 min, at room temperature in darkness). Fluorescence signal acquired by Cytell Imaging System (GE, USA), E_{ex}=350 nm, E_{em}=461 nm (blue). Scale bar: 10 μm.

ARPE-19 cells basally secreted VEGF under normal cell culture conditions. Afterwards, secreted VEGF can form an autocrine loop by binding VEGF-R expressed in ARPE-19 cells. As a result, proliferation of ARPE-19 cells is stimulated. To confirm the functional activity of biohybrid containing anti-VEGF peptide, an analysis of the inhibition of ARPE-19 cell proliferation was performed. In our experimental settings we performed culture of ARPE-19 cells with Jurkat-anti-VEGF peptide biohybrid (Figure 3.6.A) and Jurkat cells as control (Figure 3.6.B). Figure 3.6 shows that coculture of ARPE-19 cells with Jurkat-anti-VEGF biohybrid resulted in dose-dependent decreases ARPE-19 cell proliferation while coculture of ARPE-19 cells with non-modified Jurkat cells has no effect on ARPE-19 cells proliferation. Taken together, our data demonstrate that the obtained biohybrid based on the anti-VEGF peptide blocks the VEGF signaling pathway, which leads to the suppression of proliferation of the human retinal pigmented epithelial cells (ARPE-19). The results can be used to suppress vascular growth and reduce microvascular permeability in the

treatment of ophthalmic diseases (age-related macular degeneration of the retina, diabetic retinopathy, retinal occlusion, retinopathy in premature infants).

A.

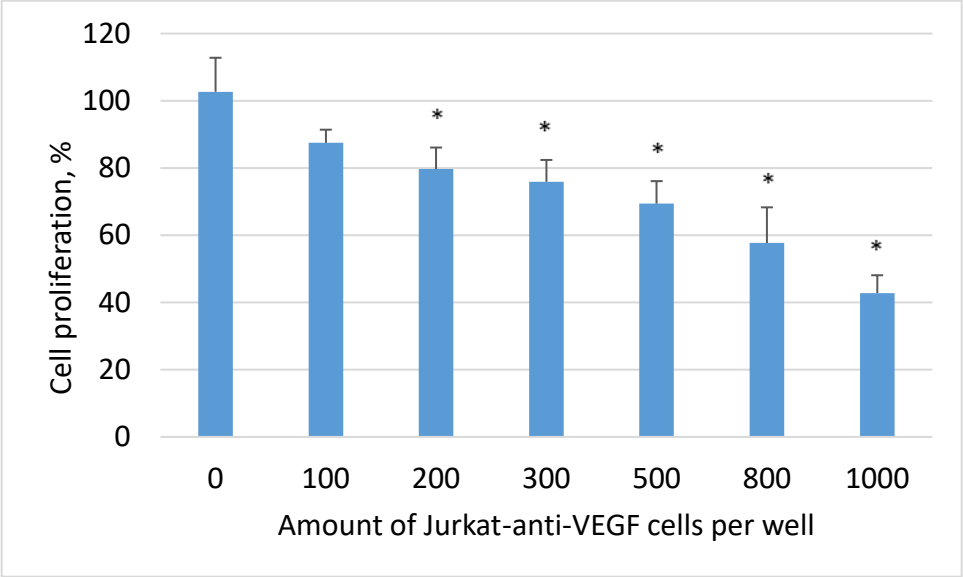

B.

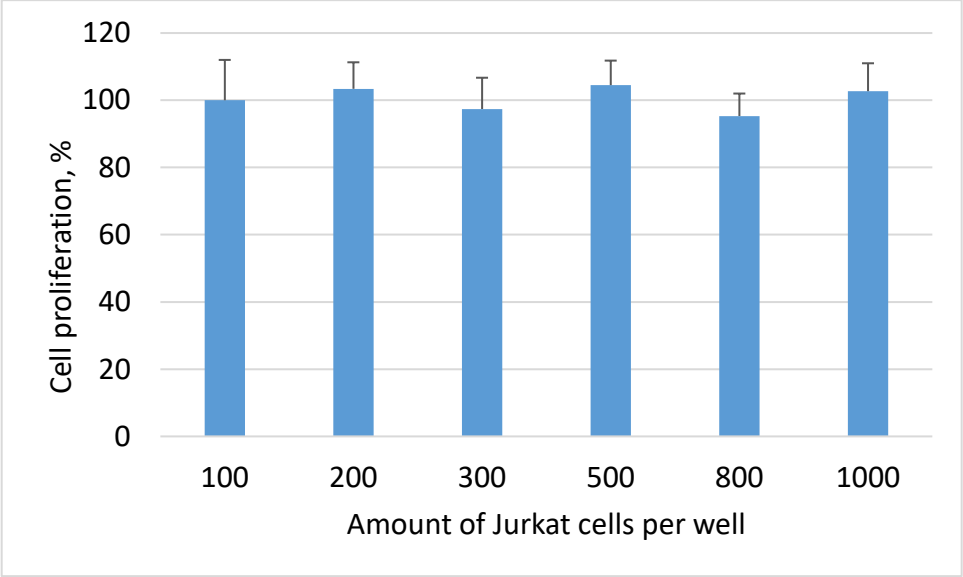

Figure 3.6 Effect of Jurkat-anti-VEGF biohybrid on ARPE-19 cell proliferation (A), effect of Jurkat on ARPE-19 cell proliferation (B) (48 h culture).

3.3 Creation of biohybrids capable of selectively recognizing tumor cells overexpressing folate receptor

The proposed strategy to prepare “clickable” conjugate relies on a simple reaction between folate ethylenediamine and DBCO–NHS ester. The synthesis of the ethylenediamine folate precursor is known. Anhydrous folic acid structure was confirmed by 1H NMR and IR spectrum (Figure 2.7) and (Figure 2.7). Chromatographic purity of folic acid was ≥95%.

Folic acid was activated in the presence of DCC 2 eq. and NHS 2 eq. at 25 °C for 17 h. Under these conditions the γ-conjugate was obtained with 92% selectivity. Kinetic studies revealed that suboptimal conversion and selectivity were obtained for shorter reaction times [100].

The excess of DCC is mandatory to achieve quantitative conversion of folic acid, while the addition of basic additives did not impact positively the selectivity or the conversion. The conjugation was performed with N-Boc-ethylenediamine, the conjugate was isolated in 69.6 % yield (Scheme 3.3). Figure 3.7 demonstrates ^{1}H NMR spectrum of N-BOC ethylenediamine-folate which is consistent with the one available in the literature. Treatment with TFA for 2 h resulted in BOC deprotection and delivered the folate ethylenediamine in 72 % isolated yield (Scheme 3.4). The ^{1}H NMR spectra of folate N-ethylenediamine was consistent with the one published in the literature (Figure 3.8).

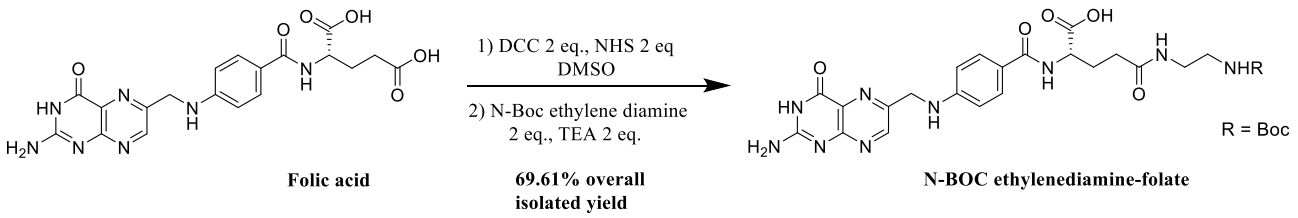

Folic acid — **69.61% overall isolated yield** — **N-BOC ethylenediamine-folate**

Scheme 3.3 Synthesis of N-BOC ethylenediamine-folate

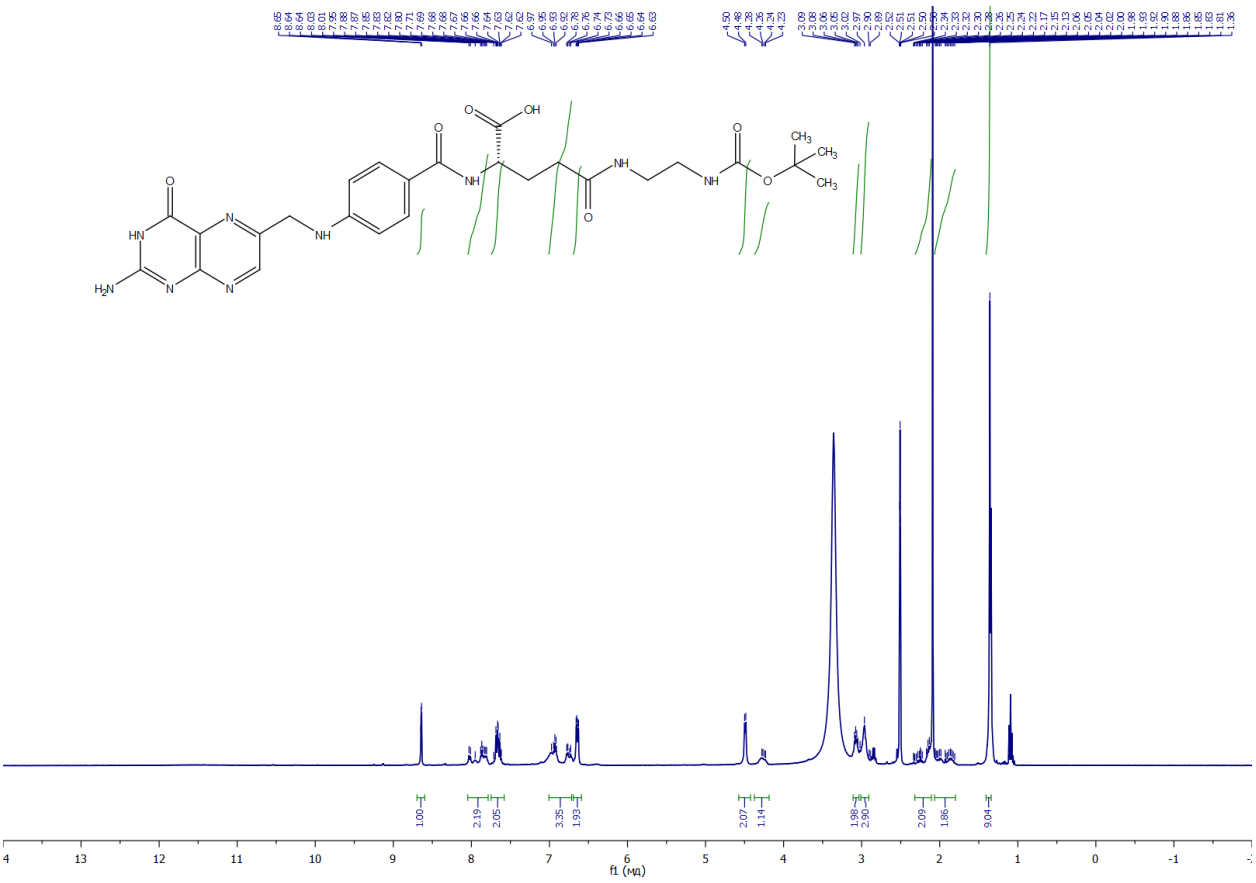

Figure 3.7 ^{1}H NMR Spectrum of N-BOC ethylenediamine folate.

^{1}H NMR (400 MHz, DMSO-d_6) δ 8.89 – 8.48 (m, 1H), 8.13 – 7.77 (m, 2H), 7.73 – 7.45 (m, 2H), 7.16 – 6.84 (m, 3H), 6.82 – 6.69 (m, 2H), 6.69 – 6.51 (m, 2H), 4.49 (d, *J* = 6.1 Hz, 2H), 4.35 – 4.18 (m, 1H), 3.12 – 3.03 (m, 2H), 3.02 – 2.89 (m, 2H), 2.35 – 2.12 (m, 2H), 2.07 – 1.79 (m, 2H), 1.36 (s, 9H) ppm.

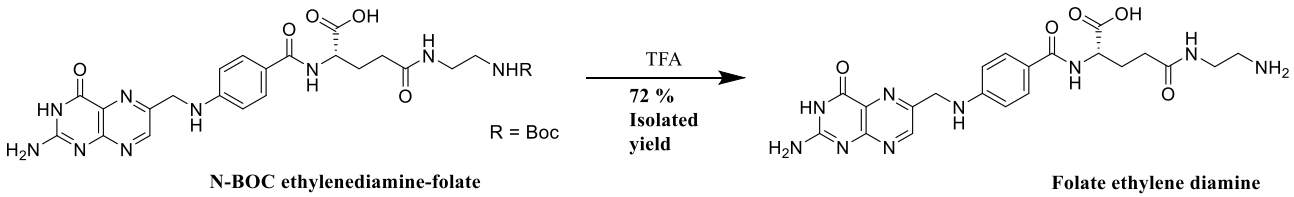

Scheme 3.4 Synthesis of folate ethylenediamine.

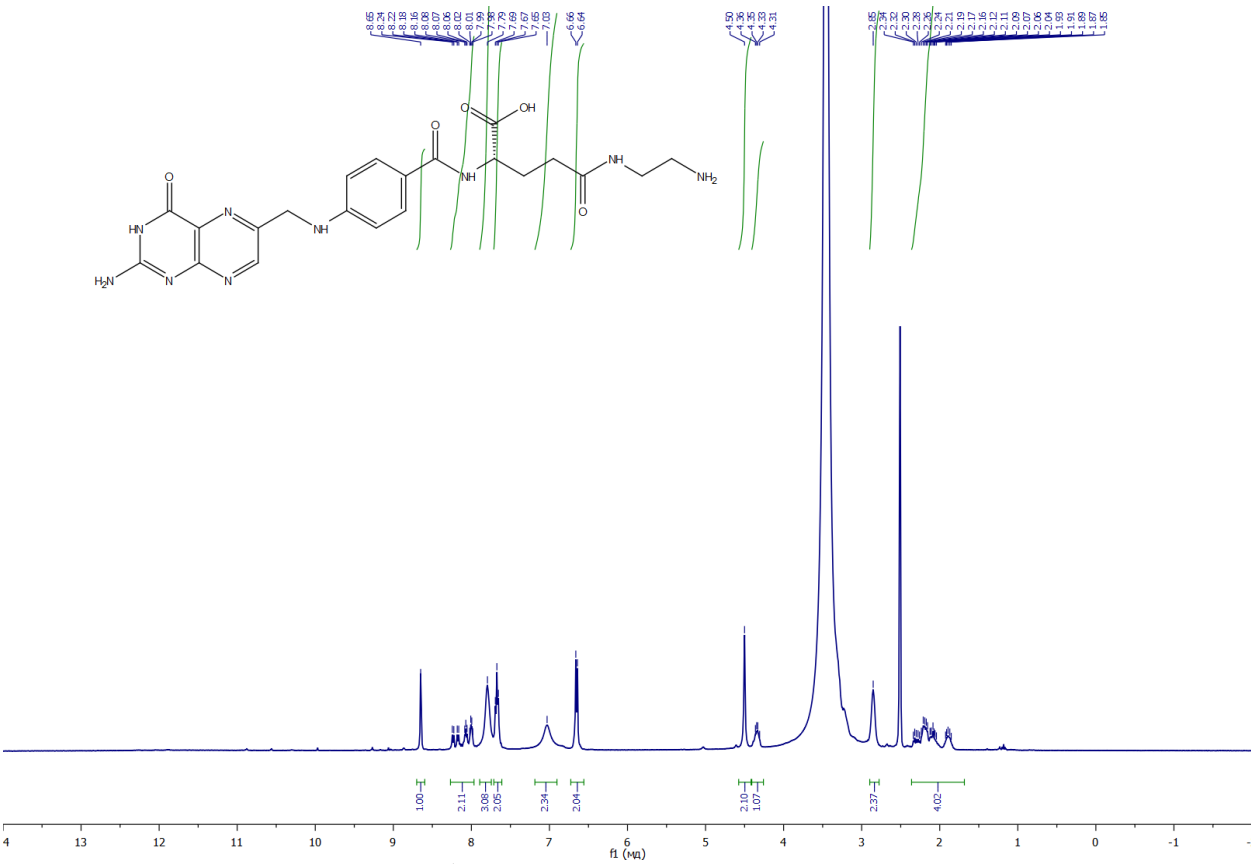

Figure 3.8 ^{1}H NMR Spectrum of folate ethylenediamine

^{1}H NMR (400 MHz, DMSO-d_6) δ 8.65 (s, 1H), 8.31 – 7.96 (m, 2H), 7.89 – 7.74 (m, 1H), 7.67 (t, J = 7.7 Hz, 2H), 7.03 (br. s, 2H), 6.65 (d, J = 8.3 Hz, 2H), 4.53 – 4.47 (m, 2H), 4.40 – 4.27 (m, 1H), 2.85 (s, 2H), 2.37 – 1.76 (m, 4H) ppm.

Subsequently, folate ethylene diamine 1 eq. conjugate was reacted for 30 min with 1.4 eq. of DBCO–NHS ester in the presence of 4 eq. of DIPEA yielding the desirable DBCO-folate ethylenediamine conjugate in 65 % isolated yield after purification (Scheme 3.5). For the first time, the folic acid conjugate with DBCO was synthetized. ^{1}H NMR spectrum contains signals of all structural fragments of the synthesized conjugate (Figure 3.9). In particular, the characteristic signals for the DBCO in the ^{1}H NMR spectrum are in good agreement with the previously published ones [101].

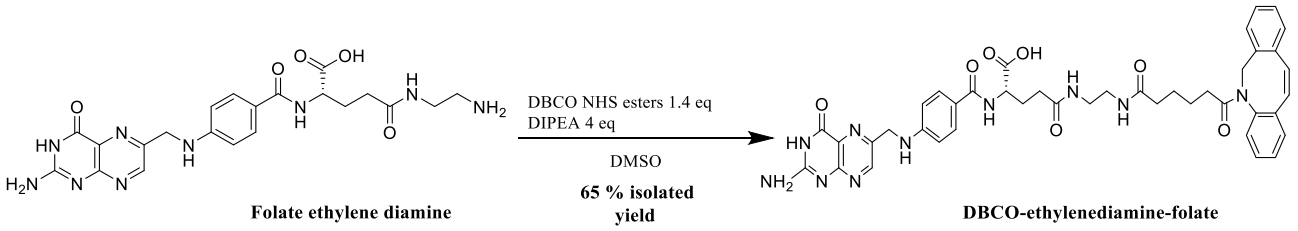

Scheme 3.5 Synthesis of conjugate of ethylenediamine-folate with DBCO

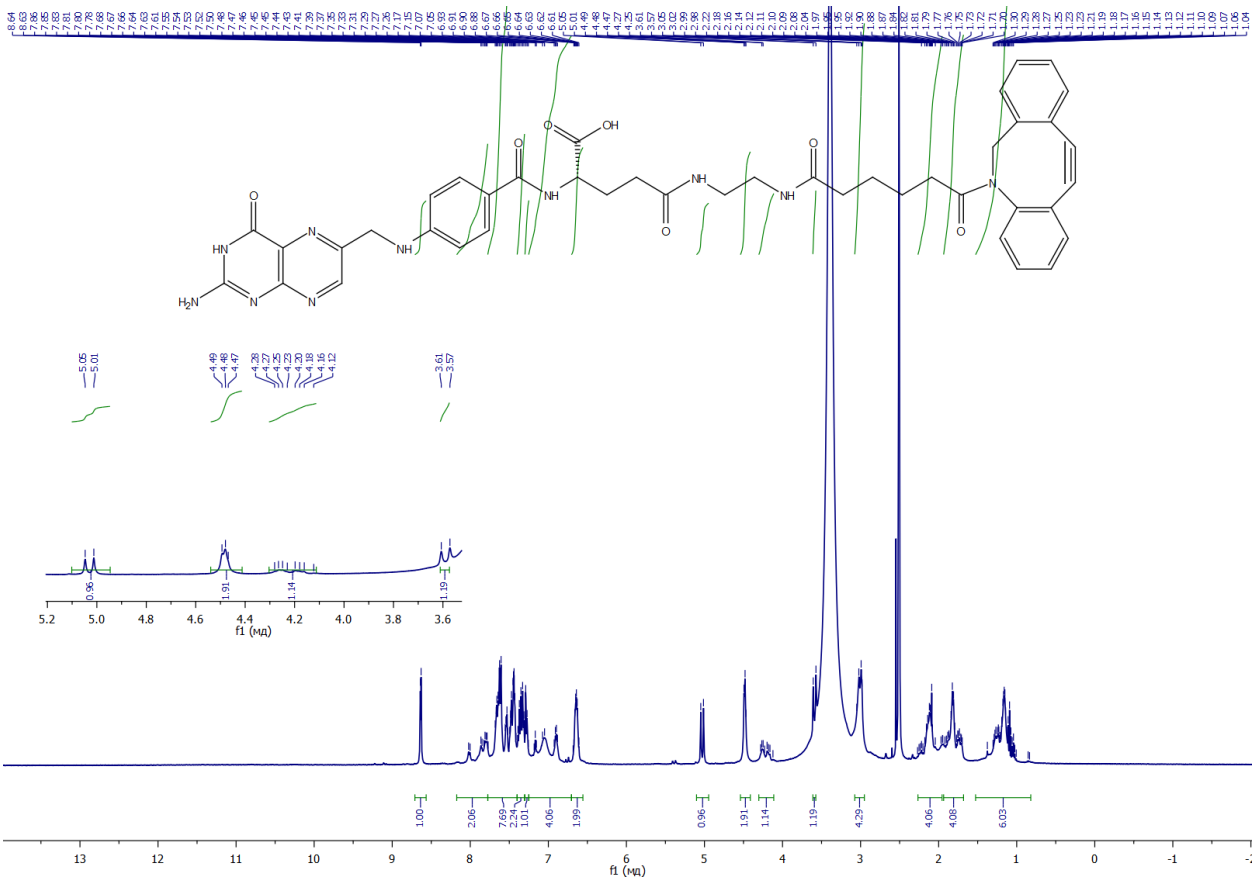

Figure 3.9 ^{1}H NMR Spectrum of DBCO-ethylenediamine folate

^{1}H NMR (400 MHz, DMSO-d_6) δ 8.63 (d, J = 3.7 Hz, 1H), 8.18 – 7.77 (m, 2H), 7.77 – 7.40 (m, 8H), 7.40 – 7.31 (m, 2H), 7.30 – 7.25 (m, 1H), 7.25 – 6.71 (m, 4H), 6.70 – 6.56 (m, 2H), **5.03 (d, J = 14.0 Hz, 1H)**, 4.49 (d, J = 5.6 Hz, 2H), 4.30 – 4.11 (m, 1H), **3.59 (d, J = 14.0 Hz, 1H)**, 3.08 – 2.93 (m, 4H), 2.28 – 1.95 (m, 4H), 1.94 – 1.67 (m, 4H), 1.36 – 0.95 (m, 6H) ppm.

Subsequently, DBCO-ethylenediamine folate and T-lymphocyte Jurkat cells were employed in SPAAC reaction for creation of biohybrids (Scheme 3.6). T-lymphocyte Jurkat cells were metabolically labeled with N-azidoacetylmannosamine tetraacetate (Ac_4ManNAz) as described above and imaged by fluorescence microscopy (Figure 3.5).

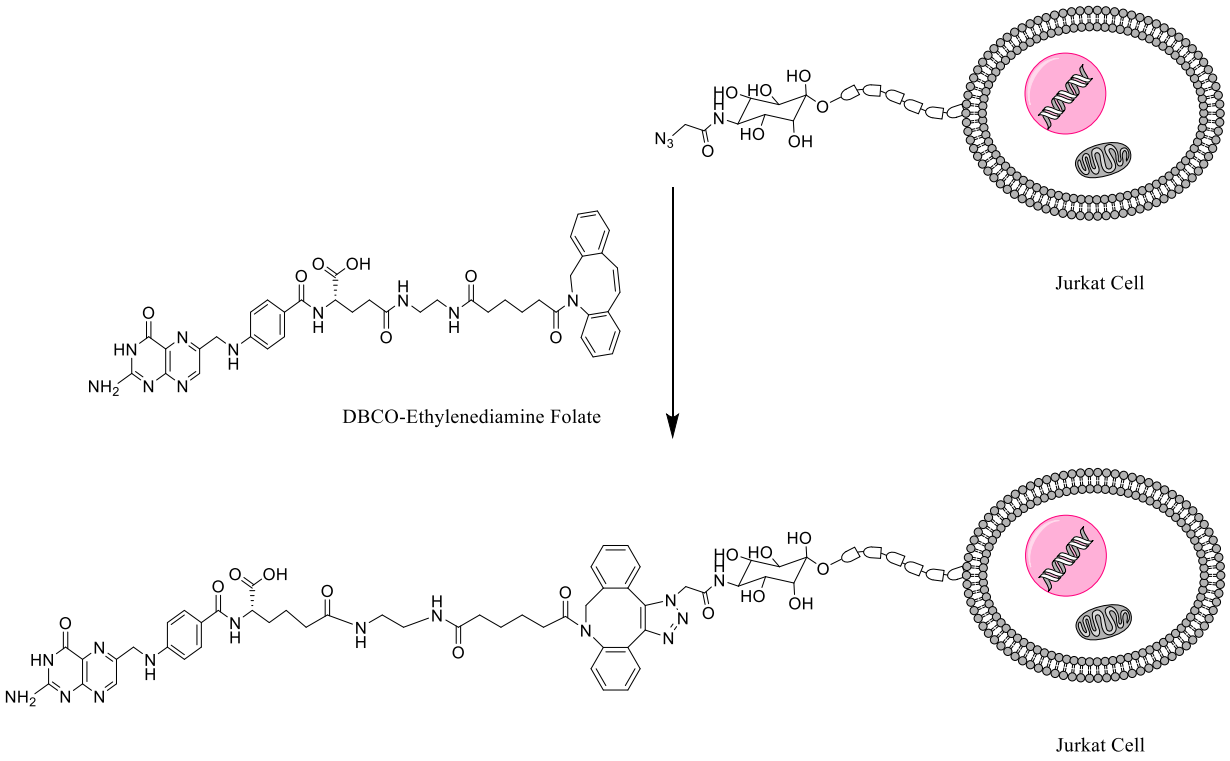

Scheme 3.6 Strategy of creation of biohybrid of T-lymphocyte Jurkat cells with DBCO-ethylenediamine folate (Jurkat-folate).

Figure *3.10* shows the results of measuring the fluorescence of metabolically labeled T-lymphocytes Jurkat cells with $Ac_4ManNAz$ with following reaction of chemoselective ligation with DBCO-ethylenediamine folate conjugate. These measurements indicate the strong fluorescent signal of DBCO-ethylenediamine folate moiety on the plasmalemma of T-lymphocytes Jurkat cells.

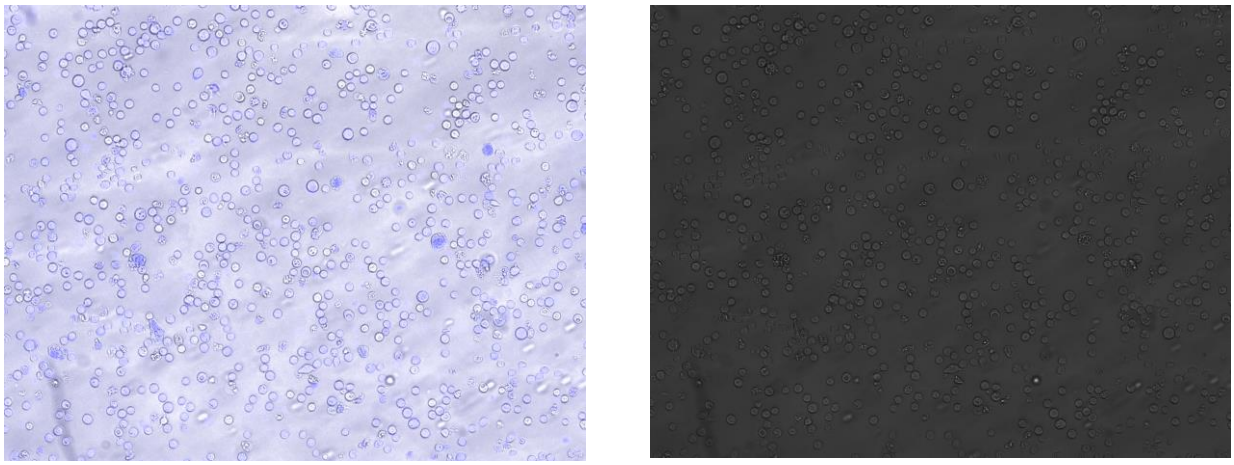

Figure 3.10 Chemoselective ligation of T-lymphocyte Jurkat cell line with 2.5 μM DBCO-ethylenediamine folate (incubation time 15 min, at room temperature in darkness). Fluorescence signal acquired by Cytell Imaging System (GE, CIIIA), E_{ex}=350 nm, E_{em}=461 nm (blue). Scale bar: 10 μm.

As presented herein, the copper-free SPAAC between DBCO-ethylenediamine-folate conjugate and azide containing cell peptidoglycans constitutes a powerful synthetic tool to introduce folic acid-based targeting vector into living cells. The obtained biohybrid is intended to use for selective recognition of human retinoblastoma Weri-Rb1 cells overexpressing folate receptor (FOLR1). The specificity of recognition of Weri-Rb1 cells by biohybrids based on T-lymphocytes Jurkat cell will be further evaluated. The obtained biohybrid for the selective recognition of tumor cells overexpressing folate receptor can be loaded with an antitumor agent or a fluorescent dye with desired photophysical properties for targeted drug delivery, diagnostics and theranostics.

Conclusion

1. The optimal conditions for chemoselective ligation of the surface of living human cells (suspension T-lymphocyte Jurkat and adherent prostate carcinoma PC3 cells) were found. The developed approaches are of great importance for creation of biohybrids.

2. The biohybrid composed of T-lymphocyte Jurkat cells ligated with anti-VEGF peptide was produced. The obtained biohybrid possess a biological activity which was confirmed by partial suppressing of proliferation of human retinal pigmented epithelial cells (ARPE-19).

3. The biohybrid composed of T-lymphocyte Jurkat cells ligated with folic acid was created. The cancer cells targeting activity of obtained biohybrid further needed to be evaluated.

4. The developed chemical and biological technologies for the construction of biohybrid platforms might be the basis of new approaches to personalized therapy of a wide range of diseases.

References

1. Tennikova T., Urtti A. Modified cells as potential ocular drug delivery systems // Drug Discov. Today. Elsevier Ltd, 2019. Vol. 24, № 8. P. 1621–1626.

2. Hu X. et al. A simple approach to bioconjugation at diverse levels: Metal-free click reactions of activated alkynes with native groups of biotargets without prefunctionalization // Research. 2018. Vol. 2018.

3. Algar W.R. A Brief Introduction to Traditional Bioconjugate Chemistry // Chemoselective Bioorthogonal Ligation React. 2017. P. 1–36.

4. Stephanopoulos N., Francis M.B. Choosing an effective protein bioconjugation strategy // Nat. Chem. Biol. Nature Publishing Group, 2011. Vol. 7, № 12. P. 876–884.

5. Hermanson G.T. Bioconjugate Techniques: Third Edition // Bioconjugate Techniques: Third Edition. 2013.

6. Hermanson G.T. Bioconjugate Techniques // Bioconjugate Techniques. Elsevier Inc., 2008.

7. Zheng M. et al. Development of bioorthogonal reactions and their applications in bioconjugation // Molecules. 2015. Vol. 20, № 2. P. 3190–3205.

8. Sletten E. Bioorthogonal Chemistries for Labeling Living Systems // UC Berkeley Electronic Theses and Dissertations. 2011. 705 p.

9. Sletten E.M., Bertozzi C.R. From Mechanism to Mouse: A Tale of Two Bioorthogonal Reactions // Acc. Chem. Res. 2011. Vol. 44, № 9. P. 666–676.

10. Zhang X., Zhang Y. Applications of azide-based bioorthogonal click chemistry in glycobiology // Molecules. 2013. Vol. 18, № 6. P. 7145–7159.

11. Prescher J.A., Bertozzi C.R. Chemistry in Living Systems // Nat. Chem. Biol. 2005. Vol. 1, № 1. P. 13–21.

12. Kenry, Liu B. Bio-orthogonal Click Chemistry for In Vivo Bioimaging // Trends Chem. Elsevier Inc., 2019. Vol. 1, № 8. P. 763–778.

13. Sletten E.M., Bertozzi C.R. Bioorthogonal chemistry: Fishing for selectivity in a sea of functionality // Angew. Chemie - Int. Ed. 2009. Vol. 48, № 38. P. 6974–6998.

14. Lim R.K.V., Lin Q. Bioorthogonal chemistry: A covalent strategy for the study of biological

systems // Sci. China Chem. 2010. Vol. 53, № 1. P. 61–70.

15. Kalia J. Advances in Bioconjugation // Curr Org Chem. 2010. Vol. 14, № 2. P. 24.

16. Horisawa K. Specific and quantitative labeling of biomolecules using click chemistry // Front. Physiol. 2014. Vol. 5, № Nov. P. 1–6.

17. Chen Y., Tong Z.R. Click chemistry: Approaches, applications and challenges // Click Chemistry: Approaches, Applications and Challenges. 2017.

18. Christopher D. Hein, Xin-Ming Liu and D.W. Click Chemistry, a Powerful Tool for Pharmaceutical Sciences Christopher // Pharm Res. 2008. Vol. 25, № 10. P. 30.

19. Takayama Y., Kusamori K., Nishikawa M. Click chemistry as a tool for cell engineering and drug delivery // Molecules. 2019. Vol. 24, № 1.

20. Lahann J. Click Chemistry: A Universal Ligation Strategy for Biotechnology and Materials Science // Click Chem. Biotechnol. Mater. Sci. 2009. P. 1–7.

21. Jung N., Bräse S. Click Reactions: Azide-Alkyne Cycloaddition // Kirk-Othmer Encycl. Chem. Technol. 2013.

22. Ramapanicker R., Chauhan P. Click Chemistry: Mechanistic and Synthetic Perspectives // Click React. Org. Synth. 2016. P. 1–24.

23. Pandey B., Demchenko A. V., Stine K.J. Nanoporous gold as a solid support for protein immobilization and development of an electrochemical immunoassay for prostate specific antigen and carcinoembryonic antigen // Microchim. Acta. 2012. Vol. 179, № 1–2. P. 71–81.

24. Saleh A.M. et al. Non-canonical amino acid labeling in proteomics and biotechnology // J. Biol. Eng. Journal of Biological Engineering, 2019. Vol. 13, № 1. P. 1–14.

25. Fisher S.A., Baker A.E.G., Shoichet M.S. Designing Peptide and Protein Modified Hydrogels: Selecting the Optimal Conjugation Strategy // J. Am. Chem. Soc. 2017. Vol. 139, № 22. P. 7416–7427.

26. Chen X., Voss S., Wu Y.-W. Chemoselective Modification of Proteins // Chem. Ligation. 2017. P. 285–338.

27. Kellam B., De Bank P.A., Shakesheff K.M. Chemical modification of mammalian cell surfaces // Chem. Soc. Rev. 2003. Vol. 32, № 6. P. 327–337.

28. Kim E.J. Chemical reporters and their bioorthogonal reactions for labeling protein O-GlcNAcylation // Molecules. 2018. Vol. 23, № 10.

29. Scientific T.F. CHAPTER 3 Fluorophores and Click Chemistry and Their Amine-Reactive Other Fu nctional Derivatives Group Modifications // Mol. Probes ® Handb. 2010.

30. Yoon H.I. et al. Bioorthogonal Copper Free Click Chemistry for Labeling and Tracking of Chondrocytes In Vivo // Bioconjug. Chem. 2016. Vol. 27, № 4. P. 927–936.

31. Koo H. et al. Bioorthogonal Copper-Free Click Chemistry In Vivo for Tumor-Targeted Delivery of Nanoparticles // Angew. Chemie. 2012. Vol. 124, № 47. P. 12006–12010.

32. Lee S. et al. Chemical tumor-targeting of nanoparticles based on metabolic glycoengineering and click chemistry // ACS Nano. 2014. Vol. 8, № 3. P. 2048–2063.

33. Xie R. et al. Cell-selective metabolic glycan labeling based on ligand-targeted liposomes // J. Am. Chem. Soc. 2012. Vol. 134, № 24. P. 9914–9917.

34. Wang H. et al. Selective in vivo metabolic cell-labeling-mediated cancer targeting // Nat. Chem. Biol. Nature Publishing Group, 2017. Vol. 13, № 4. P. 415–424.

35. Layek B., Sadhukha T., Prabha S. Glycoengineered mesenchymal stem cells as an enabling platform for two-step targeting of solid tumors // Biomaterials. Elsevier Ltd, 2016. Vol. 88. P. 97–109.

36. Harmey J.H. et al. Vascular Endothelial Growth Factor (VEGF) and Its Role in Non-Endothelial Cells: Autocrine Signalling by VEGF // VEGF and Cancer. 2004.

37. Sullivan L.A., Brekken R.A. The VEGF family in cancer and antibody-based strategies for their inhibition. 2010. P. 165–175.

38. Ria R. et al. Vascular endothelial growth factor and its receptors in multiple myeloma // Leukemia. 2003. Vol. 17, № 10. P. 1961–1966.

39. Roskoski R. Vascular endothelial growth factor (VEGF) signaling in tumor progression // Crit. Rev. Oncol. Hematol. 2007. Vol. 62, № 3. P. 179–213.

40. Pandey A.K. et al. Mechanisms of VEGF (vascular endothelial growth factor) inhibitor-associated hypertension and vascular disease // Hypertension. 2018. Vol. 71, № 2. P. E1–E8.

41. Lal N., Puri K., Rodrigues B. Vascular Endothelial Growth Factor B and Its Signaling // Front. Cardiovasc. Med. 2018. Vol. 5, № April. P. 1–9.

42. Uccelli A. et al. Vascular endothelial growth factor biology for regenerative angiogenesis // Swiss Med. Wkly. 2019. Vol. 149, № January. P. w20011.

43. Krilleke D., Ng Y.S.E., Shima D.T. The heparin-binding domain confers diverse functions of

VEGF-A in development and disease: A structure-function study // Biochem. Soc. Trans. 2009. Vol. 37, № 6. P. 1201–1206.

44. Azimi-Nezhad M. Vascular endothelial growth factor from embryonic status to cardiovascular pathology. // Reports Biochem. Mol. Biol. 2014. Vol. 2, № 2. P. 59–69.

45. Ho Q.T., Kuo C.J. Vascular endothelial growth factor: Biology and therapeutic applications // Int. J. Biochem. Cell Biol. 2007. Vol. 39, № 7–8. P. 1349–1357.

46. Bruno J.B., , M.H.T. Matos, R.N. Chaves, J.J.H. Celestino, M.V.A. Saraiva, I.B. Lima-Verde, V.R. Araújo J.R.F. Angiogenic factors and ovarian follicle development // Anim. Reprod. 2009. Vol. 6, № 2. P. 371–379.

47. Ferrara N. Vascular endothelial growth factor: Basic science and clinical progress // Endocr. Rev. 2004. Vol. 25, № 4. P. 581–611.

48. Hicklin D.J., Ellis L.M. Role of the vascular endothelial growth factor pathway in tumor growth and angiogenesis // J. Clin. Oncol. 2005. Vol. 23, № 5. P. 1011–1027.

49. GERA NEUFELD, TZAFRA COHEN, STELA GENGRINOVITCH A.Z.P. Vascular endothelial growth factor (VEGF) and its receptors // Drugs of Today. 2003. Vol. 39, № SUPPL. C. P. 81–93.

50. Kaseb A.O. et al. Vascular endothelial growth factor in the management of hepatocellular carcinoma: A review of literature // Cancer. 2009. Vol. 115, № 21. P. 4895–4906.

51. Ferrara N., Adamis A.P. Ten years of anti-vascular endothelial growth factor therapy // Nat. Rev. Drug Discov. Nature Publishing Group, 2016. Vol. 15, № 6. P. 385–403.

52. Takahashi H., Shibuya M. The vascular endothelial growth factor (VEGF)/VEGF receptor system and its role under physiological and pathological conditions // Clin. Sci. 2005. Vol. 109, № 3. P. 227–241.

53. Holmes D.I., Zachary I. The VEGF family - angiogenic factors in health and disease // Genome Biol. 2005. Vol. 6. P. 209.

54. Robert S. Kerbel. Tumor Angiogenesis Robert // N Engl J Med. 2008. Vol. 358, № 19. P. 2039–2049.

55. Emma Roberts, Davina A. F. Cossigny and G.M.Y.Q. The Role of Vascular Endothelial Growth Factor in Metastatic Prostate Cancer to the Skeleton // Can. J. Urol. 2013. Vol. 2013. P. 8.

56. Marla V., Hegde V., Shrestha A. Relationship of angiogenesis and oral squamous cell

carcinoma // Kathmandu Univ. Med. J. 2015. Vol. 13, № 50. P. 178–185.

57. Shibuya M. Vascular Endothelial Growth Factor (VEGF) and Its Receptor (VEGFR) Signaling in Angiogenesis: A Crucial Target for Anti- and Pro-Angiogenic Therapies // Genes and Cancer. 2011. Vol. 2, № 12. P. 1097–1105.

58. Epstein R.J. VEGF signaling inhibitors: More pro-apoptotic than anti-angiogenic // Cancer Metastasis Rev. 2007. Vol. 26, № 3–4. P. 443–452.

59. Ferrara N. The biology of VEGF and its receptors // Nat. Med. 2003. Vol. 9, № 6. P. 669–676.

60. Hoeben A. et al. Vascular endothelial growth factor and angiogenesis // Pharmacological Reviews. 2004. Vol. 56, № 4.

61. Francis S. Markland , Stephen Swenson , Radu Minea. Tumor Angiogenesis: From Molecular Mechanisms to Targeted Therapy. Wiley-Blackwell, 2010. 351 Pages p.

62. Ferrara N. Vascular endothelial growth factor // Arterioscler. Thromb. Vasc. Biol. 2009. Vol. 29, № 6. P. 789–791.

63. Castilla M.Á. et al. Tumor-induced endothelial cell activation: Role of vascular endothelial growth factor // Am. J. Physiol. - Cell Physiol. 2004. Vol. 286, № 5 55-5. P. 1170–1176.

64. Hong T. et al. Expression of angiogenic factors and apoptotic factors in leiomyosarcoma and leiomyoma. // Int. J. Mol. Med. 2001. Vol. 8, № 2. P. 141–148.

65. Elizabeth R. Gerstner, MD, A. Gregory Sorensen, MD, Rakesh K. Jain, PhD, and Tracy T. Batchelor, MD. Anti–Vascular Endothelial Growth Factor Therapy for Malignant Glioma // Curr Neurol Neurosci Rep. 2009. Vol. 9, № 3. P. 254–262.

66. Qi N. et al. Combination use of paclitaxel and avastin enhances treatment effect for the NSCLC patients with malignant pleural effusion // Med. (United States). 2016. Vol. 95, № 47.

67. Mukherji S.K. Bevacizumab (avastin) // Am. J. Neuroradiol. 2010. Vol. 31, № 2. P. 235–236.

68. Zafar S.Y. et al. Early dissemination of bevacizumab for advanced colorectal cancer: A prospective cohort study // BMC Cancer. 2011. Vol. 11.

69. FILIS KAZAZI-HYSENI, JOS H. BEIJNEN, JAN H. M. SCHELLENS. Bevacizumab // Oncol. 2010. 2010. Vol. 15. P. 819–825.

70. Keating G.M. Bevacizumab: A review of its use in advanced cancer // Drugs. 2014. Vol. 74, № 16. P. 1891–1925.

71. De Falco S. Antiangiogenesis therapy: An update after the first decade // Korean J. Intern. Med. 2014. Vol. 29, № 1. P. 1–11.

72. Balaratnasingam C. et al. Aflibercept: A review of its use in the treatment of choroidal neovascularization due to age-related macular degeneration // Clin. Ophthalmol. 2015. Vol. 9, № December. P. 2355–2371.

73. Aprile G. et al. Ramucirumab: Preclinical research and clinical development // Onco. Targets. Ther. 2014. Vol. 7, № October. P. 1997–2006.

74. Papadopoulos Z. Aflibercept: A review of its effect on the treatment of exudative age-related macular degeneration // European Journal of Ophthalmology. 2019. Vol. 29, № 4.

75. Stewart M.W. A Review of Ranibizumab for the Treatment of Diabetic Retinopathy // Ophthalmol. Ther. Springer Healthcare, 2017. Vol. 6, № 1. P. 33–47.

76. Giuliari G., Guel D., Gonzalez V. Pegaptanib Sodium for the Treatment of Proliferative Diabetic Retinopathy and Diabetic Macular Edema // Curr. Diabetes Rev. 2009. Vol. 5, № 1. P. 33–38.

77. Haas B. et al. Is sunitinib a Narrow Therapeutic Index Drug? - A systematic review and in vitro toxicology-analysis of Sunitinib vs. Imatinib in cells from different tissues // Regul. Toxicol. Pharmacol. 2016. Vol. 77. P. 25–34.

78. Iyer R. et al. Sorafenib: A clinical and pharmacologic review // Expert Opin. Pharmacother. 2010. Vol. 11, № 11. P. 1943–1955.

79. Adhip P.N. Majumdar, Udayini Kodali, Richard Jaszewski. CHEMOPREVENTIVE ROLE OF FOLIC ACID IN COLORECTAL CANCER // Front. Biosci. 9,. 2004. Vol. 9. P. 2725–2732.

80. Vergote I.B., Marth C., Coleman R.L. Role of the folate receptor in ovarian cancer treatment: evidence, mechanism, and clinical implications // Cancer Metastasis Rev. 2015. Vol. 34, № 1. P. 41–52.

81. Kelemen L.E. The role of folate receptor α in cancer development, progression and treatment: Cause, consequence or innocent bystander? // Int. J. Cancer. 2006. Vol. 119, № 2. P. 243–250.

82. Chittiboyina S. et al. The role of the folate pathway in pancreatic cancer risk // PLoS One. 2018. Vol. 13, № 2. P. 1–15.

83. Chen C. et al. Structural basis for molecular recognition of folic acid by folate receptors // Nature. 2013. Vol. 500, № 7463. P. 486–489.

84. Drakos S.S. et al. The role of folate metabolism-related gene polymorphisms in the

development of meningiomas // Cancer Genomics and Proteomics. 2010. Vol. 7, № 2. P. 105–109.

85. Ledermann J.A., Canevari S., Thigpen T. Targeting the folate receptor: Diagnostic and therapeutic approaches to personalize cancer treatments // Ann. Oncol. Elsevier Masson SAS, 2015. Vol. 26, № 10. P. 2034–2043.

86. Marchetti C. et al. Targeted drug delivery via folate receptors in recurrent ovarian cancer: A review // Onco. Targets. Ther. 2014. Vol. 7. P. 1223–1236.

87. Yi Y.S. Folate Receptor-Targeted Diagnostics and Therapeutics for Inflammatory Diseases // Immune Netw. 2016. Vol. 16, № 6. P. 337–343.

88. Maurer A.H. et al. Imaging the folate receptor on cancer cells with 99mTc- etarfolatide: Properties, clinical use, and future potential of folate receptor imaging // J. Nucl. Med. 2014. Vol. 55, № 5. P. 701–704.

89. Leamon C.P. et al. Synthesis and biological evaluation of EC20: A new folate-derived, 99mTc-based radiopharmaceutical // Bioconjug. Chem. 2002. Vol. 13, № 6. P. 1200–1210.

90. Assaraf Y.G., Leamon C.P., Reddy J.A. The folate receptor as a rational therapeutic target for personalized cancer treatment // Drug Resist. Updat. Elsevier Ltd, 2014. Vol. 17, № 4–6. P. 89–95.

91. Leamon C.P., Low P.S. Folate-mediated targeting: From diagnostics to drug and gene delivery // Drug Discov. Today. 2001. Vol. 6, № 1. P. 44–51.

92. Hilgenbrink A.R., Low P.S. Folate receptor-mediated drug targeting: From therapeutics to diagnostics // J. Pharm. Sci. 2005. Vol. 94, № 10. P. 2135–2146.

93. Vergote I., Leamon C.P. Vintafolide: A novel targeted therapy for the treatment of folate receptor expressing tumors // Ther. Adv. Med. Oncol. 2015. Vol. 7, № 4. P. 206–218.

94. Kamen B.A., Smith A.K. Farletuzumab, an anti-folate receptor α antibody, does not block binding of folate or anti-folates to receptor nor does it alter the potency of anti-folates in vitro // Cancer Chemother. Pharmacol. 2012. Vol. 70, № 1. P. 113–120.

95. Teng L. et al. Clinical translation of folate receptor-targeted therapeutics // Expert Opin. Drug Deliv. 2012. Vol. 9, № 8. P. 901–908.

96. Luyckx M. et al. Profile of vintafolide (EC145) and its use in the treatment of platinum-resistant ovarian cancer // Int. J. Womens. Health. 2014. Vol. 6, № 1. P. 351–358.

97. Riss T.L. et al. Cell Viability Assays. 2016. № Md. P. 1–25.

98. Aslantürk Ö.S., Aslantürk S. In Vitro Cytotoxicity and Cell Viability Assays:Disadvantages In Vitro Cytotoxicity and Viability Assays : Principles , Advantages, and Disadvantages. P.1-18.

99. Kumar P., Nagarajan A., Uchil P.D. Analysis of Cell Viability by the MTT Assay. 2018. P. 469–472.

100. Trindade A.F. et al. “Click and go”: simple and fast folic acid conjugation† // Org. Biomol. Chem. 2014. P. 3181–3190.

101. Debets M.F. et al. ChemInform Abstract: Aza-Dibenzocyclooctynes for Fast and Efficient Enzyme PEGylation via Copper-Free [3 + 2] Cycloaddition. // ChemInform. 2010. Vol. 41, № 22. P. no-no.